AD NUMBER

AD835810

LIMITATION CHANGES

TO:

Approved for public release; distribution is unlimited.

FROM:

Distribution authorized to U.S. Gov't. agencies and their contractors; Critical Technology; APR 1968. Other requests shall be referred to Naval Weapons Center, China Lake, CA 93555. This document contains export-controlled technical data.

AUTHORITY

NWC per DTIC Form 55

COMBUSTION OF SOLID PROPELLANTS AND LOW FREQUENCY COMBUSTION INSTABILITY PROGRESS REPORT 1 APRIL–30 SEPTEMBER 1967

by

Aerothermochemistry Division

Research Department

ABSTRACT. This semiannual report summarizes studies of ammonium perchlorate decomposition and deflagration, behavior of aluminum in the combustion zone of propellants, and oscillatory combustion of propellants in several types of experimental arrangements.

NAVAL WEAPONS CENTER
CHINA LAKE, CALIFORNIA * APRIL 1968

NAVAL WEAPONS CENTER
AN ACTIVITY OF THE NAVAL MATERIAL COMMAND

M. R. Etheridge, Capt., USN ..... Commander
Thomas S. Amlie, Ph.D. ..... Technical Director

FOREWORD

This report summarizes progress on a continuing program sponsored by the Office of Advanced Research and Technology of the National Aeronautics and Space Administration (NASA) under NASA Work Order 6030 during the period April through September, 1967. The preceding report on this work was NOTS TP 4244.

The following persons contributed to this report: M. W. Beckstead, T. L. Boggs, J. E. Crump, G. L. Dehority, J. D. Hightower, K. J. Kraeutle, H. Krier, H. S. Mathes, and E. W. Price.

This report is released at the working level for information purposes and does not represent the final judgement of the Center.

Released by
J. E. CRUMP, Head (Acting)
Aerothermochemistry Division
16 April 1968

Under authority of
HUGH W. HUNTER, Head
Research Department

NWC Technical Publication 4478

Published by.....Research Department
Collation.....Cover, 57 leaves, DD Form 1473, abstract cards
First printing.....230 unnumbered copies
Security classification.....UNCLASSIFIED

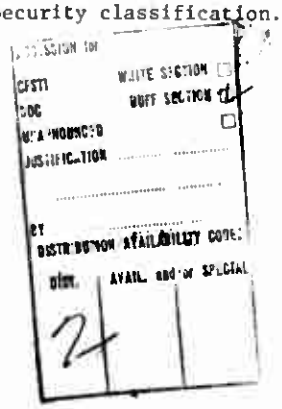

CONTENTS

NOMENCLATURE

A	Nondimensional parameter, $\frac{E_s}{R\bar{T}_s}\left(1 - \frac{T_o}{\bar{T}_s}\right)$
A'	Nondimensional parameter, $\left(\frac{E_s}{R\bar{T}_s} - 1/2\right)\left(1 - \frac{T_o}{\bar{T}_s}\right)$
A_b	Area of burning surface
A_t	Throat area of sonic nozzle
a	Acoustic wave velocity
B_{DB}	Nondimensional parameter (see Eq. 4.9)
B_{HFC}	Nondimensional parameter (see Eq. 4.10)
C_s, C_p	Specific heat of solid and gas, respectively
c^*	Characteristic velocity of exhaust gases
D	Diameter
E_s, E_f	Activation energy of the solid and the flame, respectively
j	Temperature sensitivity of propellant, $\frac{T_o}{\bar{r}}\frac{\partial \bar{r}}{\partial T_o}$
K	A constant, ≤ 1
L	Length of T-burner
L^*	Characteristic length of chamber (free volume divided by nozzle throat area)
ℓ_s	Distance between entropy extremes
m	Mass burning rate

n	Pressure exponent in steady state burning rate law, $\bar{r} = bp^{-n}$
p	Pressure
$\bar{p}$	Mean or time-average pressure
p'	Pressure perturbation
p_r	Reference plane pressure
R	Gas constant
Re()	Real part of a complex expression
r'	Burning rate perturbation
s	Entropy
s_o	Reference entropy
T	Temperature
$\bar{T}$	Mean or time average temperature
T'	Tempersture perturbation
T_f	Adiabstic flame temperature
T_o	Initial temperature of the propellant
T_r	Reference plane temperature
T_s	Surface temperature of burning propellant
$\mathcal{T}$	Period of acoustic oscillation
V	Volume
$\bar{V}$	Velocity amplitude
v	Velocity perturbation
$\bar{v}$	Mean or time-average velocity
v_g	Mean gas velocity
X	Displacement
Y	Acoustic admittance

α Exponential growth constant

α_t Thermal diffusivity of aolid

ε Ratio of maximum presaure perturbation to mean pressure

λ Characteristic root of the aolid phase energy equation (see Eq. 4.7 and wavelength in Section 5)

μ/ε Ratio of masa perturbation to pressure perturbation. Also deaignated the propellant responae function.

ρ Density

σ/ε Ratio of denaity perturbation to preaaure perturbation

τ Characteriatic time to burn through a particle

τ_{ch} Residence time of the chamber

τ_{tw} Thermal wave relaxation time, $\frac{\alpha_t}{r^2}$

ϕ Phase of combuation relative to preasure

ψ Phaae between preaaure and emergence of element of gaa from the combuation zone

Ω Non-dimensional frequency, $\frac{\alpha_t \omega}{\bar{r}^2}$

ω Frequency in radiana/aecond

SUPERSCRIPTS

$-$ Bar over a aymbol (e.g., $\bar{r}$) refera to a time averaged value

SUBSCRIPTS

b Burning aurface

g Gas

o Total

c Chamber

1. INTRODUCTION

1.1. CONCEPT OF STUDIES

The research work described in this report is part of a continuing program (Ref. 1) of inveatigation of the processes involved in low frequency acoustic and nonacoustic type oscillatory behavior in solid propellant rocket motors and in various aspects of steady-state combustion and ingredient decomposition believed to be related to solid propellant combustion instability. The present program was initiated at a time when there were two concurrent trends in the development of solid propellant rocket motors. The first of these was the development of very large solid propellant booster rockets, whose dimensions were such as to permit oscillatory behavior in acoustic modes at frequencies down to about 10 cps. The second was the growing interest in motors intended for space applications which possessed very high volumetric loading density and were designed to operate at relatively low pressures; both of these features are important for favorable mass ratios required for upper stage applications. Some motors of this type were observed to exhibit oscillatory behavior in a low frequency, nonacoustic mode, particularly in the frequency range of 10 to 200 cps (Ref. 2-4). Considering the extremely high cost of individual firings of the very large rocket motors under development and the cost of trial and error corrections should low frequency combustion instability occur, it was advantageous to develop laboratory scale tests which would permit qualitative evaluation of the susceptibility of propellants to low frequency combustion instability and to determine those attributes of the combustion responsible for instability.

A review of the general character of solid propellant combustion and of oscillatory combustion were presented in the previous report (Ref. 1); that review should be considered as background information for the work reported here.

1.2. PLAN OF THE REPORT

This report aummarizes work that has been done on this program from April through September, 1967. Each section deals with a specific aspect of the program and in some cases is complete in itself. Although the sections are independent, they are mutually complementary; results in one area often suggest investigations that should he pursued in others.

Section 2 describes the continued investigations of decomposition and deflagration of large single ammonium perchlorate (AP) crystals. The

work included investigations with MnO_4^--doped crystals and combustion of crystals in low pressure methane.

Section 3 reports the improvements in the apparatus and techniques for photographing propellant samples in a window bomb and also the progress in understanding the detailed aspects of aluminum accumulation in "real propellants".

Section 4 covers the work, both experimental and theoretical, on nonacoustic combustion instability. Experimental data was reasonably well correlated by the models of Denison and Baum and of Hart, Farrell, and Cantrell. A phenomenological concept is presented which partially explains the deviation of experimental data for several bimodal oxidizer propellants from the one-dimensional thermal theory.

Section 5 deals with the work on low frequency acoustic instability with particular emphasis on the dynamics of the combustion zone as inferred from streak photographs and gas temperature measurements taken during oscillatory combustion.

Section 6 is a brief summary of the more significant observations made during this reporting period and their relation to previous work on the program.

Appendix A consists of burning rate data and tabular experimental data obtained on nonacoustic combustion instability. Appendix B presents the results of testing some of the NASA big booster candidate propellants in both the acoustic and nonacoustic laboratory burners and discusses their significance.

2. AMMONIUM PERCHLORATE OECOMPOSITION AND OEFLAGRATION

2.1. INTROOUCTION

Ammonium perchlorate (AP) is the oxidizer and principal ingredient in most modern composite propellants and its behavior in the combustion wave ia an essential aspect of the combustion as a whole. The knowledge of the major aspecta of the low temperature decompoaition and high temperature deflagration of AP was summarized in the previoua report (Ref. 1). Work has continued in both these areas of AP behavior. In the thermsl decomposition ares, single crystals of pure AP were partially decomposed and subsequently studied with a scanning electron microscope and the interfacial decomposition of MnO_4^--doped AP crystala was investigated. In the area of AP deflagration, further studies were conducted to elucidate the extent of the occurrence of a melt on the surface of pure AP crystala undergoing self-deflagration. Also, deflagration studies have been started on doped AP single crystals.

2.2. LOW TEMPERATURE OECOMPOSITION EXPERIMENTS[1]

2.2.1. Surface Structure of Partially Oecompoaed AP Crystals

To gain additional insight into the low temperature decomposition of AP, s series of experiments were undertaken to systematically study the surface features of partially decomposed AP crystala.[2] The isothermal decompoaition of single crystala of AP was monitored with a hot atage microscope and stopped at a predetermined stage. The samples were then vacuum coated with an Au/Pd alloy and kept under vacuum until they could be photographed with the scanning electron microscope (SEM). Several seriea of SEM photographs are shown of AP samples decomposed under various conditions. Each figure containa pictures of four different magnifications to allow the study of details as well aa bigger areas of a crystal surface. Rectangular-shaped holea are characteristic for decomposition

---

1 This work waa supported by Naval Ordnance Systems Command ORO-033 129/200 1/R001-06-01, Problem Assignment #5 and is reported here for continuity.

2 Both the pure and doped AP crystals uaed in the studiea in this section were grown by Or. W. R. McBride of the Research Oepartment, Michelson Laboratory, NWC, China Lake, California. A description of the techniques is given in Ref. 1.

sites on *m*-faces whereas rhombohedral-shaped holes are characteristic for the decomposition sites on c-faces. Figure 2.1 shows the *m*-face of a crystal which was decomposed isothermally at 226°C for 40 minutes at an air pressure of 20 mm Hg. The characteristic feature is the rectangular structure of the holes which make up the decomposition nucleus. The holes have the shape of the *m*-face with edges running parallel to the edges of the *m*-face. They are arranged in a disk-like pattern and eventually develop into a porous residue. Furthermore, the decomposition seems to occur in layers with the size of the holes becoming smaller and smaller with depth. There is a second type of decomposition site which generally does not develop into growing nuclei composed of holes. They appear immediately after reaching the decomposition temperature and were not observed under atmospheric pressure.

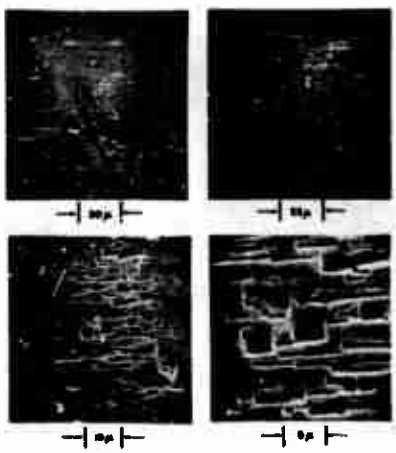

FIG. 2.1. Decomposition Site on *m*-Face of Pure AP After 40 Minutes Decomposition at 226°C and 20mm Hg.

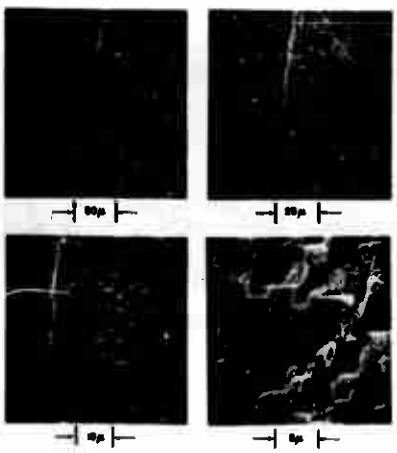

FIG. 2.2. Decomposition Site on c-Face of Pure AP After 60 Minutes Decomposition at 226°C and 20mm Hg.

Figure 2.2 shows part of a c-face on a crystal which was decomposed for 60 minutes at 226°C and 20 mm Hg of air. Analogous to *m*-faces there are two types of decomposition sites which have the shape of rhombohedrons. One type consists of holes arranged in a streak-like pattern. The streaks grow faster along the b-axis than along the a-axis and, after overlapping, constitute the porous residue layer. The other type comprises very flat rhombohedral holes which are spread all over the c-faces and appear only under low pressure. Both the streaks and the long diagonals of both types of decomposition sites are parallel to the b-axis of the crystal. If the decomposition is carried on for a longer time the

surfsce becomes less regular, although some of the rectsngular structure is still preserved, as can be seen in Fig. 2.3, which shows part of an *m*-fsce after 140 minutes decompoaition at 226°C and a pressure of 20 mm Hg sir. There is s very different type of structure at the very top of the decomposition site in Fig. 2.3. It appears to consist of clusters of very small AP particles. The clusters may be products of a complex dissociation-desorption-adsorption process or may be residues of advsnced sublimation of the porous lsyer.

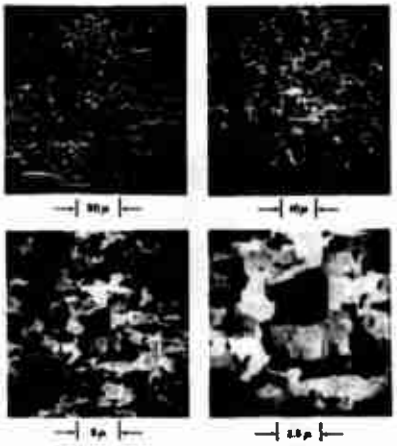

FIG. 2.3. Decomposition Site on *m*-Fsce of Pure AP After 140 Minutes Decomposition at 226°C snd 20 mm Hg.

The decomposition under atmospheric pressure does not change the general appesrance of the decomposition sites. Figure 2.4 shows part of sn *m*-fsce sfter 90 minutes decomposition at 226°C and Fig. 2.5 psrt of a c-fsce after 120 minutes decomposition.

However, some differences from vacuum decomposition csn be seen. First, the size of the holes is amaller although the crystals decomposed about twice ss long as under vacuum. This is probably due to s suppression of sublimstion st atmospheric pressure. Second, there is a great number of fine crscks not visible on vscuum decomposed samples, snd third, there sre spots of elevated surfsce. These spots sre concentrated at the rim of an *m*-face decompoaition site whereas they are abundant over the whole streak on s c-fsce.

Aa a by-product of the decomposition at both 20 mm Hg and st atmospheric pressure a condensste was obtsined on a cool (about 50°C) quartz plate. Figure 2.6 shows a SEM photogrsph of the condensste obtained during the decomposition of an AP crystal at one atmoaphere of air. The condensste wss in the esrly stsge of development. An x-ray powder pattern showed the condensate to be pure AP. This indicates that there waa

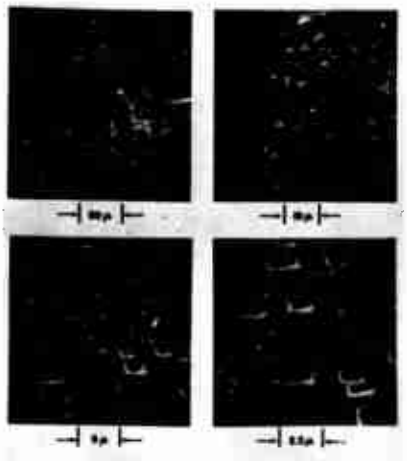

FIG. 2.4. Decompoaition Site on *m*-Face of Pure AP After 90 Minutea Decomposition at 226°C and Atmospheric Presaure.

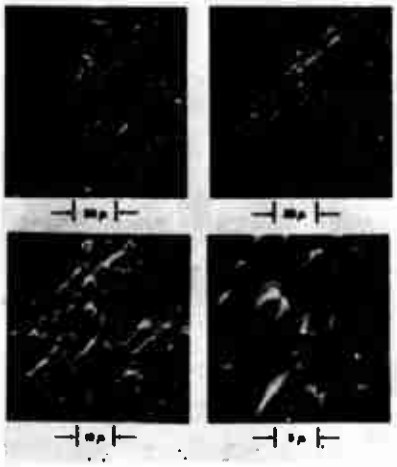

FIG. 2.5. Decomposition Site on c-Face of Pure AP After 120 Minutes Decomposition at 226°C and Atmoapheric Pressure.

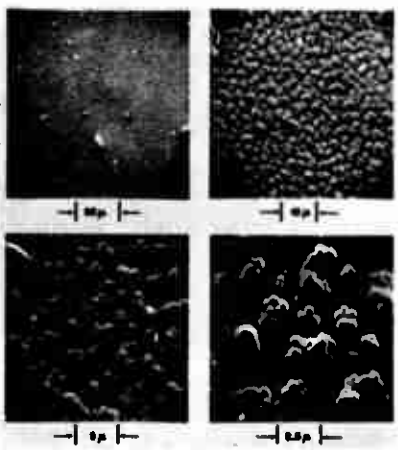

FIG. 2.6. Condensate of Pure AP on Quartz Disk.

an appreciable sublimation of AP even at atmospheric pressure. No condensate is obtained if the whole reaction vessel (volume) is kept at decomposition temperature. In that case, the part of AP which sublimes subsequently decomposes in the gas phase or, heterogeneously, on the hot surface (walls) of the oven. In view of continuing discussions of condensed and/or gas phase reactions during the decomposition of AP, and in light of the above observations, an effort should be made to obtain data simultaneously for reactions occurring in the condensed phase and away from the condensed phase of decomposing AP.

2.2.2. Interfacial Decomposition of Doped AP Crystals

Work in this area as reported in Ref. 1 has been expanded to include two additional concentrations of MnO_4^- in the doped AP single crystals. The procedure is described and results for pure AP crystals were reported in Ref. 1.

Single AP crystals containing 0.009 weight percent, 0.04 weight percent, and 0.11 weight percent MnO_4^- were decomposed isothermally under atmospheric pressure. The advance of the decomposition interface as a function of time was obtained by cleaving the crystals and measuring the thickness of the residue layers at different stages of decomposition. The total weight loss after a complete partial decomposition was between 35 and 40% of the original weight as compared with 35% for pure AP and about 30% measured by Bircumshaw and Newman (Ref. 5).

As in the case of pure AP, it was found that the decomposition interface advanced linearly with time into the crystal. Figures 2.7 through 2.12 show data of *m*- and *c*-face decomposition. The decomposition parallel to *c*-faces is about 10-20% slower than the decomposition parallel to *m*-faces. With the rate values evaluated from Fig. 2.7 through 2.12 one can calculate the fractional decomposition at a given time for crystals which were cleaved to the shape of a parallelepiped. Of more interest, however, are the kinetic parameters of the isothermal decomposition which can be obtained from Arrhenius plots of rates versus 1/T. Figure 2.13 shows the diagrams for *m*-face decomposition and Fig. 2.14 for *c*-face decomposition. The kinetic parameters calculated from these figures are listed in Table 2.1. Values reported for pure AP single crystals (Ref. 1) were 6.5×10^3 cm/sec for the preexponential factor and 21.9 kcal/mole for the activation energy (average values for *m*- and *c*-faces). All of the doped AP had preexponential factors and activation energies smaller than the values for pure AP. Accordingly, at higher temperatures and under the assumption that the decomposition mechanism stays the same, one would expect smaller burning rates for doped AP because the preexponential term becomes more and more dominant and the Arrhenius plots intersect at relatively low temperatures. This was in fact observed (Section 2.3.2), but it does not infer that the combustion of AP obeys the same or similar mechanisms as the low temperature decomposition. This would be a gross simplification of a very complex process.

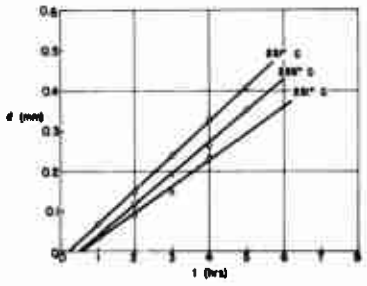

FIG. 2.7. 0.009 Wt.% MnO_4^-. *m*-Face Decompoaition.

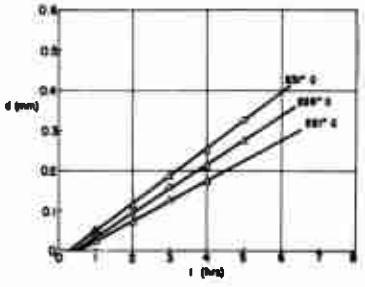

FIG. 2.8. 0.009 Wt.% MnO_4^-. c-Face Decompoaition.

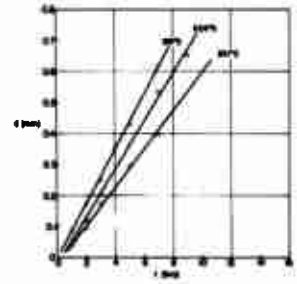

FIG. 2.9. 0.04 Wt.% MnO_4^-. *m*-Face Decomposition.

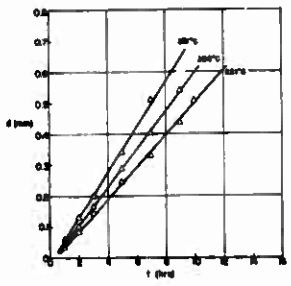

FIG. 2.10. 0.04 Wt.% MnO_4^-. c-Fsce Decomposition.

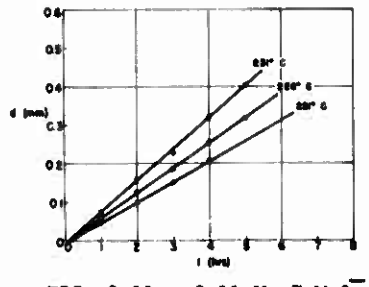

FIG. 2.11. 0.11 Wt.% MnO_4^-. *m*-Face Decompoaition.

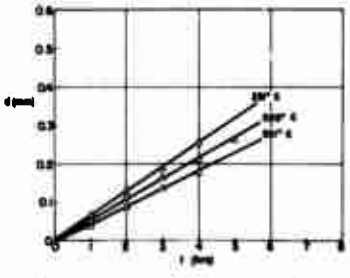

FIG. 2.12. 0.11 Wt.% MnO_4^-. c-Face Decompoaition

FIG. 2.7-2.12. Penetration of the Decompoaition Interface Into NH_4MnO_4-Doped Ammonium Perchlorate Single Crystals. d = distance from crystal aurface to interface.

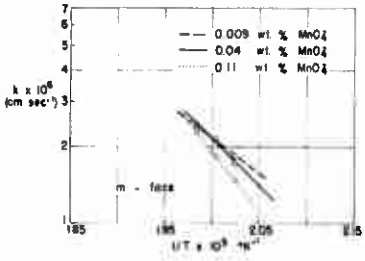

FIG. 2.13. Arrhenius Plot for NH_4MnO_4-Doped AP. *m*-Face Decomposition.

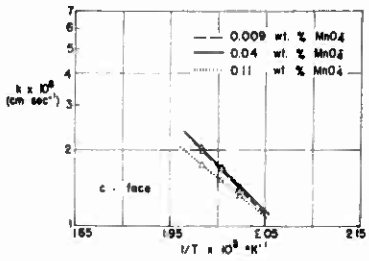

FIG. 2.14. Arrhenius Plot for NH_4MnO_4-Doped AP. c-Face Decomposition.

TABLE 2.1.

KINETIC PARAMETERS FOR THE DECOMPOSITION OF NH_4MnO_4-DOPED AMMONIUM PERCHLORATE SINGLE CRYSTALS

SAMPLE	PREEXP. FACTOR (cm/sec)		ACTIVATION ENERGY kcal/mole	
	m-face	c-face	m-face	c-face
AP + 0.009 WT. % MnO_4^-	0.9	62.0	12.9	17.3
AP + 0.04 WT. % MnO_4^-	47.3	39.0	16.8	16.7
AP + 0.11 WT. % MnO_4^-	4180.0	2.5	21.4	14.2

A theoretical interpretation of the results has not been tried yet in view of the uncertainty concerning the nucleation rate and rate of nuclei growth. In preliminary experiments using a hot stage optical microscope it was found that the nucleation rate of doped AP is much higher than that of pure AP. In addition, the number of nucleation sites in orders of magnitude greater for doped than for undoped AP if both are compared after the same decomposition time. This may affect the preexponential factors as well as the activation energies and a careful study of nucleation and nuclei growth, both for pure and doped AP, will be necessary to give an interpretation of the variety of kinetic parameters available.

2.3. SINGLE CRYSTAL DEFLAGRATION STUDIES

2.3.1. Combustion In Reactive Atmoapheres

In earlier work (Ref. 1, 6 and 7) evidence wss reported which indicated that a thin layer of melt wss present on the aurface of pure AP crystals undergoing self-austained deflagration. The studies have been extended to determine the extent of occurrence of the melt and ita importance to the deflagration process. The use of reactive atmospheres auch as methsne and ammonis have allowed atudiea to be made at reduced pressures corresponding to regresaion ratea intermediate between those of self-deflagration and low tempersture decompoaition.

Single crystals of pure AP and crystals doped with varioua concentrations of NH_4MnO_4 and $KClO_4$ were grown in the appsratus described in Ref. 1. Figure 2.15 shows crystals typical of those used in the present work. Samples were burned in the flushed window bomb described in Section 3.2. High speed motion pictures were taken to study the qualitstive aspecta of combuation and to determine the burning rates. For photographic purpoaea pure AP and K^+-doped cryatals were illuminated by a 2,500-watt xenon lamp. The purple MnO_4^--doped AP crystals were photographed with transmitted, low intensity polarized light to prevent heating the crystals by optical rsdiation sbaorption.

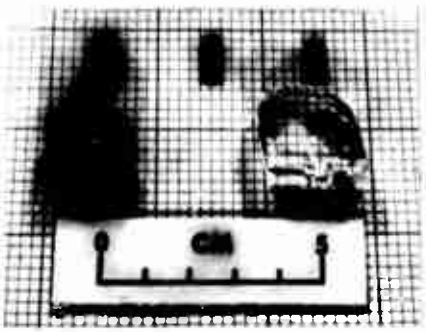

FIG. 2.15. Single Cryatsls Typical of Those Used in the Present Work. At left is a MnO_4^--doped crystal which hss deep purple color and slightly modified growth habit. At right e pure AP cryetal snd above amall, clsaved segmenta of MnO_4^--doped AP in various concentration.

High apeed motion pictures of the deflagration in methane st pressures between etmospheric and 100 psis were of perticular interest. Under these conditions a variety of surface heating conditiona end, hence, regression retes was possible. Figure 2.16 showa s pure AP crystal burning st 15 psie in methane. At this pressure the surface regressed with a pronounced coning due to flsme spresd down the sidee of the crystsl; the upper portion of the coned eurface had a regression rate of approximately 0.03 in/sec. The surfsce had e froety, trsnslucent eppearsnce. Quenched ssmples st these lower pressures were obteined by rspidly flooding the combustion bomb with nitrogen. Figure 2.17 is a scsnning electron microacope (SEM) photograph of the surface of a

FIG. 2.16. Single Frame of Motion Picture of Pure AP Burning in Methane Atmosphere at 15 psia. Crystal approximately 0.5 cm wide.

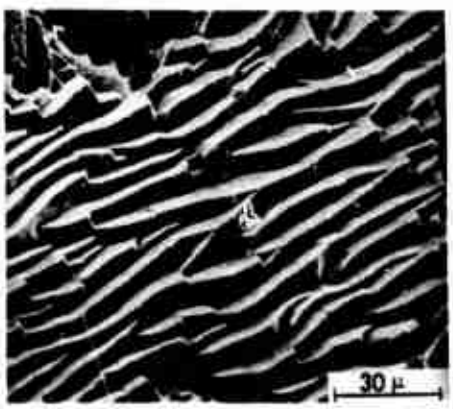

FIG. 2.17. Scanning Electron Microscope Photomicrograph of the Burned Surface of Pure AP Quenched from Combustion in 15 psia methane.

quenched sample that was burned in this intermediate regression rate domain. The surface structure that results from this mode of combustion gives the appearance of a crystal structure but differs from the structure of an "undisturbed" AP crystal. Figure 2.18 shows a pure AP crystal burning at 65 psia. At this pressure the surface was clear and transparent and resembled melting ice. Occasional boiling activity could be clearly seen on the surface. At 100 psia in methane movies taken at a magnification of 4X of AP crystals approximately 250 micron thick showed a definite "flowing" motion associated with portions of the burning surface as well as patches of rapidly boiling "froth". It was not possible to quench samples under these conditions of higher pressure.

FIG. 2.18. Single Frame of Motion Picture of Pure AP Burning in Methane Atmosphere st 65 psia. Crystal approximately 0.5 cm wide.

The K^+-doped AP, as observed in the movies, behaved eaaentially like pure AP when burning in methane except that the tendency for surface boiling waa more pronounced and eaaily observed.

In low pressure (15 to 50 paia) methaoe the MnO_4^--doped crystals were observed to burn with a white porous material covering the regressing surface. Figure 2.19 is a SEM photograph of the aurface of a MnO_4^--doped cryatal quenched at low preaaure. This atructure is very aimilar to the water vapor "rejuvinated" low temperature decompoaition reaidue shown in Fig. 2.20. At higher preasure (200 psia) the poroua material sppeared to undergo a cyclic accumulation-rapid consumption process which gave a strsnge pulsating character to the deflagration process.

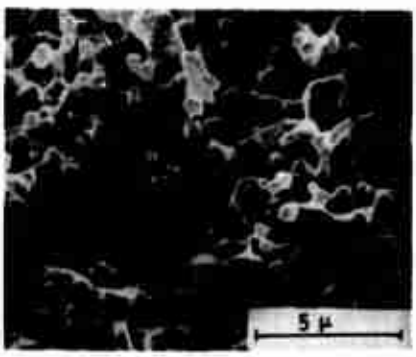

FIG. 2.19. Scanning Electron Microscope Photomicrograph of the Burned Surface of MnO_4^--Doped AP Quenched from Combustion in 15 psia Methane.

FIG. 2.20. Scanning Electron Microscope Photomicrograph of the Reaidue of Partially Decompoaed Pure AP (st 220°C) Which has Been Rejuvinated by Exposure to Water Vapor.

Low speed motion pictures (24 to 100 fps) were taken utilizing the self-illumination of the AP decomposition flame. At atmospheric pressure in methane a pink-orange flame approximately 175 microns thick was observed (by visual observation the flame color was the same as was observed with single crystals burning in nitrogen at elevated pressure). The decomposition flame appeared to commence right at the condensed phase surface.

In addition to the samples burned in methane, several pure AP crystals were burned in an atmosphere of ammonia at atmospheric pressure. The combustion behavior was essentially the same as in methane atmospheres. It was not possible to burn samples at elevated pressure in ammonia since the crystals rapidly dissolved in the ammonia.

2.3.2. Deflagration at High Pressure

Additional measurements were made of the deflagration rates for single crystals. The rates were measured from high speed motion pictures of the combustion and are shown in Fig. 2.21. The previously reported AP burning rate data (Ref. 6) were repeated and verified with larger cross-section (0.5 cm on a side) crystals.

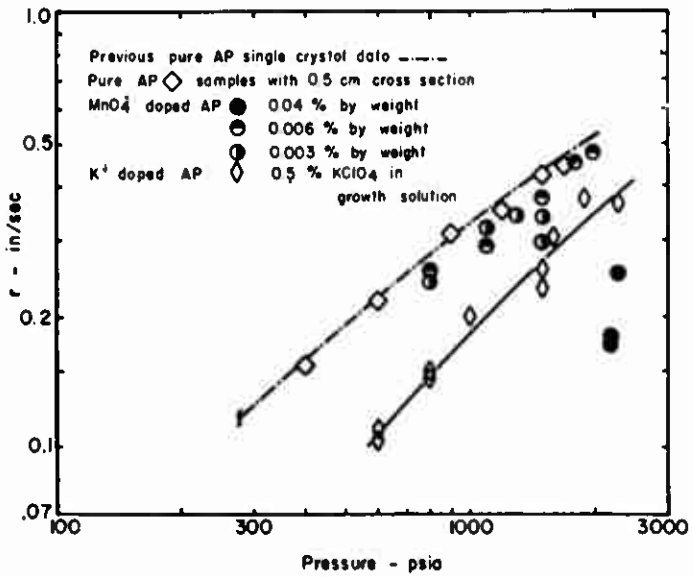

FIG. 2.21. Deflagration Rate of Pure and Doped AP Single Crystals.

The burning rates for the single AP crystals doped with K^+ and three concentrations of MnO_4^- exhibited one consistent feature even though there was inconsistency in some of the rate-concentration dats; that festure was thst the burning rates for the doped crystals were always below the pure AP rate over the pressure range tested. In addition, the K^+-doped AP had a pressure exponent of spproximately 1.0 as compared to approximately 0.77 for pure AP. Motion pictures of this material undergoing deflagration showed definite melting snd boiling on the surfsce with occssional ejection of molten materisl (presumed KCl) from the surfsce.

In the case of the MnO_4^--doped crystals, the burning rate data at the lowest concentrstions was too scattered to warrant drawing conclusions concerning rate-concentration trends. In addition, it was difficult to precisely measure the MnO_4^- concentration. The highest (0.04%) concentration MnO_4^--doped AP which would undergo self-deflsgration displayed a much lower burning rste so it is presumed thst increasing MnO_4^- concentration results in lowering the single crystal deflagrstion rste. Light transmission through the gaseous combustion products was observed to be much higher for the MnO_4^--doped AP than for the pure AP. Figure 2.22 shows a comparison of doped versus pure AP photographed under the same test conditions with transmitted illumination by polarized light.

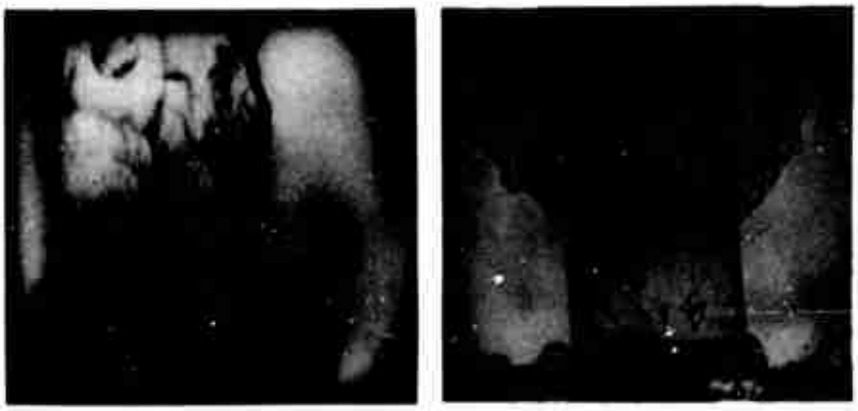

(a) (b)

FIG. 2.22. Single Frame of Motion Picture of (a) Pure AP and (b) AP Doped With 0.006% MnO_4^-. Both samples deflagrating st 800 psia, photographed with transmitted, polarized illuminstion. Note difference in optical density of combustion products.

The low pressure deflagration limit for all of the doped crystals was much higher than that of the pure material (275 psia, Ref. 6) with MnO_4^- being apparently more effective in raising the limit than K^+. Friedman, et al (Ref. 9), also observed that $NaMnO_4 \cdot 3H_2O$) and MnO_2 raised the deflagration limit of pressed AP pellets. The low pressure deflagration limits in the present work were found to be approximately 600 psia for the 0.5% $KClO_4$-doped AP and 800 psia for the 0.003 to 0.006% MnO_4^--doped AP. The AP doped with 0.04% MnO_4^- could not be made to deflagrate below about 2000 psia.

2.3.3. Interpretation and Discussion

The work here and in Ref. 1 has revealed several qualitative aspects of combustion that were previously unknown, or were matters of speculation. The most important aspect is the decisive evidence for a frothy liquid on the surface of the burning AP. The exact chemical nature of the liquid is not known, although x-ray diffraction tests on residues indicate only AP. It is not surprising that a liquid layer should be present at the high surface heating rates associated with self-deflagration of crystalline AP. The temperature gradient resulting from this heat flux is of such magnitude that it could raise the temperature of the subsurface AP to its melting point in less time than it would take to gasify the material. Thus, a melting point would be encountered which would not be observed at lower heating rates, i.e., such as associated with differential thermal analysis, where the sample would gasify before the melting point was reached.

The results suggest that the melt plays an important role in self-deflagration of the AP. There has been continuing difficulty in reconciling the amount of heat required for the initial decomposition of AP with the amount of heat that could be supplied by the AP flame, because the heat balance dictates a flame standing only a few mean free paths from the surface (assuming a one-dimensional regressing surface). On the other hand, a frothy melt on the surface provides opportunity for both heterogeneous and gas phase reactions in the froth, with a very large area for heat transfer. Thus, it seems plausible to assume that the liquid froth is an essential feature of the self-deflagration of AP, and that the low pressure deflagration limit corresponds to attainment of heating rates so low that surface material gasifies without reaching a melting temperature. Under these conditions, a major portion of the exothermic reactions would occur only in the gas phase flame, which apparently does not have any equilibrium position satisfying heat balance requirements.

Microscopic examination of quenched samples indicate no optically detectable changes in the AP below the melt region other than the phase transition region. This implies that there is probably no significant contribution to the heat release during deflagration by solid phase reactions. This is not really surprising because the decomposition reactions of solids include an induction period followed by a growth and

decay period. The induction period may be long or at least comparable to the time it takes for the very thin thermal wave associated with combustion to traverse a given layer of material. Ammonium perchlorate does decompose in a combustion wave, and on a molecular scale the actual decomposition mechanism may be the same as for the "low temperature" thermal decomposition, e.g., a proton transfer. The kinetics of the overall process are expected to be different if they occur in s melt as opposed to a crystalline solid.

It aeems reasonable to asaume then, that slteration of the thermal stability of the surface melt or auppresaing its formation would produce a corresponding change in the deflagration behavior of AP. Earlier work (Ref. 9) showed that a rapidly heated mixture of granular AP and lithium fluoride produced a residue mixture of AP-lithium perchlorate. Markowitz and Harris (Ref. 10) have shown that the decomposition rste of AP in solution with lithium perchlorate is lower than that of pure AP at corresponding temperatures. It is possible that a similar process may occur on the surface of deflagrating crystals doped with the K^+ ion resulting in the formation of an AP-potaasium perchlorate solution. There is also an accumulation of liquid balls (probably KCl, a stable product of KCl4 decomposition) on the burning surface of K^+ doped crystals which may affect the deflagration rate. In the case of MnO_4^--doped crystala both the deflagration limit and the burning rate were influenced tremendously by small concentrations of this ion. The preasure deflagration limit is increased accordingly along with a reduced burning rate.

2.4. SUMMARY

The present work (including Ref. 1) has revealed rather decisively that the physical character of the surface residue of AP is significantly dependent on the imposed heating rate. Under conditions of iaothermal decomposition the AP apparently sublimes and there is no evidence of a surface melt. Under conditions of rapid heating, a surface melt is observed and in the case of self-deflagration the surface melt is frothy and may contribute significantly to the heat release necessary to sustain deflagration. Also, the substitution of foreign iona in the AP crystal structure in amall qusntities reduced the activation energy of the isothermal decomposition snd also altered the combustion behavior of the crystal either by altering the thermal stability of the aurface melt and/or the gas phase kinetics.

3. BEHAVIOR OF ALUMINUM IN COMPOSITE PROPELLANTS

Certain aspects of aluminum agglomeration in the combustion zone of composite propellants were described in detail in the previous progress report (Ref. 1). During this reporting period, emphasis has been placed on investigating the mechanism of agglomeration. In particular, the photographic technique has been improved to increase the resolution of the high speed motion pictures, and quenched propellant samples have been examined in detail with a scanning electron microscope (SEM) to investigate the early (preignition) phases of aluminum agglomeration.

3.1. EXPERIMENTAL TECHNIQUE DEVELOPMENTS

3.1.1. Cinephotomicrography Improvements

The basic arrangement for high speed motion picture photography with magnification has been described in Ref. 1. However, improvements have been made in each of the three major components of the experimental setup.

The improved arrangement is shown in Fig. 3.1. The original Fastax camera was replaced by a Hycam 16 mm high speed motion picture camera, Model K3004E. This camera provides more uniform exposure over the entire film frame, more versatility in speed selection and, due to its internal optics, provides a somewhat larger magnification than the Fastax. The original xenon arc external illumination arrangement was replaced with a Strong X-16 xenon arc assembly which includes a 2,500 watt xenon arc lamp, dichroic main mirror and external focusing controls. This assembly permits better control of external illumination and can supply considerably more intensity, if desired, than the previous arrangement. The greatest improvement has been made in the window bomb itself. The new bomb provides complete flushing of the interior without recirculation, permits more versatility in the mounting of propellant samples (Fig. 3.2), and provides better mechanical support for the fused quartz windows.

Figure 3.3 illustrates the details of combustion that can now be resolved with the improvements in the experimental arrangement. In the first picture, an accumulation of several hundred 15μ aluminum particles have melted together to form a sphere of molten aluminum, as indicated by the highlight on the sphere. Some unmelted material, including several original aluminum particles, is visible on the left side of the agglomerate. In the second picture (one millisecond later) most of the remaining material on the agglomerate has melted except for the crusty,

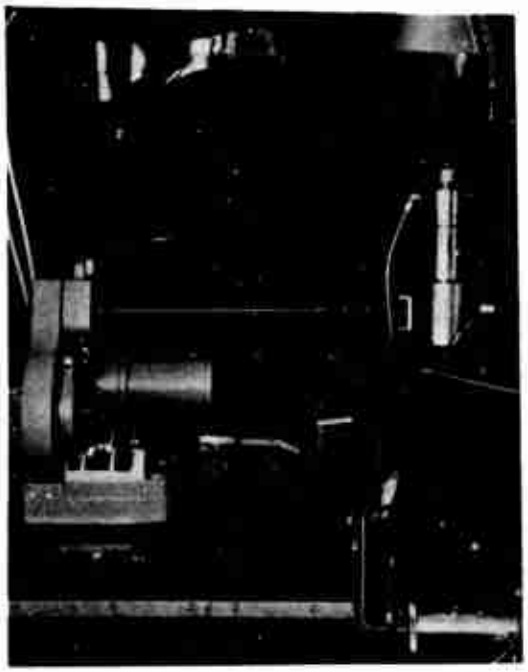

FIG. 3.1. Photographic Arrangement.

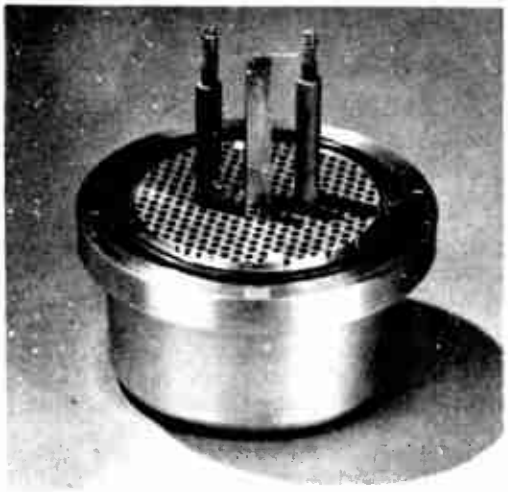

FIG. 3.2. Propellan. Sample Holder.

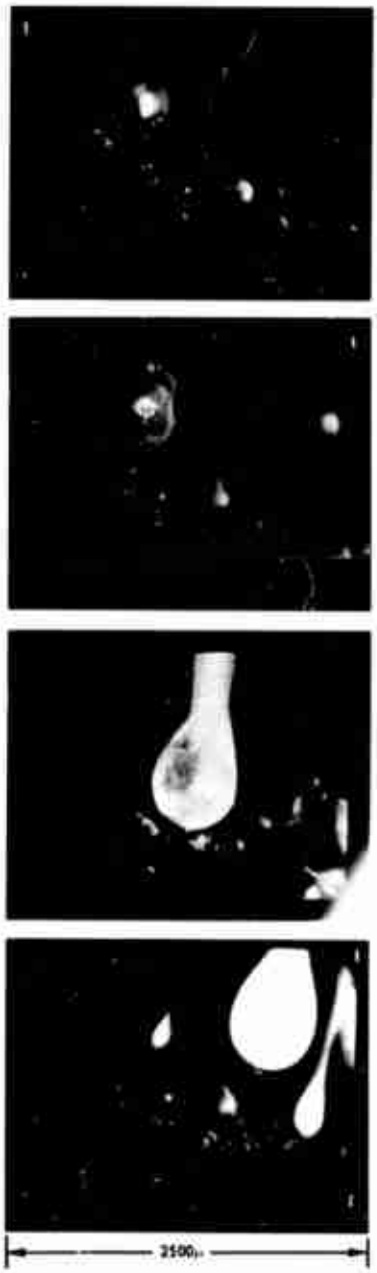

FIG. 3.3 Selected frames from high speed motion picture of composite propellant containing 18% aluminum burning at 100 psi.

irregular appearing aluminum oxide surface. The aluminum oxide "smoke" indicates the developing reaction region of the aluminum combustion. At five milliseconds the droplet shows a well-developed combustion envelope which flows outward with the propellant combustion products. In the final picture the spherical droplet appears to be burning vigorously and highlights from the liquid surface are visible through the combustion envelope. The disc centered on the sphere in this picture is a luminous cap which probably contains most of the preignition oxide of the original aluminum particles. Such oxide caps are readily discernible in the photographs in Ref. 1 (Fig. 3.3). The final picture also shows the heterogeneity of the propellant surface underneath the aluminum agglomerate. The motion pictures show this area to be almost entirely "uncluttered" with pyrolysis residue. Assuming that the residue is a thermal insulator, energy from the gas phase could be more easily transferred to this "clean" spot and could result in a momentary increase in energy release in that localized area. This possibility along with the energy release following ignition of the aluminum agglomerate quite conceivably could play an important role in driving gas oscillations.

3.1.2. Propellant Quench Technique

Quenching propellants by rapid depressurization of the window bomb was performed earlier in this program (Ref. 11). High speed motion pictures taken during the quench indicated that the majority of aluminum in the later stage of agglomeration was removed from the surface during the rapid depressurization. In order to preserve the large accumulates during quench for later microscopic study, a new quench technique was employed. A freshly cut piece of propellant (approximately a 1/4 in. cube but with the top surface cut at a 30° angle to the horizontal) was placed on a clean metal plate and ignited by a hot Michrome wire in the pressurized bomb. As the burning surface approached the metal plate, the combustion was thermally quenched. A small portion of unburned propellant as well as aluminum particles in various stages of agglomeration remained on the plate. Plates of copper, aluminum, and stainless steel were evaluated as heat sinks; the stainless steel plates were most satisfactory in that a larger portion of unburned propellant remained after quench. Some residuums have been examined with a scanning electron microscope (SEM) and the results are discussed in later sections.

3.2. DETAILED ASPECTS OF ALUMINUM AGGLOMERATION

The preignition behavior of the aluminum in composite propellants has received increased attention during this reporting period and the more important processes are reasonably well understood. An exploratory experiment which yielded the greatest insight into the agglomeration mechanism was performed by dropping 100μ spherical aluminum particles (in air) onto a sapphire disk heated by a torch to approximately 1,400°C (Ref. 12) and subsequently examining the particles using a scanning electron microscope (SEM). A series of resulting SEM photographs with

increasing magnification are shown in Fig. 3.4. The important feature shown in Fig. 3.4a is that two aluminum particles are rigidly connected by a "bridge" of material. This interaction of the particles occurred at an environmental temperature (< 1,400°C) well below the melting point of aluminum oxide (2,050°C), even though the original aluminum particles had an oxide coating. Examination at higher magnifications shows numerous ridges approximately 1/2μ in width which resemble welding joints. These observations on the microscopic scale probably explain the details of aluminum agglomeration in propellants and are interpreted in the following manner. As the aluminum particles are heated (in this experiment by conduction from the 1,400°C sapphire disk), the stresses produced by the differential thermal expansion of the aluminum and aluminum oxide caused the aluminum oxide covering to fracture. The particles in Fig. 3.4 were evidently heated to above the melting point of aluminum and hence, liquid aluminum started to flow through the cracks. The aluminum was rapidly oxidized, thus producing the "weld joint" appearance. The heat liberated by the aluminum oxidation conceivably could produce additional stresses and cracking if radiative heat losses, for instance, were not too great. As in Fig. 3.4, where the particles are in contact, a "bridge" can be formed by the cracking of oxide and flow of molten aluminum. In Fig. 3.4d it appears that additional "thermal cracking" occurred after the bridge was formed. This is indicated by the two ridges that run across the bridge.

It is felt that this phenomens is the first step in the agglomeration (or sintering together) process. Combustion residues obtained from thermal quenching (Section 3.1.2) were examined with the SEM for evidence of the "bridging" phenomena. Figure 3.5a is a series of SEM photographs of an agglomerate from a composite propellant containing 16% of 15μ diameter aluminum. The successively larger magnifications show the pattern of the aluminum flowing to form a large agglomerate. For comparison, Fig. 3.5b shows an analogous situation of agglomerate formation with 100μ aluminum particles rapidly heated to 1,400°C on a sapphire disk in atmospheric air. The details of oxide cracking and healing are not at all evident in the agglomerate from the propellant. This agglomerate was formed in a more complicated environment and undoubtedly there are numerous pyrolysis and oxidation products present which could greatly modify the appearance of the agglomerate. However, efforts are continuing to conclusively demonstrate this "bridging" phenomena because of the importance of relating the metal particle behavior with behavior in propellants.

3.3. INTERPRETATION AND SUMMARY

A detailed, qualitative description of the behavior of aluminum in composite propellants can now be made based on (1) high speed motion pictures of aluminized propellants, especially the observations of a liquid phase on the propellant surface for the early stages of accumulation, (2) on interpretation of and deductions from the observations of

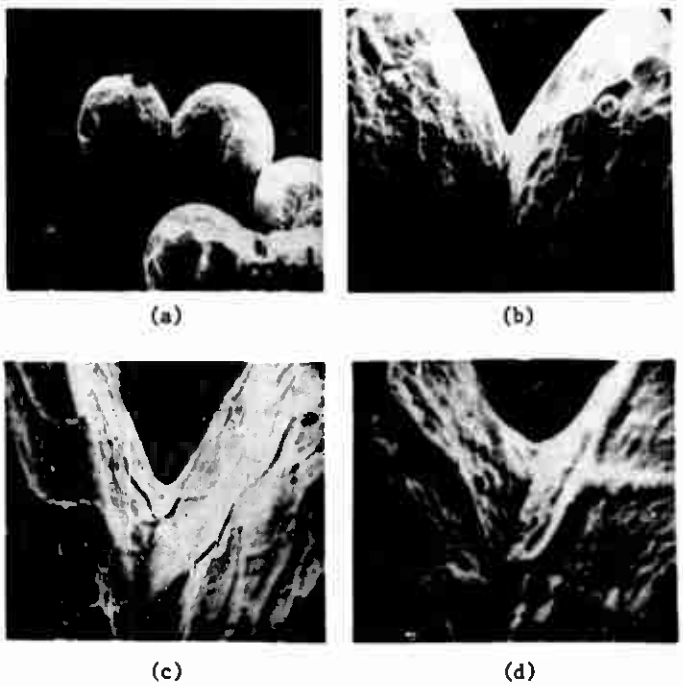

FIG. 3.4. SEM Photographa of "Bridgea" Joining 100μ Aluminum Particles. Aluminum particles were dropped onto sapphire plate heated to 1,400°C in air.

the behavior of rapidly heated single particles in Section 3.2 and similar, though less conclusive, studies of residual accumulates from propellant quench tests, and (3) on high speed motion pictures (Section 3.1.1 and Ref. 1 and 13) of burning propellants as exemplified by the four frames shown in Fig. 3.3.

The sequence of events in the agglomeration of aluminum is believed to be as follows. The original aluminum particles with thin oxide coatings are distributed in the binder of the propellant. As the combustion front movea through the propellant, the temperature of the aluminum particlea begina to riae as the thermal wave proceeds. As the binder and the ammonium perchlorate pyrolize, the aluminum recedea with the aurface until it comes into contact with other aluminum particles. The decomposing surface of the propellant ia liquid and thus the individual aluminum particlea are readily retained on the surface. Aa the aluminum particles accumulate in the melt, they are heated by conduction to at least the local surface temperature (typically on the order of 400°C-700°C) and probably reach a somewhat higher temperature due to oxidative

(a)

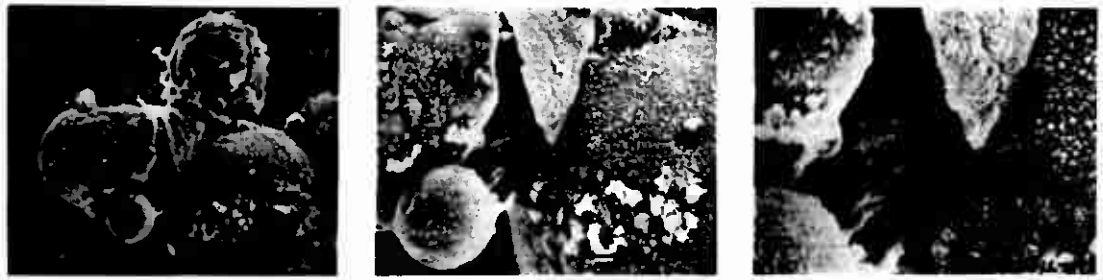

(b)

FIG. 3.5. SEM Photographs of Aluminum Agglomeration. (a) Particles dropped onto 1,400°C plate, (b) Quenched particles from composite propellant.

self-heating. In this situation with the aluminum particles in contact with one another and with the aluminum at a temperature above its melting point, the adjacent particles interact as described in Section 3.2. The molten aluminum flows through the thermal expansion cracks in the aluminum oxide ahell and is probably quickly oxidized. When cracks roughly coincide with the contact pointa with adjacent particles, the flowing aluminum can "wet" the adjacent particle. Thua, the aluminum particles are joined together at their contact points by aluminum and aluminum oxide "bridges". The agglomerate as s whole can be described as numerous drops of liquid sluminum encspsulated in aluminum oxide shells. These drops and ahella are linked together by oxide "bridgea". Figure 3.4 representa thia type of structure. As the binder and AP recede beyond thia region of the sluminum agglomerste, the aluminum-aluminum oxide atructure haa enough atrength to physically withatand the flow of binder and oxidizer gases away from the aurface and, nence, remains on the surface until it ignites or is completely undermineò and drifts away with the flow of gsa from the aurface.

In the case where the sgglomerate is not undermined and removed, oxidative self-heating, oxide cracking and aluminum flow continues until the molten aluminum from one ahell joins with aluminum from another and a large molten ball of aluminum has formed. The latter stage of the formation of a large molten ball of aluminum is shown in the "t" portion of Fig. 3.3. The next picture (t + 1 msec) ahows the ball increasing in aize to engulf the entire agglomerate contained in that particular binder "pocket". These two picturea alao show that the aluminum oxide on the large molten ball ia irregular in ahape indicating that the oxide has not yet melted. In the t + 5 msec picture the oxide has melted (no aharp irregularities) and vigorous combustion of the aluminum has begun as indicated by the pronounced aluminum oxide smoke that has developed. The molten aluminum oxide cap characteristic of burning aluminum droplets ia distinguishable in the t + 8 msec picture.

Future effort in thia area will be directed at obtaining even more conclusive evidence on the aluminum sintering proceaa and the tranaition to a large molten ball in experimenta closely simulating the propellant combustion situation.

4. NONACOUSTIC INSTABILITY

4.1. INTRODUCTION

A general review of the statua of nonacoustic combustion inatability (NAI) in aolid propellants was presented in the previous report (Ref. 1). The principal effort during this reporting period has been (1) to compare nonacoustic experimental results with one-dimensional theories and (2) to examine the effect of oxidizer particle size on NAI.

In the past, theoretical models describing the interaction of the pressure perturbations with the combustion zone have mainly been applied to acoustic inatability (for example, Ref. 14-17). However, the combustion inatability models that describe the dynamics of the combustion zone and are applicable in the low frequency rcgime should apply to nonacoustic as well as acoustic instability. Several recent papers (Ref. 18-20) have discussed NAI in terms of the response function normally associated with acoustic instability which evolved from the above models. In the previous report (Ref. 1) the analysis relating to the combustor was separated from the analysis of the combustion so that theoretical combustion modela could be combined with the combustor analysis quite readily. A method was also presented for reducing NAI data (obtained from L* burners) in terms of the response function and the phase of the combustion. In the present report, some of the same NAI data are compared with response function curves calculated from models which are directly applicable to the low frequency regime but which have normally been applied to acoustic instability. For this purpose the model of Denison and Baum (Ref. 16) and a recent model proposed by Hart, Farrell and Cantrell (Ref. 17) have been chosen as being representative and have been utilized to compare the relative applicability of these types of models.

Experimental experience plus the understanding obtained from studies such as outlined above have advanced the level of understanding of NAI so that predictions can be made as to the general behavior of a given propellant. However, there are many instances where the behavior has been different than expected. For example, the one-dimensional models predict that for a given propellant and a given set of conditions, pressure oscillations should occur at one particular frequency. However, two previous instances are known (Ref. 1 and 21) where propellants have oscillated at two different frequencies, under essentially the same conditions, and in each case one of the frequencies was much different than expected. A close scrutiny of the propellant characteristics and the conditions

under which the anomalies occurred has led to the belief that the oxidizer particle size was a major factor producing the unexpected frequency. This provided the motivation which led to the atudy which ia outlined in Section 4.5.

4.2. NONACOUSTIC COMBUSTOR ANALYSIS

In NAI it sppesrs thst the combustion couplea with the flow out of the rocket chamber in order to induce and sustain instsbility. Thua, the maas balsnce for a rocket motor contsining burning propellant snd exhauating through a sonic nozzle can be written

$$\rho r\, A_b - \frac{pA_t}{c^*} = \frac{d}{dt}\ (\rho_g\, V_c) \tag{4.1}$$

where c* ia the charscteristic velocity for the products of combuation. Assuming ideal gaa conditions, a thin combustion zone, s spacewise isothermsl gas, and the density of the propellant to be much greater than that of the gas, Eq. 4.1 can be written (For a more complete derivation of Eq. 4.1 and 4.2, aee Ref. 18 and 22)

$$\frac{r}{\bar{r}} - \frac{p}{\bar{p}} = \tau_{ch}\ \frac{d(p/\bar{p})}{dt} \tag{4.2}$$

Applying standsrd perturbstion techniques snd conaidering an exponentially growing, sinusoidal perturbation such as

$$r = \bar{r}\left(1 + \left(\frac{r'}{\bar{r}}\right)\ e^{i(\omega - i\alpha)t}\right) \tag{4.3}$$

Equation 4.2 reduces to

$$\frac{r'/\bar{r}}{p'/\bar{p}} = 1 + \alpha\tau_{ch} + i\ \omega\tau_{ch} \tag{4.4}$$

where α is a growth coefficient and τ_{ch} representa the residence time of the chamber and is directly proportional to L*. The left hand side of Eq. 4.4 is the response of the mass flow rate in the combustor to the pressure of the combustor and is equal both in magnitude and phase to a similarly defined response of the combustion. All of the terms on the right hand aide of Eq. 4.4 are quantities that can be determined experiemntslly in an L*-type of burner. Thua, the nonacoustic response of the combustor can be determined experimentally snd compared with the

response of the combustion as determined from models such as those of Denison and Baum and Hart, Farrell and Cantrell.

Figure 4.1 is a schematic of an L* burner (Ref. 18, 21, and 22) from which nonacoustic instability data can be obtained. Data have been obtained for two propellants and reduced to the format suggested by Eq. 4.4 in order to make a comparison with one-dimensional models. Both are composite propellants but vary widely in compositions and properties. A-35 is a polyurethane-AP propellant, containing 75% AP, while Utah-TF is a PBAA-AP-Al propellant containing 5% Al, 18% PBAA, 2% copper chromite burning rate catalyst and the remainder AP (see Ref. 1 and 21).

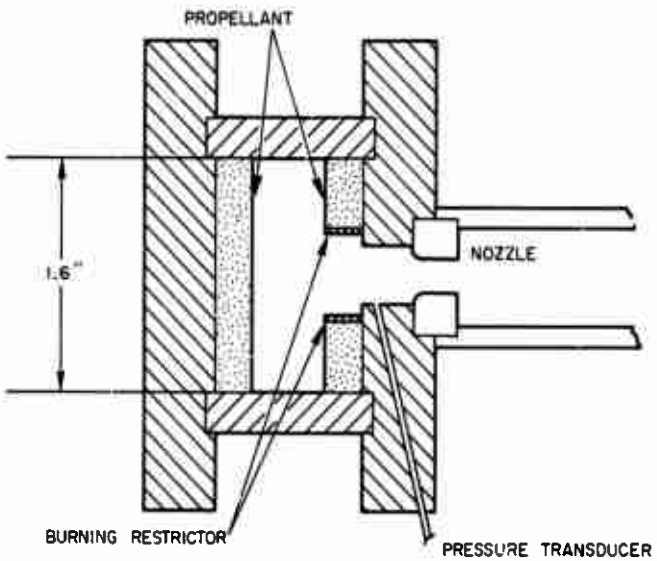

FIG. 4.1. The L* Burner.

4.3. COMBUSTION DYNAMICS MODELS

The model of Denison and Baum (denoted DB) was chosen to provide a basis of comparison for several reasons. First of all it applies specifically to the low frequency range that is of interest in NAI. Secondly, as has been pointed out by Culick (see Appendix A of Ref. 1), the form of the derived response function is extremely simple, containing only two parameters (A and B_{DB}) and the independent variable Ω. Culick has also shown that virtually all of the one-dimensional models reduce to the same function as the DB model. The model of Hart, Farrell, and Cantrell (denoted HFC) was also chosen because it too is directly applicable to

the low frequencies of interest in the present study, and because it contains the effects of a pressure dependent surfsce reaction.

4.3.1. Comparing the Models

The assumptions involved in both of the analyses are very similar. Both assume a homogeneous, one-dimensional solid, quasi-steady gas phase, and are applicable in the same low frequency range. The principsl difference in the models (other thsn the actual method of analysis) is that Denison and Baum arrive at a burning rate lsw by starting with the conservation equstions and reducing the complexity of these equations with several assumptions. In so doing, the effects of diffusion in the gas phase sre included (however, the Lewis number is sssumed to be unity). In the original Hart-McClure model (Ref. 14), snd in the HFC model, the burning rate is assumed to be a function only of the pressure and the temperature gradient in the gas phase and the latter is then related to the initial temperature of the propellant. By so doing, diffusion in the gss phase is circumvented. The HFC model also takes into account the effects of a surfsce reaction between a gas phase component and the solid surface. However, the resultant response function can easily be reduced to what will be referred to here as the thermal case (essentially the results derived by Bird, et al (Ref. 15) snd in the same form as the Denisor-Baum results), or in other words, the snalysis without the pressure dependent surface resction. Throughout the remainder of this section the HFC model will be considered as containing two separate cases, one with and one without the surface reaction.

If the response functions of both models (initially considering the thermal csse for the HFC model) sre reduced to a common set of nomenclature and put in the form suggested by Culick (see Appendix A of Ref. 1), it is found that there is very little difference. The DB response function is

$$\frac{1}{n}\,\frac{r'/\bar{r}}{p'/\bar{p}} = \frac{AB_{DB}}{AB_{DB} + \frac{A}{\lambda} + \lambda - (A + 1)} \tag{4.5}$$

and the HFC response function is

$$\frac{1}{n}\,\frac{r'/\bar{r}}{p'/\bar{p}} = \frac{A'B_{HFC} + \frac{\lambda-1}{n}}{A'B_{hfc} + \frac{A'}{\lambda} + \lambda - (A' + 1)} \tag{4.6}$$

where λ is the characteristic root of the energy equation for the solid and is equal to

$$\lambda = 1/2\ [1 + (1 + 4i)^{1/2}] \tag{4.7}$$

It is apparent that the two response functions are essentially the same except for a term in the numerator. This term results from the fact that the HFC model includes pressure dependent surface reactions. If the thermal case of the HFC model is considered (i.e., neglecting the surfsce reaction) the response function reduces to

$$\frac{1}{n}\ \frac{r'/\bar{r}}{p'/\bar{p}} = \frac{AB_{HFC}}{AB_{HFC} + \frac{A}{\lambda} + \lambda - (A + 1)} \tag{4.8}$$

Equations 4.5 and 4.8 are identical, differing only in the definition of B. For the two models the definition of this parameter is

$$B_{DB} \equiv \frac{C_p\ T_f}{C_s\left(\bar{T}_s - T_o\right)\ \left(n + 1 + \frac{E_f}{2RT_f}\right)} \tag{4.9}$$

and

$$B_{HFC} \equiv \frac{T_o}{j\left(\bar{T}_s - T_o\right)} \tag{4.10}$$

The differences in the two definitions can readily be traced to the basic difference in the two models involving the form of the burning rate law. In the DB model (as has been mentioned) a burning rate law is derived from the energy and species conservation laws which relate the burning rate to the pressure and the flame parameters. In perturbation form the term

$$\frac{n + 1 + E_f/2RT_f}{T_f}$$

is introduced. It has also been pointed out that in the HFC model the burning rate is assumed to be a function of the pressure and the temperature gradient in the gas phase. The burning rate is then written as a perfect differential in terms of the appropriate pressure and gradient terms. The latter is then related to the initial temperature of the propellant which results in the factor j/T_o

$$(\text{where } j \equiv \frac{T_o}{\bar{r}} \frac{\partial \bar{r}}{\partial T_o}).$$

Thus, the only real difference in the two models being compared (considering the HFC thermal case only) is in the burning rate law that is employed, and for the sake of numerical calculations, the models are identical. The only difference lies in relating the original parameters from the respective models to the value of B.

4.3.2. Comparing Calculated Response Functions and Data

The purpose of this section is to compare the predictions of the chosen instability models with the results obtained from actual NAI data. In order to evaluate Eq. 4.5, 4.6, and 4.8, values for A and B must be obtained. Values of the individual parameters have been measured or obtained from the literature wherever possible, and most probable ranges of values have been obtained where a precise value is not available. These are tabulated in Table 4.1, with literature references given, where available. The corresponding parameter values are also tabulated in Table 4.1 where possible.

TABLE 4.1. Values of Parameters for Numerical Calculation

	Representative values	Values used in calculations	Corresponding parameter values
T_o	300°K	300°K	. . . .
n	0.46[a] and 0.49[b]	0.50	. . . .
T_a	750 to 1,000°K[23,24][c]	900°K	. . . .
E_a	22[25] and 30[26] Kcal	22, 30 Kcal	A = 8, 11
j	0.6 to 0.7[27,28]	0.65	B_{HFC} = 0.77
T_f	2160[d] and 2860°K[e]	2160, 2860°K	See Fig. 4.2
E_f	10 to 50 Kcal	10, 30, 50 Kcal	See Fig. 4.2

[a] Measured for A-35 propellant.
[b] Measured for UTAH-TF propellant (See Ref. 22).
[c] Superscripts refer to references.
[d] Calculated adiabatic flame temperature for A-35 propellant.
[e] Calculated adiabatic flame temperature for UTAH-TF propellant.

Figures 4.2, 4.3, and 4.4 show how the nondimensional parameters A and B vary as functions of the physical parameters. In determining B_{DB} it was assumed that the specific heat of the gas phase is equal to that of the solid, and that the mean flame temperature, the mean surface temperature and the burning rate exponent, n, are all constant. Substituting the values of Table 4.1 into Eq. 4.9, the range of B_{DB} is from 0.55 to 2.0 for the two propellants. This range of values reflects the uncertainty in the value of the activation energy of the flame which is the parameter having the greatest uncertainty. This is graphically demonstrated in Fig. 4.2.

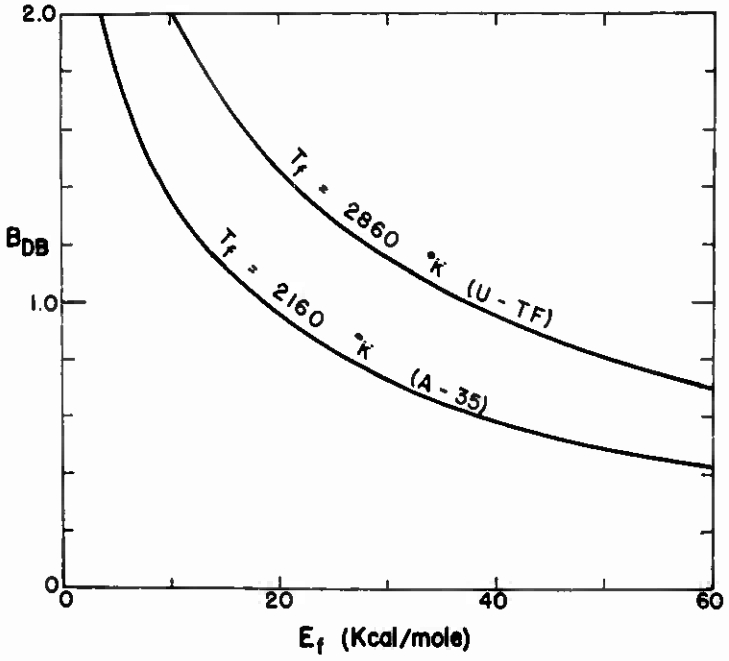

FIG. 4.2. The Denison and Baum Gas Phase Parameter B as a Function of E_f With the Flame Temperature as a Parameter.

From Fig. 4.3, it is seen that the parameter B_{HFC} does not vary greatly but is close to 0.8 for reasonable values of the parameters. The values of the parameters in Table 4.1 result in B_{HFC} = 0.77 which was subsequently used in all the calculations for that model. In Fig. 4.4 A would appear to have a value on the order of 10. Combining the

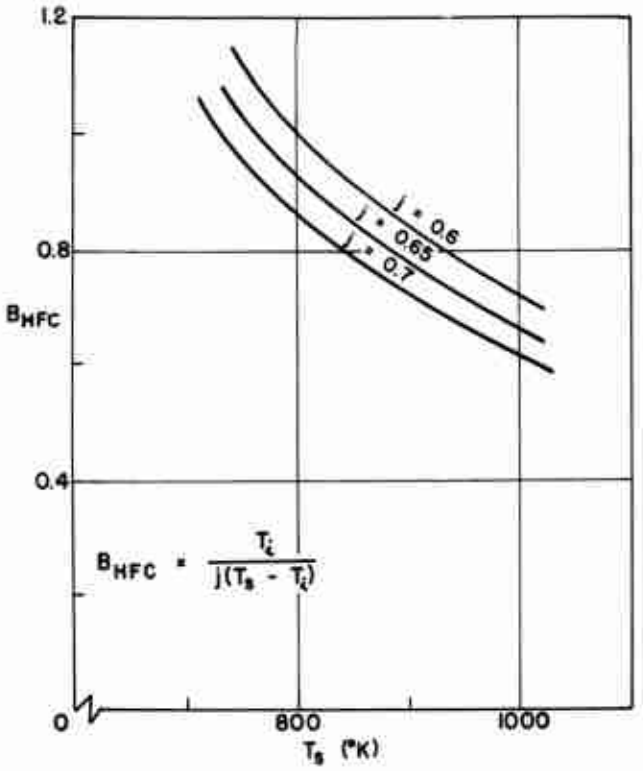

FIG. 4.3. The Hart, Farrell, Cantrell Parameter B as a Function of T_s With the Temperature Sensitivity j aa a Parameter.

values of the various parameters given in Table 4.1 results in valuea of approximately 8 and 11 for the nondimensional parameter A, and these values (for a constant aurface temperature of 900°K) have been used in the calculations for both models.

Using the values of the various parametera aa noted above, the real part and the phase of the response function have been calculated from Eq. 4.5, 4.6, and 4.8 and are compared with the data for one of the particular propellants in each of the following figures. Thus, Fig. 4.5 and 4.6 contain the data of A-35 propellant (Ref. 1) and the curvea calculated from the models using the parameters that are indicated in the

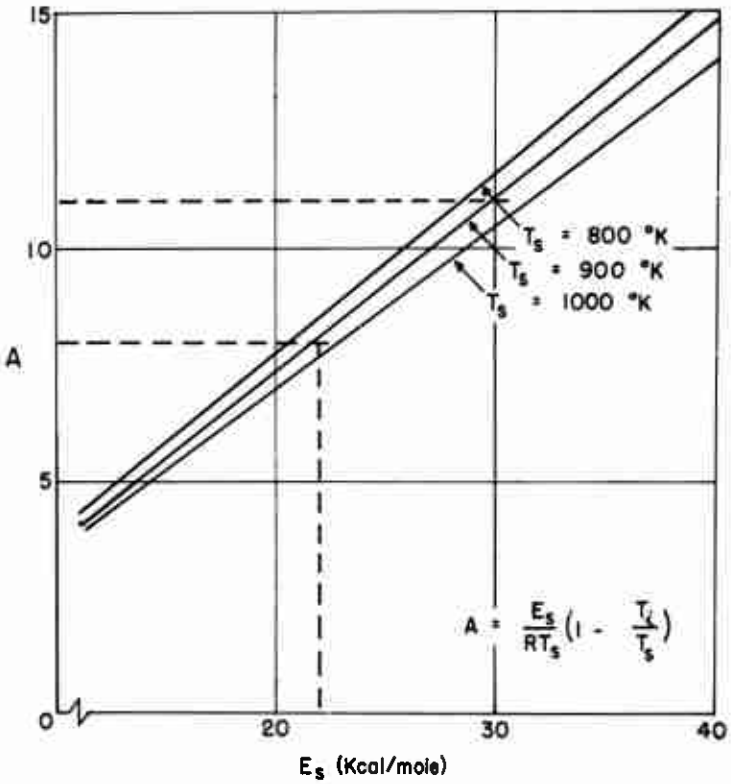

FIG. 4.4. The Solid Phase Parameter A Plotted Versus E_s With the Surface Temperature as a Parameter.

figures. It should be noted here that even though the scatter in the data is considerable, the fact that a comparison can actually be made between data of this nature and the theoretical models is considered significant. In comparing the two different cases for the HFC model, it is apparent that the addition of a pressure-dependent surface reaction greatly enhances the predicted response of the propellant.

Of the calculations for the DB model, only the curve corresponding to the flame-activation energy of 30 Kcal/mole is included in the two plots. The curves for E_f = 10 Kcal/mole resulted in responses that were entirely too low to predict instability, while the curves for E_f = 50 predicted exponential instability (nonsinusoidal instability; see the discussion in Ref. 16 on this subject). Therefore, these curves were not included in Fig. 4.5 and 4.6. Although each of the curves is quite

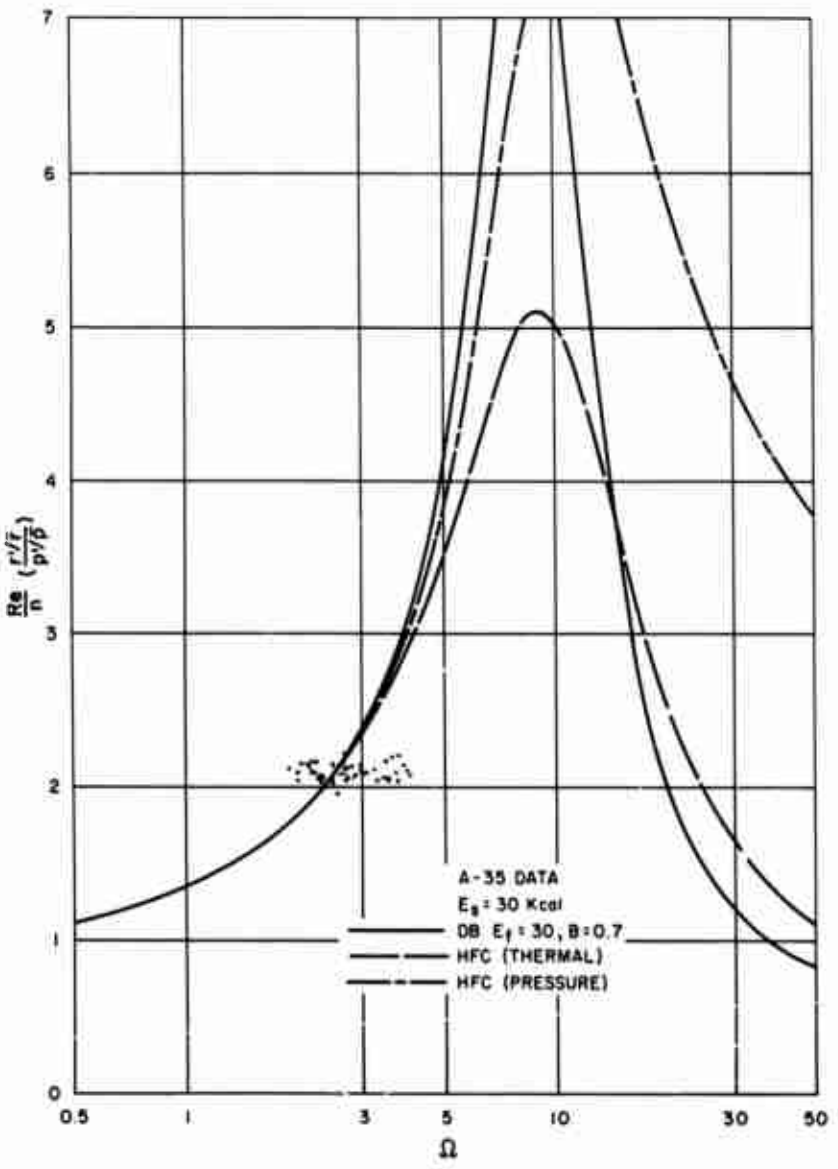

FIG. 4.5. Reaponae Functiona aa a Function of the Nondimenaional Frequency. Ω, and for the Given Parametera Compared With A-35 Data. HFC (thermal) refera to the HFC model, thermal caae. HFC (preasure) refers to the HFC model including the presaure dependent aurface reaction term.

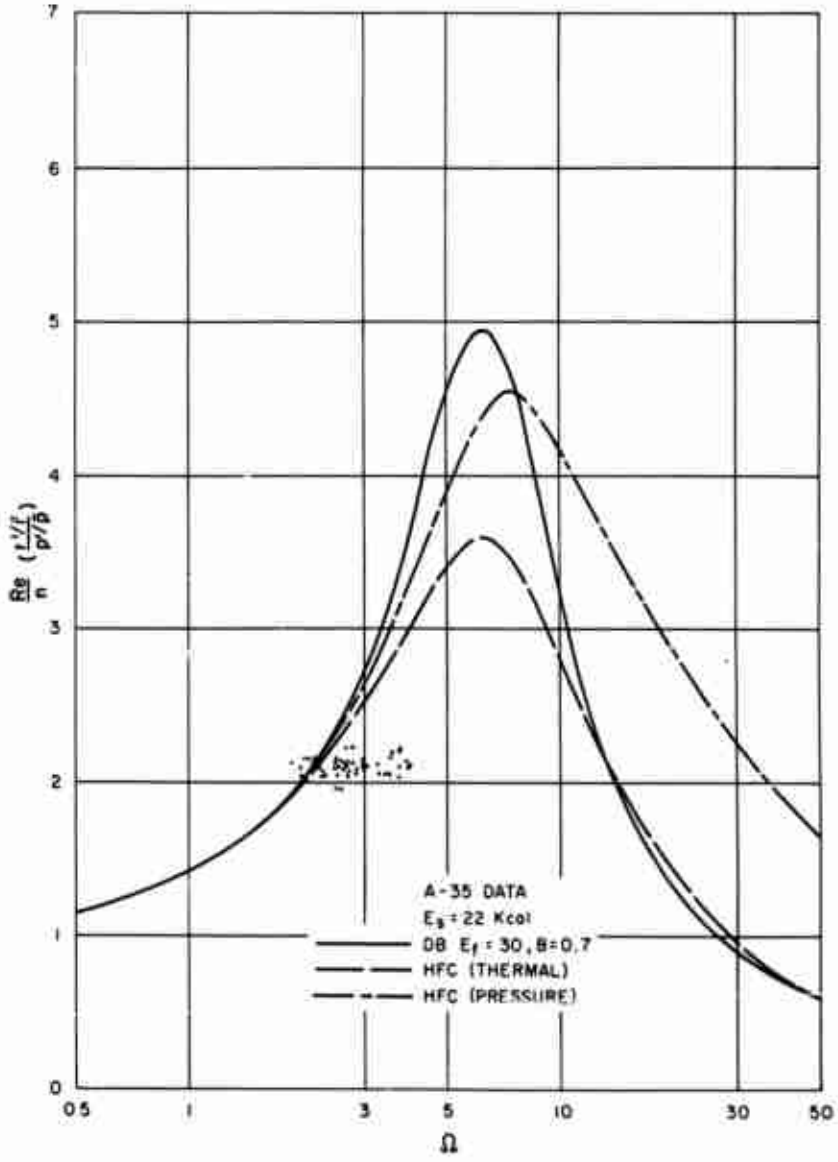

FIG. 4.6. The Response Functions for E_s = 22 (A = 8) Compared With A-35 Data.

different from the others it would be impossible to judge from the data which set of parameters more nearly predicts actual behavior. However, the phase has also been calculated for these parameters and is compared with the L* burner data in Fig. 4.7 and 4.8. Again, the scatter is considerable, but a much more definite trend is apparent. On the basis of these latter figures, it can be concluded that for both models the curves corresponding to E_s = 22 Kcal/mole and, in particular, the purely thermal part of the HFC model, provide the better fit with the data. The results from these latter two curves will be used later in a comparison with basic NAI data.

Figures 4.9 through 4.12 contain the Utah TF propellant data and are compared with the theoretical curves. Two curves for the DB model have been included, corresponding to E_f = 30 and 50. In Fig. 4.9 and 4.10 the value of 50 provides the better fit with the data. The curves for E_f = 30 are both much lower than the data. Based on these two figures, it would appear that the surface-activation energy of 50 in both models provides the better fit of the data. Turning again to the calculated values of the phase, Fig. 4.11 and 4.12 provide additional information upon which a judgement msy be based. In Fig. 4.11, the curve that most closely fits the data corresponds to the DB model with E_f = 30, but this set of parameters has already been rejected on the basis of Fig. 4.8. From Fig. 4.12 it is again concluded that the best fit of the data is obtained for E_s = 22 for both models, utilizing the thermal part of the HFC model (B = 0.77) and E_f = 50 for the DB model (B = 0.8).

In summarizing the results of this section, it seems appropriate to choose the sets of psrameters for the calculations that result in the best fit of the data for the two models to be coupled with NAI combustor theory. The only parameter that was varied in the HFC model was the surface-activation energy and the results indicate that the value of 22 Kcal/mole (A = 8) gives the best results for both propellants. It also appears that the thermal case of the HFC model is more applicable than the pressure-dependent case. This observation is not apparent from an examination of the response function results alone ss the real part of the two cases does not vary much at low frequencies. However, the phase is different over the range of frequencies and upon this basis, it is possible to draw the conclusion that the thermal case is more applicable. With the DB model the surface-activation energy of 22 Kcal/mole also gave the best results for both propellants. This would be snticipated because the surface-sctivation energy is containcd in the psrameter A in exactly the ssme manner for both models. However, for the TP propellant a flame-activation energy of 50 Kcal/mole gave the best fit while the value of 30 Kcal/mole was best for A-35. A mechanistic argument explaining the difference between the two propellants is beyond the scope of this report snd will not be attempted at this time. This difference in flame-activation energy is not so dramatic when the pronounced differences of the propellant compositions are taken into sccount.

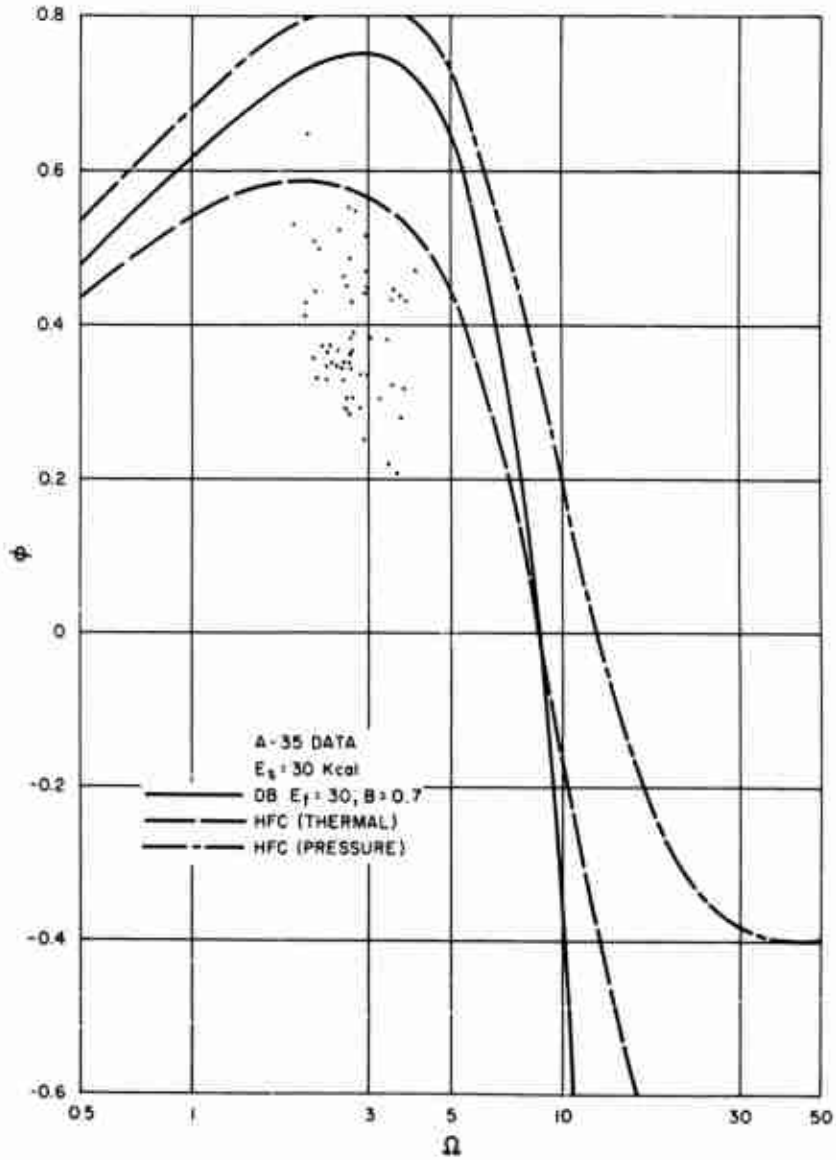

FIG. 4.7. Theoretical Phase Versus Nondimensional Frequency for E_s = 30, (A = 11), Compared to A-35 Data.

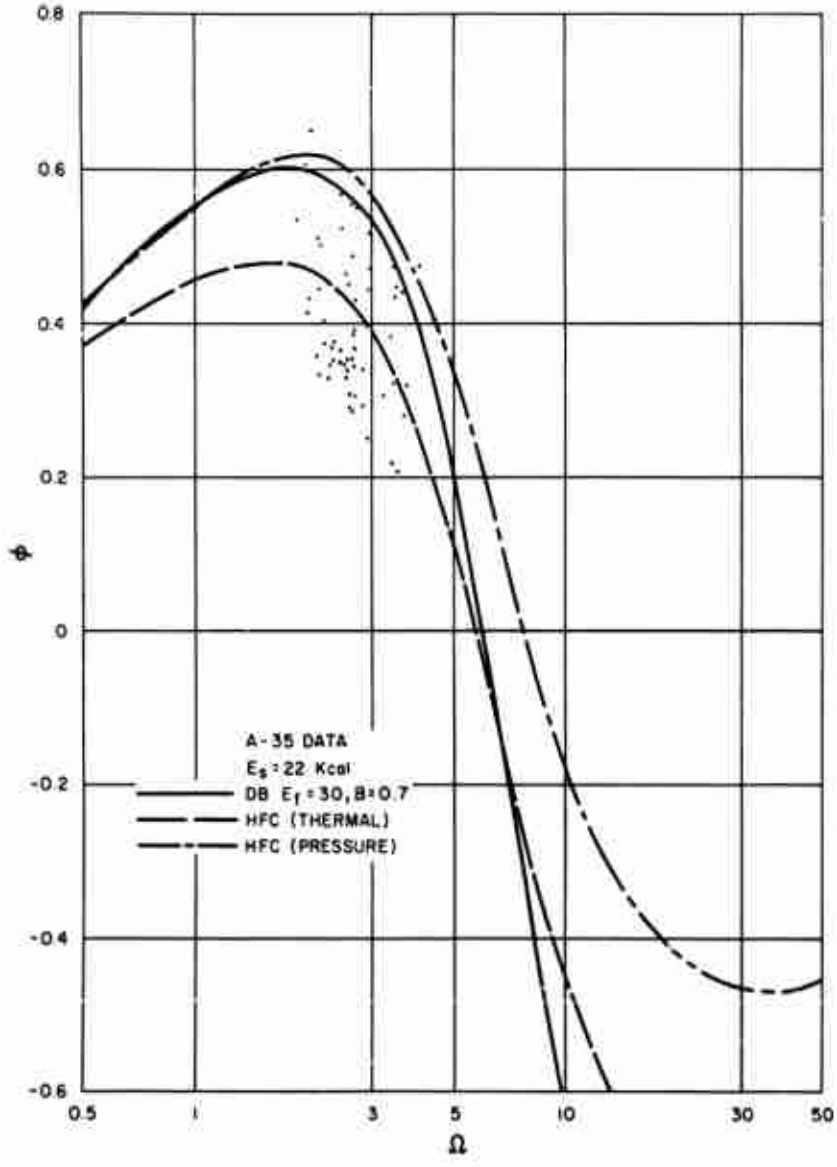

FIG. 4.8. Theoretical Phase Versus Ω for E_s = 22, (A = 8), Compared to A-35 Dsta.

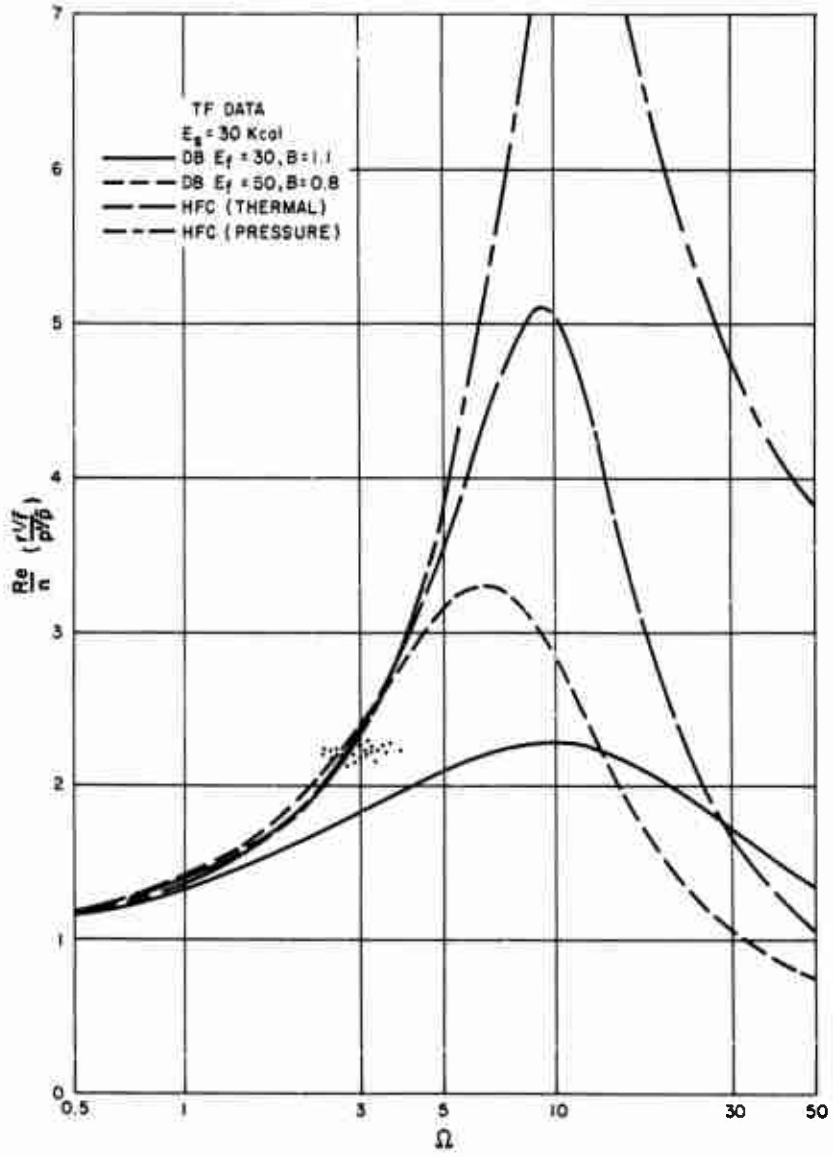

FIG. 4.9. The Response Functions for E_s = 30, (A = 11), Compared With Utah-TF Data.

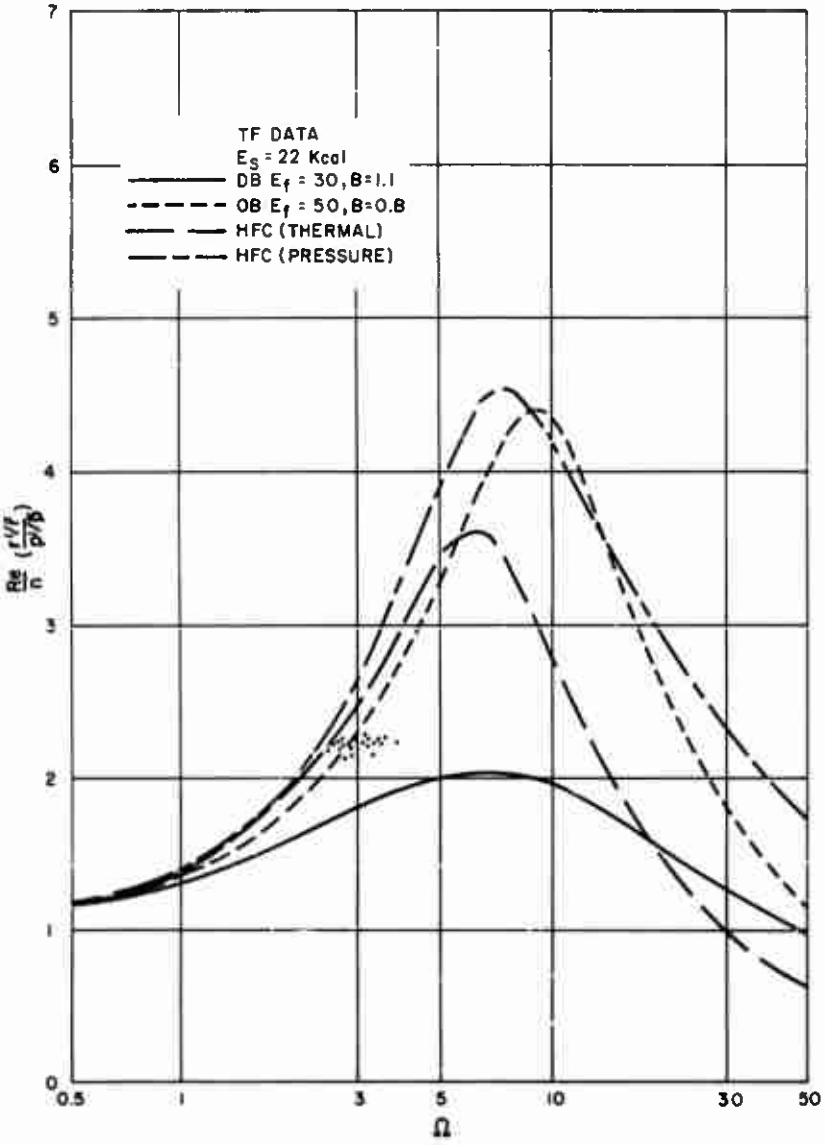

FIG. 4.10. The Response Functions for E_s = 22, (A = 8), Compared With Utah-TF Dsts.

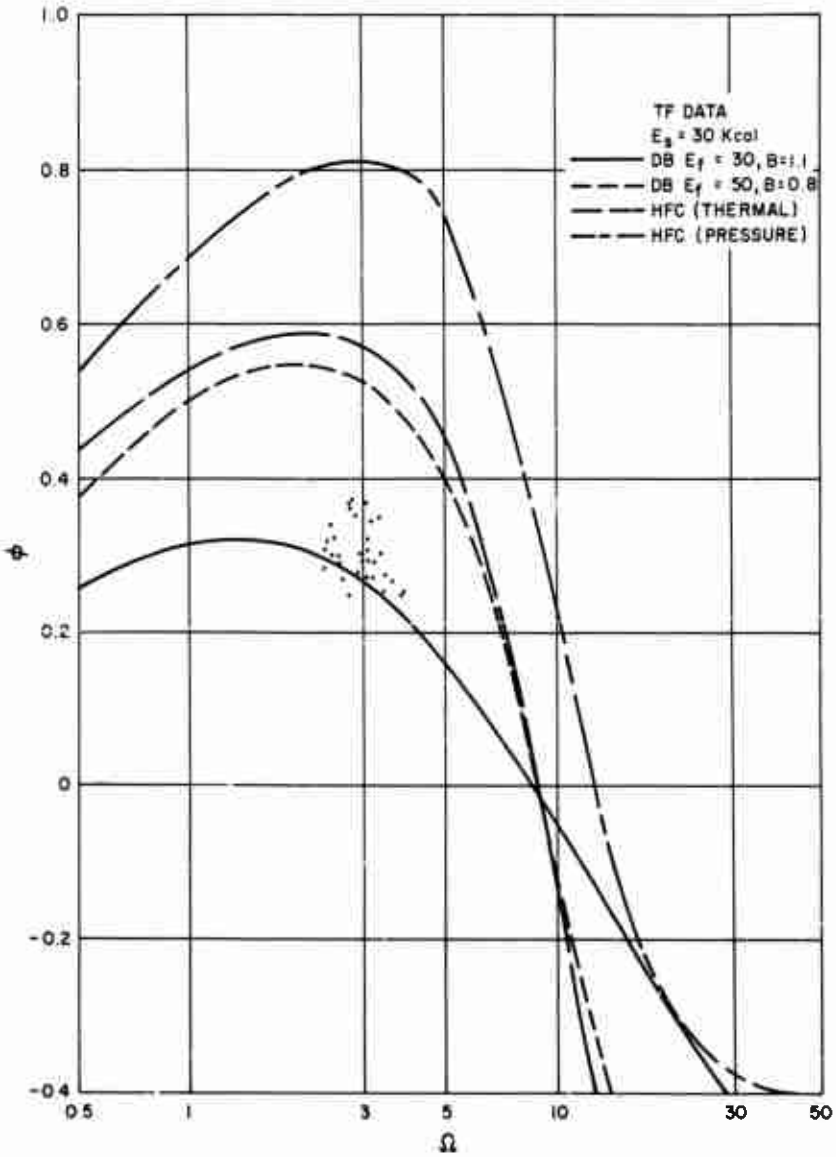

FIG. 4.11. rhase Versus Ω for E_s = 30, (A = 11), Compared to Utah-TF Data.

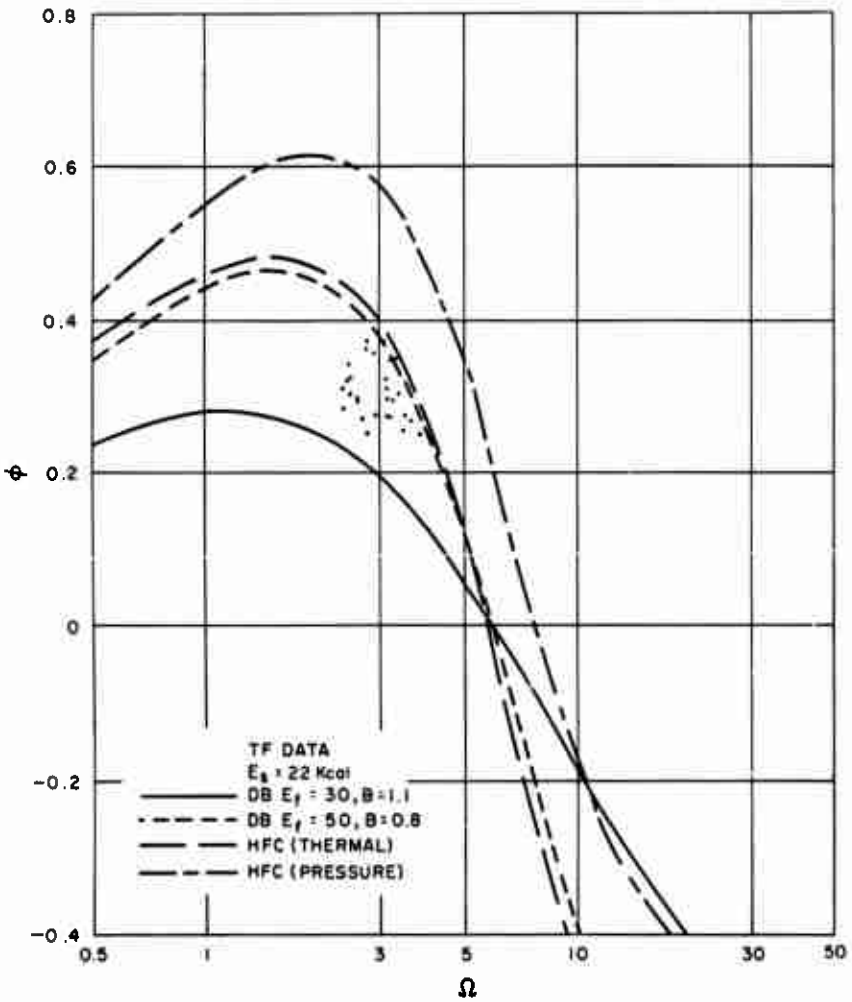

FIG. 4.12. Phase Versus Ω for E_S = 22, (A = 8), Compared to Utsh-TF Data.

It should be noted here that the value of B in these two cases is 0.8 and 0.7, respectively, while B_{HFC} was 0.77. Due to the numerical identity of the models there is essentially one set of nondimensional parameters that give the best fit for both propellants and for both models, i.e., A = 8, B = 0.7-0.8.

4.4. NAI CHARACTERISTICS FROM THEORETICAL MODELS

If the various parameters discussed in the previous section were known a priori, the response function could be calculated directly from the models. This information could then be combined with Eq. 4.2 to give the nonacoustic instability characteristics of a rocket motor or a laboratory burner.

In the following, the NAI characteristics for the two propellants studied will be calculated utilizing the models and the apparently best parameters as determined from Fig. 4.5 through 4.12. This will permit the direct comparison of the one-dimensional models with experimental data from an L* burner. Because of the numerical similarity between the two models only one set of parameters was used in the calculations for each propellant (for A-35: A = 8, B = 0.77 and for Utah TF: A = 8, B = 0.8). From Eq. 4.4

$$\mathrm{Re}\left(\frac{r'/\bar{r}}{p'/\bar{p}}\right) = 1 + \alpha\tau_{ch} \tag{4.11}$$

and

$$\tan\phi = \frac{\omega\tau_{ch}}{1 + \alpha\tau_{ch}} \tag{4.12}$$

where ϕ represents the phase of the combustion relative to pressure. Combining these equations and nondimensionalizing them with the thermal wave time constant after solving for τ_{ch} yields

$$\frac{\tau_{ch}}{\tau_{tw}} = \frac{\mathrm{Re}\left(\frac{r'/\bar{r}}{p'/\bar{p}}\right)\tan\phi}{\omega\tau_{tw}} = \frac{\mathrm{Re}\left(\frac{r'/\bar{r}}{p'/\bar{p}}\right)\tan\phi}{\Omega} \tag{4.13}$$

The right-hand side of the equation can be completely determined theoretically from the models, thus relating the nondimensionalized L* ($\tau_{ch} \propto L^*$) to the nondimensional frequency. Similar relationships have been derived previously (Ref. 22), but without considering the details of the gas-phase combustion. Utilizing the parameters for the given propellants as discussed above, values for the response function and phase as a function of the nondimensional frequency can be substituted

into Eq. 4.13 to give the nondimensional, L*-frequency relationship. In Fig. 4.13 theoretical curves of this nature are compared with the actual data for the two propellants. The theoretical curves are much more curved than one would expect from the trend of the actual data, but other than this, the agreement is quite reasonable.

Because of the intimate relationship between the growth constant and the stability of the system, it would be worthwhile to have a theoretical relationship describing the growth conatant. Thia can be determined readily by solving for α from Eq. 4.12 obtaining

$$\alpha = \frac{\omega}{\tan \phi} - \frac{1}{\tau_{ch}} \tag{4.14}$$

Evaluating τ_{ch} from Eq. 4.13 and dividing through by the frequency yields

$$\frac{\alpha}{\omega} = \frac{\mathrm{Re}\left(\frac{r'/\bar{r}}{p'/\bar{p}}\right) - 1}{\mathrm{Re}\left(\frac{r'/\bar{r}}{p'/\bar{p}}\right) \tan \phi} \tag{4.15}$$

Again, all of the terms on the right-hand side of the equation can be determined from the theoretical models. Using the parameters noted above, resulta obtained from Eq. 4.15 are compared with actual data in Fig. 4.14. Within the limits of the data scatter, the theoretical prediction is excellent.

If the growth constant is now set equal to zero, the atability limit for NAI is obtained. From Eq. 4.4 and 4.15 this condition ia aeen to be

$$\left[\mathrm{Re}\left(\frac{r'/\bar{r}}{p'/\bar{p}}\right) = 1\right]_{\text{stability limit}} \tag{4.16}$$

From Fig. 4.14 and the equations for the response function it is apparent that Eq. 4.16 will hold true for a particular value of the frequency (i.e., Ω_{cr}) for any given set of parameters. Substituting these reaults intα Eq. 4.13 yields

$$\tau_{ch} = \left(\frac{\tan \phi}{\Omega}\right)_{cr} \tau_{tw} \tag{4.17}$$

Thus, it should be posaible to represent the stability limit aa a straight line paaaing through the origin on a plot of τ_{ch} veraus τ_{tw}.

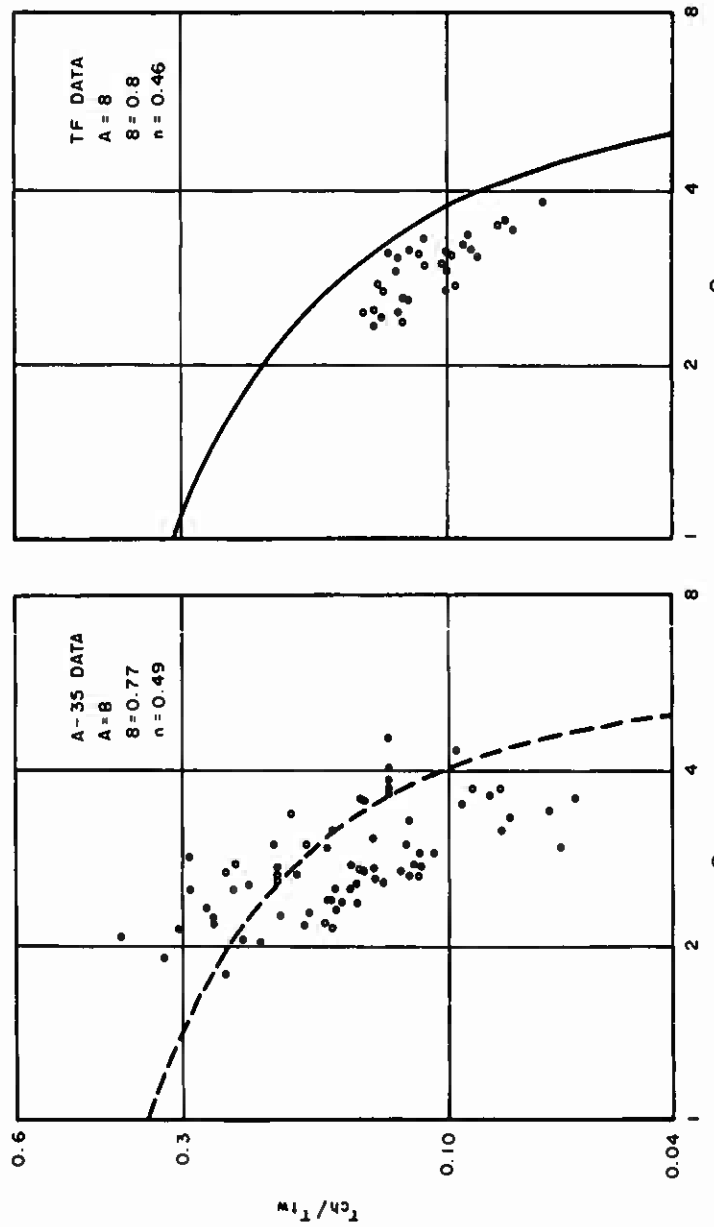

FIG. 4.13. Comparison of Theory (Using the Best Parameters as Determined by the Response Function and Phase Curves) With Experiment. Nondimensional L* versus nondimensional frequency.

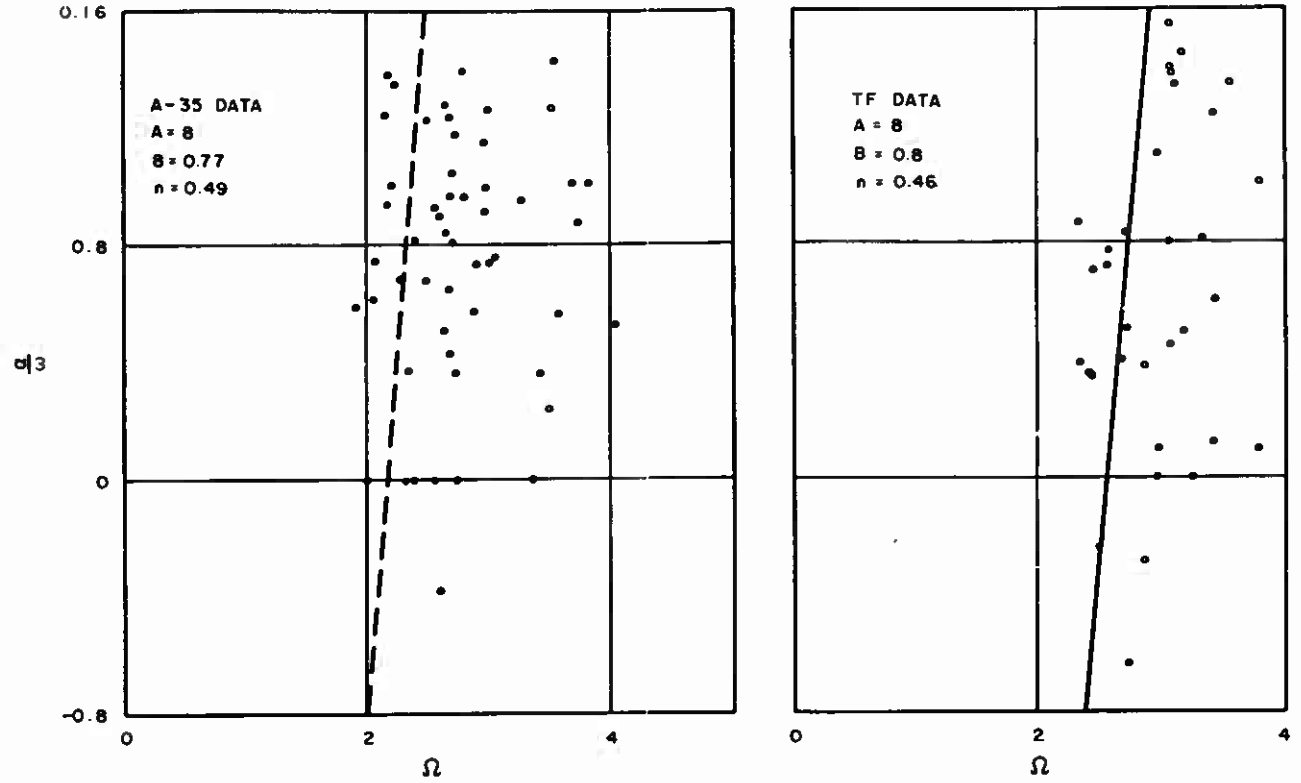

FIG. 4.14. Comparison of Theory With Experiment. Nondimensional growth constant versus nondimensional frequency.

Figure 4.15 contains such a plot--again comparing the results of the models with the actual dsta. The solid circles represent firings with $\alpha < 0$ (i.e., in a stable regime where developed oscillations decayed). Considering that data can only be obtained in the unstable region and up to the stability limit, a line drsvn along the left-hand edge of the data should represent the stability limit. For the Utah-TF propellant, the theoretical results sgree quite well with the data. However, for the case of the A-35 data, it would be virtually impossible to draw such a line and hsve it pass through the origin. Apparently something occurs with this propellant which is not accounted for by the models.

4.5. THE EFFECT OF OXIDIZER PARTICLE SIZE ON NAl

In order to make the models mathematically tractable certain ssumptions such as s homogeneous solid burning in one dimension with a quasi-steady gas phsae were made. In an effort to assess the validity of the assumption of one-dimensional burning of a homogeneous solid, a progrsm was initiated to study the effects of oxidizer particle aize distribution snd binder type on the nonacoustic combustion instability. The following sections present the effect oxidizer particle size has on NAl.

4.5.1. The Lsyer Frequency Concept

An idealized propellant can be visualized as consisting of oxidizer particles stscked one on top of snother, surrounded by binder. The characteristic time to burn through one particle is the particle diameter divided by the burning rate (i.e., $\tau = D/r$). If the particles are indeed stacked in layers then this characteristic time will be repested at a frequency of one cycle per particle, or $f = 1/\tau = r/D$ (Fig. 4.16). If the entire surface of a burning propellant regressed so that each oxidizer particle was exposed at the ssme time and burned "in phase" with enough other oxidizer particles, then this layer frequency would become a measurable phenomenon, contributing to combustion instability. This phase correlstion[3] concept is schematically pictured in Fig. 4.17.

In sn actual propellsnt the oxidizer psrticles are rsndomly distributed and therefore the phase correlation of the entire surface would be somewhat difficult to schieve and would most likely result in s frequency less than noted above. That is to say,

$$f = K/\tau = Kr/D \qquad (4.18)$$

[3] This "phase correlation" concept was first proposed by Price (Ref. 29) in connection with the shedding of sgglomerated metal from a propellant surface.

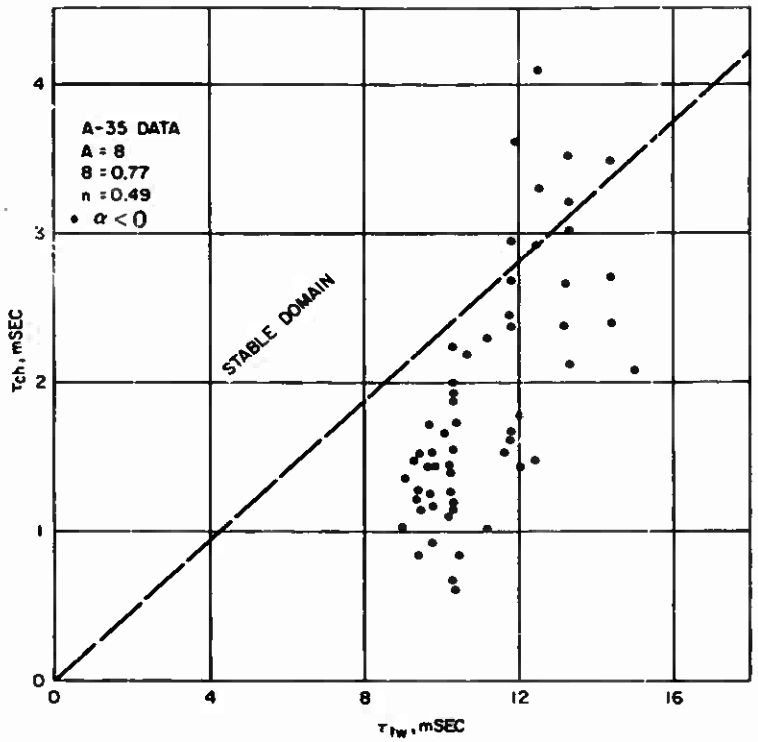

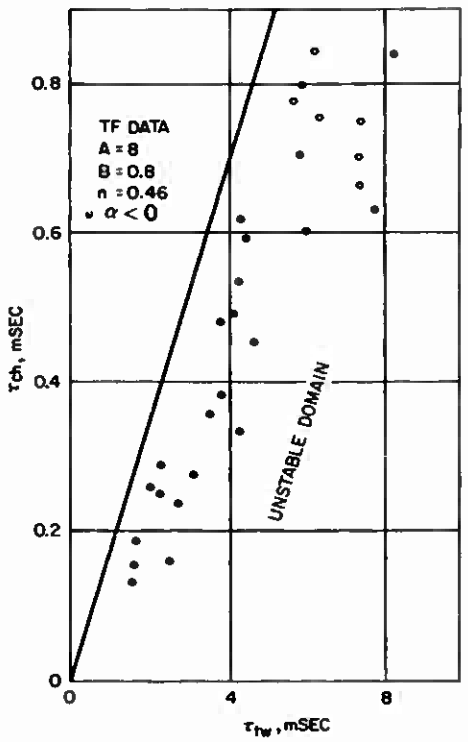

FIG. 4.15. Comparison of Theories With Experiment. Stability limit-chamber residence time versus thermal wave relsxation time. To the right of the lines is the unstable domain.

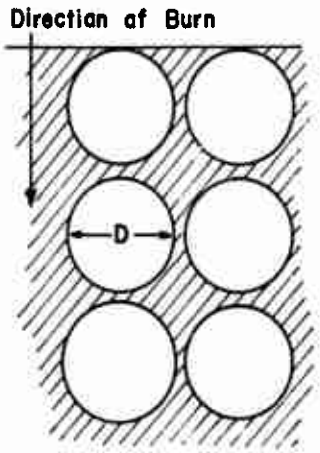

$$\text{characteristic time} = \frac{\text{oxidizer particle size}}{\text{burning rate}}$$

$$\tau = \frac{D}{r} \text{ (sec)}$$

$$\text{frequency} = \frac{\text{(constant)(one cycle/particle)}}{\text{characteristic time/particle}}$$

$$f = \frac{K}{\tau} = \frac{Kr}{D}$$

FIG. 4.16. The Layer-Frequency Concept--The Frequency at Which a Combustion Wave Burns Through Layered Particles is Directly Proportional to the Burning Rate and Inversely Proportional to the Diameter.

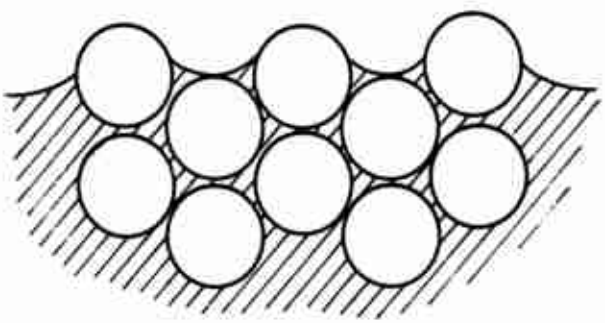

FIG. 4.17. Phase Correlation--If the Burning Surface Arranges Itself Such That Sufficient Oxidizer Particles are Exposed Simultaneously, Then the Surface is Said to be "Phase Correlated", and Measurable Oscillations will Occur at the "Layer Frequency".

where $\Gamma < 1$ due to the fact that the oxidizer particlea are not atacked uniformly one on top of the other but are randomly oriented. The poasibility of having a phaae correlated aurface can be explored by examining the surface of a quenched propellant. Figure 4.18 is a photomicrograph of the surface of a propellant that extinguished itself while chuffing. The protruding surfaces of the oxidizer particlea are readily apparent and it is not unrealistic to imagine that the aurface was indeed phase correlated to aome degree. The extent to which a surface must be "correlated" in order for instability to be obaervable ia a queation that could be pursued in the future.

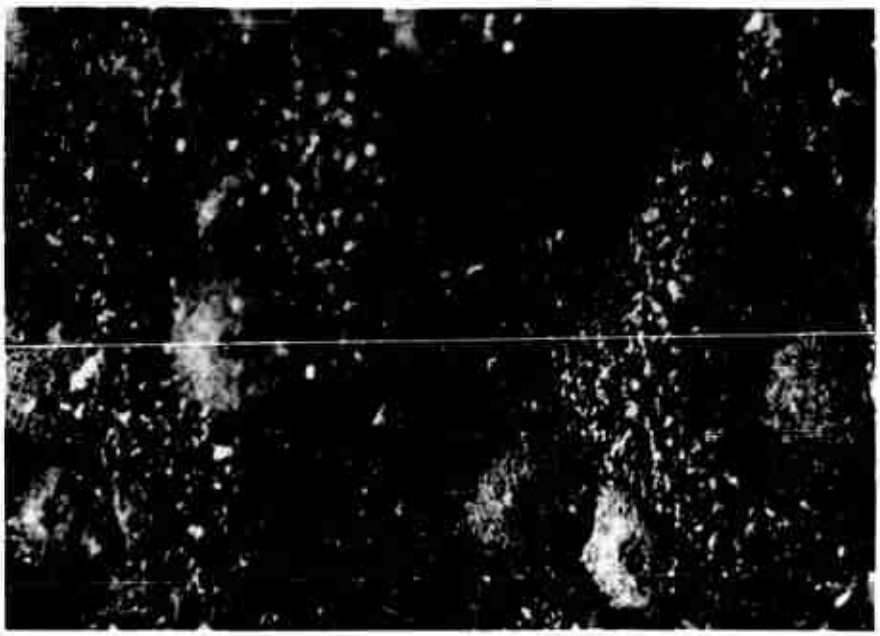

FIG. 4.18. Photomicrograph of an Extinguished Sample of A-155 Propellant. The large, protruding crystala had an initial, mean diameter of 400μ.

It was pointed out in Section 4.1 that a dual frequency nature had been exhibited by two different propellanta, and that thia duality had been attributed to the oxidizer particle aize. According to the layer frequency concept outlined above, any propellant containing a bimodal blend of oxidizer should, under the right conditions, display this dual-frequency behavior. To check this poatulate a series of bimodal AP propellants was made having 25% polyurethane binder and 75% solids (1%

carbon black was used to reduce the translucence of the propellant). Part of the AP in the propellants was a coarse oxidizer and part was finer oxidizer, with the oxidizer particle size distribution for each propellant given in Table 4.2. The AP that was used was the special spherical AP produced by the American Potash and Chemical Corporation, and all blends except the 15μ were screened to give either ±18 or ±25% of the mean particle diameter. Chemically, the propellants were the same; only the physical nature was changed by varying the oxidizer particle sizes. In the remainder of this section the results obtained with these propellants and their relationship with the layer frequency will be discussed.

TABLE 4.2. Bimodal Propellant Compositions.

Propellant designation	Ingredients and weight percent			
	Ammonium Perchlorate		Binder	Other
A-146	37.5% 15μ	37.5% 80μ	25% polyurethane	.....
A-148	37.0% 15μ	37.0% 200μ	25% do	1% carbon black
A-149	37.0% 90μ	37.0% 600μ	25% do	1% do
A-151	37.0% 45μ	37.0% 200μ	25% do	1% do
A-155	37.0% 45μ	37.0% 400μ	25% do	1% do
A-156	51.8% 15μ	22.2% 200μ	25% do	1% do
A-157	22.2% 15μ	51.8% 200μ	25% do	1% do
A-158	37.2% 90μ	37.5% 600μ	25% do	.....
A-159	36.0% 15μ	36.0% 200μ	25% do	1% carbon black 1% n-butyl ferrocene
A-160	36.0% 45μ	36.0% 400μ	25% do	1% carbon black 1% n-butyl ferrocene

4.5.2. The Non-one-dimensional Nature of Propellant

The models available (Section 4.3) to predict the general behavior of a given propellant all assume that the propellant is a homogeneous solid burning in a one-dimensional manner. The degree of validity of these assumptions may be investigated by examining the heterogeneous, non-one-dimensional nature of the propellant with respect to thermal wave penetration and oxidizer particle size. Figure 4.19 is a schematic showing the relative dimensions of typical oxidizer particles and

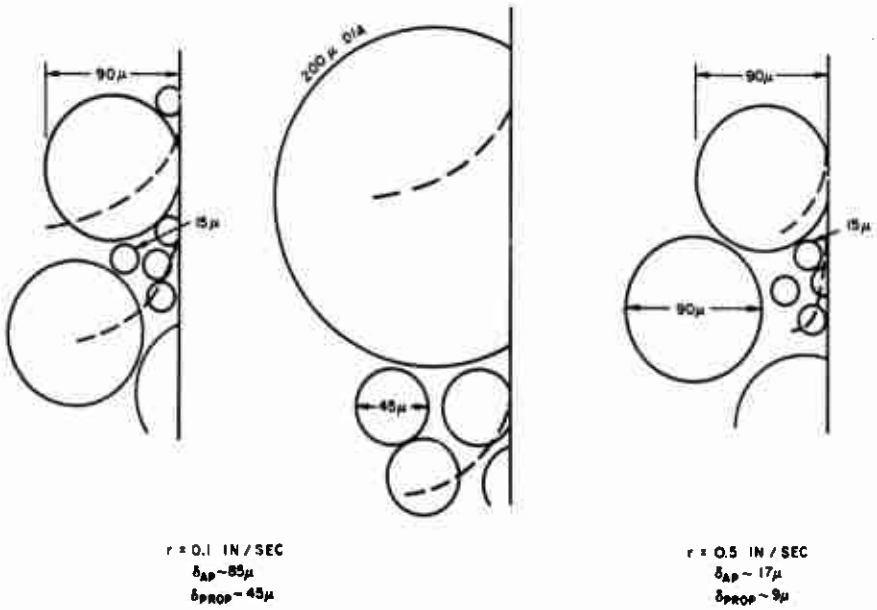

FIG. 4.19. Thermal Waves in Heterogeneous Propellants--The Circles Represent AP Crystals (Drawn to Scale) and the Dashed Lines Represent the Temperature Profile and the Distance that the Profile Penetrates Into the Crystal. The upper profile was calculated from the properties of AP alone and the bottom one is based on the average propellant properties.

temperature profiles for two different burning rates. The thermal profiles which have been included are based on the thermal properties of AP alone (top profile) and on the average properties of the propellant (bottom profile). At low pressure and low burning rate, the thermal wave thickness is quite large, and for small oxidizer particle sizes the propellant can be considered homogeneous and burning may essentially be considered one-dimensional. However, at a burning rate of 0.1 in/sec, the thermal wave thickness is the same order of magnitude as the oxidizer particle sizes used in this study. Hence, the homogeneous and one-dimensional assumptions necessary to the analytical models would appear to be tenuous under these conditions, and at the same time these are the conditions where the layer frequency would most likely be observed. If the thermal wave thickness just matches the particle size, then as the particle burns the combustion wave will soon be passing into preheated AP and the local burning rate of the particle will increase as the

particle burns out. This rapid burning of the remains of an oxidizer particle has been observed in movies such as those described in Section 3. It can readily be imagined that if such a phenomenon could be "phase correlated" over the entire propellant surface, pressure oscillations would be produced.

4.5.3. Results From Bimodal Propellants

From the above discussions the greatest departure from one-dimensional theory would be expected at high values of burning rate (smaller thermal wave) and for large oxidizer particle sizes. This is indeed the case as illustrated by the trends of the data plotted in Fig. 4.20. Test data as well as the burning rates of the various propellants are tabulated in Appendix A. The cross-hatched parabolic band represents the prediction of one-dimensional theory, and the data are for the various propellants. At low values of the burning rate, $r < .09$ in/sec, the data agree moderately well but at higher burning rates ($r > .10$ in/sec), the experimental values deviate quite significantly from the one-dimensional theory.

Whereas Fig. 4.20 is a composite plot, Fig. 4.21-4.26 present the data for each individual propellant. In the figures the shaded areas bounded by straight lines represent the mapping of the equation of $f = r/P$ for the particle size distribution used in the formulation of that propellant. These shaded areas show where the layer frequency should show the strongest effect (for $K = 1$).

Figure 4.21 presents the data for the unimodal, 90μ AP propellant, A-35. For this propellant the data agree well with both the layer frequency concept (the line labeled 85μ) and the one-dimensional theory as the two are coincident for the range of burning rates available for testing.

Figure 4.22 presents the data for the bimodal (90 and 600μ) propellant A-149. Since the large particles of AP tend to decrease the burning rate, it is to be expected that the layer frequency concept (for the 90μ AP) and the one-dimensional theory are mutually applicable for this propellant. Apparently the layer frequency corresponding to the 600μ AP was so low that it was unobservable.

The one-dimensional theory parabola deviates quite significantly from the experimental results for the A-151 propellant (45 and 200μ) as shown in Fig. 4.23. As was mentioned earlier for a burning rate of 0.10 in/sec, the thermal wave thickness for the propellant is approximately 45μ which coincides with the fine oxidizer particle size for this propellant. Hence, non-one-dimensional behavior was expected for this range of conditions. It should be noted here as well as with the other propellants that the range of conditions for which data may be obtained is very limited in an L* burner. At low burning rates where the steady-state thermal wave penetrates deeply into the solid there are ignition

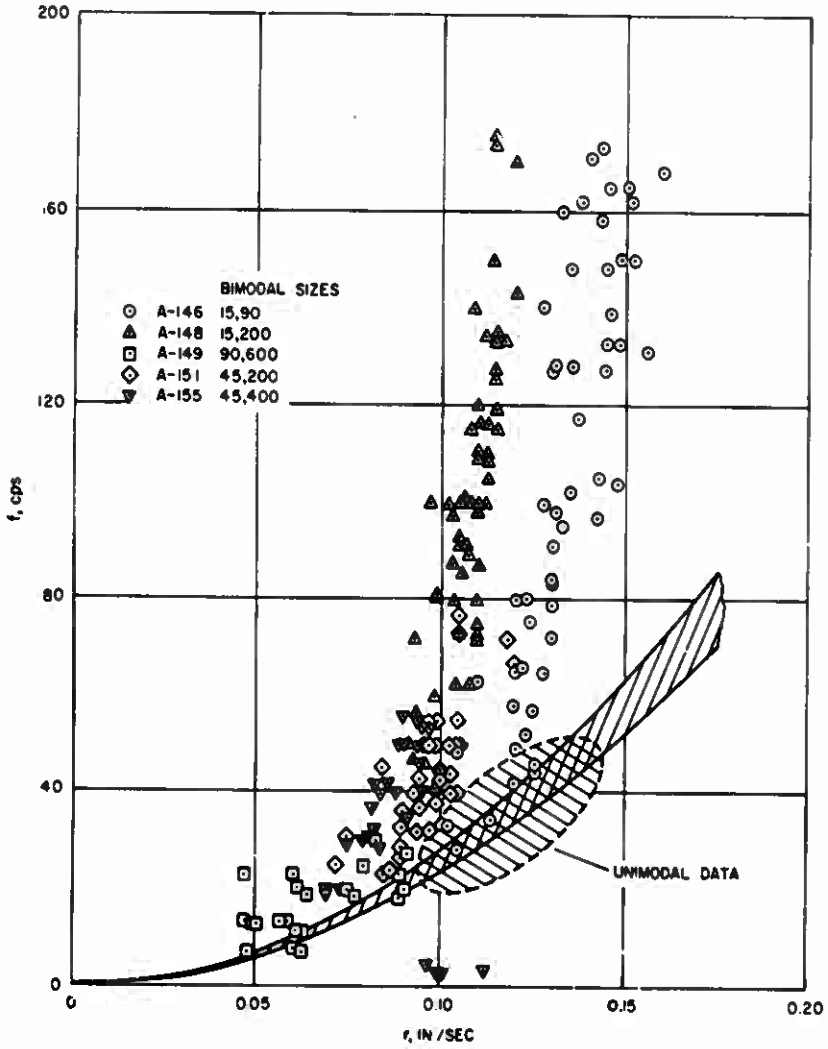

FIG. 4.20. Frequency Veraue Burning Rate for the Propellanta Teeted. The data for the reference, unimodal propellant are indicated by the ahaded area and the predicted behavior (baeed on one-dimenaional modela) ie included.

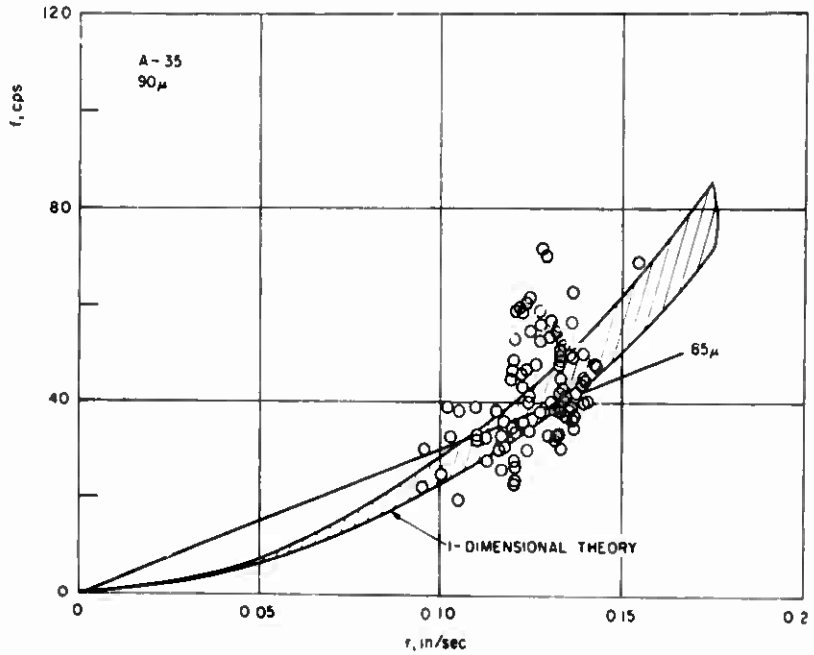

FIG. 4.21. Frequency Veraus Burning Rate for the Reference Propellant, A-35. The straight line represents the layer frequency concept based on the median of the particle distribution of the AP.

problems in establishing this profile and igniting the propellant. Also, there are aimilar problems as the low pressure deflagration limit is reached. At high burning rates, data acquisition is restricted by the stability limit of the L* burner, and by the physical limit of the burner (i.e., the smaller values of L* that would be below the stability limit are physically impossible to attain in the burner).

Figures 4.24 and 4.25 are quite similar as might be expected, due to the similarity in the propellant compositions. Both contain 15μ AP and both oscillated at frequencies two to three times what normally would have been expected. It appears as though there is a transition occurring from one-dimensional behavior at low burning rate to a layer frequency behavior st the higher burning rate.

In Fig. 4.26, propellant A-155 not only exhibits the higher trend in frequencies but also, under certain conditions, oscillated at very low frequencies. The low frequency corresponds very closely to the

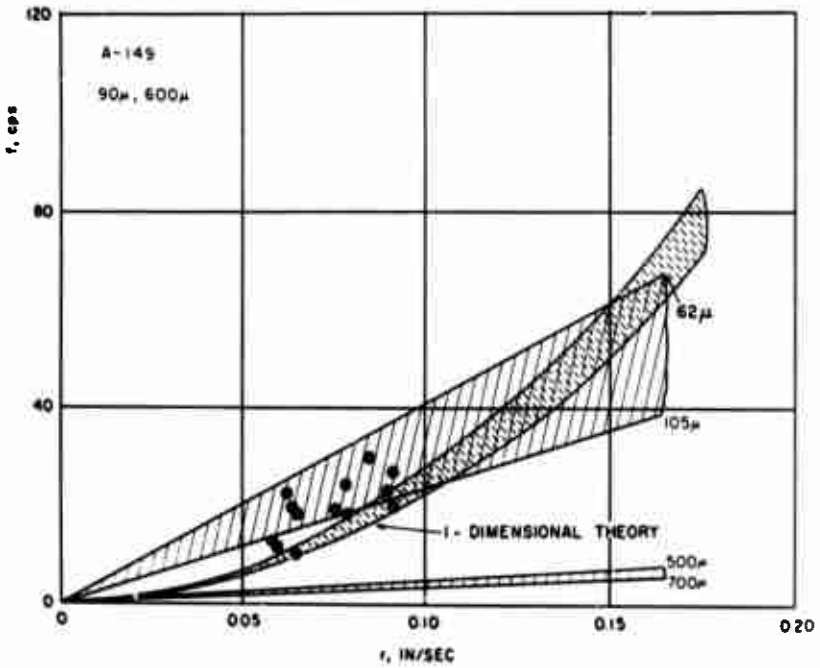

FIG. 4.22. Frequency Veraus Burning Rate for A-149.

layer frequency of the larger oxidizer particlee. This representa the dual frequency nature thet wae aought at the outaet of tha atudy. Apparently e sufficient number of the lerge oxidizer perticlea ware burning in phese with eech other to cauae en oacillation of sufficient magnitude that it could be meaeured. Figure 4.27 ia a preesure-time trece of one of the rune where the low frequency oacilletion occurred. The chuffing end oscilletions thet occur at the initial part of the test ere at a frequency of 52 cpe while the low amplitude oacillationa later in the teat ere at e frequency of 2.7 cpa. Thie ia the moet conclueive evidence aveileble thet the leyer frequency concept ia velid end produces en obeervable affect under certein conditiona. Subsequent test records have elao exhibited thie dual frequency phenomenon.

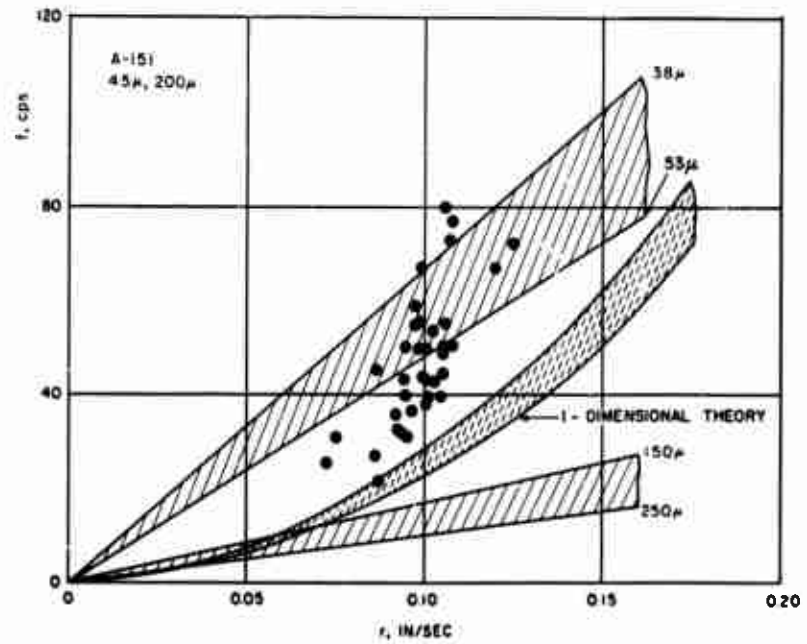

FIG. 4.23. Frequency Versus Burning Rate for A-151.

4.6. THE RELATIONSHIP BETWEEN THEORETICAL MODELS AND THE LAYER FREQUENCY CONCEPT

In order to put the results of this study in perspective with Section 4.3, the data have also been reduced to give the response function and the nondimensional frequency. Figure 4.28 contains the results of the data for four of the bimodal propellants and compares these with reaults obtained using the Denison and Baum model. The parameters used in the theoretical calculation were determined for A-35 propellant in the manner outlined in Section 4.3 and also by the method recently proposed by Beckstead and Culick (Ref. 30). Utilizing this latter technique to determine the parameters neceasary to fit the data for the bimodal propellants resulta in parameters that are totally impractical (i.e., $A < 0$). This again indicates that these propellants oscillate in a manner that cannot be predicted from one-dimenaional theories.

Another way of looking at the data ia in a stability plot aimilar to Fig. 4.15. Utilizing the data for A-155, which seemed to show the most dramatic dual frequency results, Fig. 4.29 waa constructed. The data for $\alpha > 0$ should lie to the right of the stability limit line, the

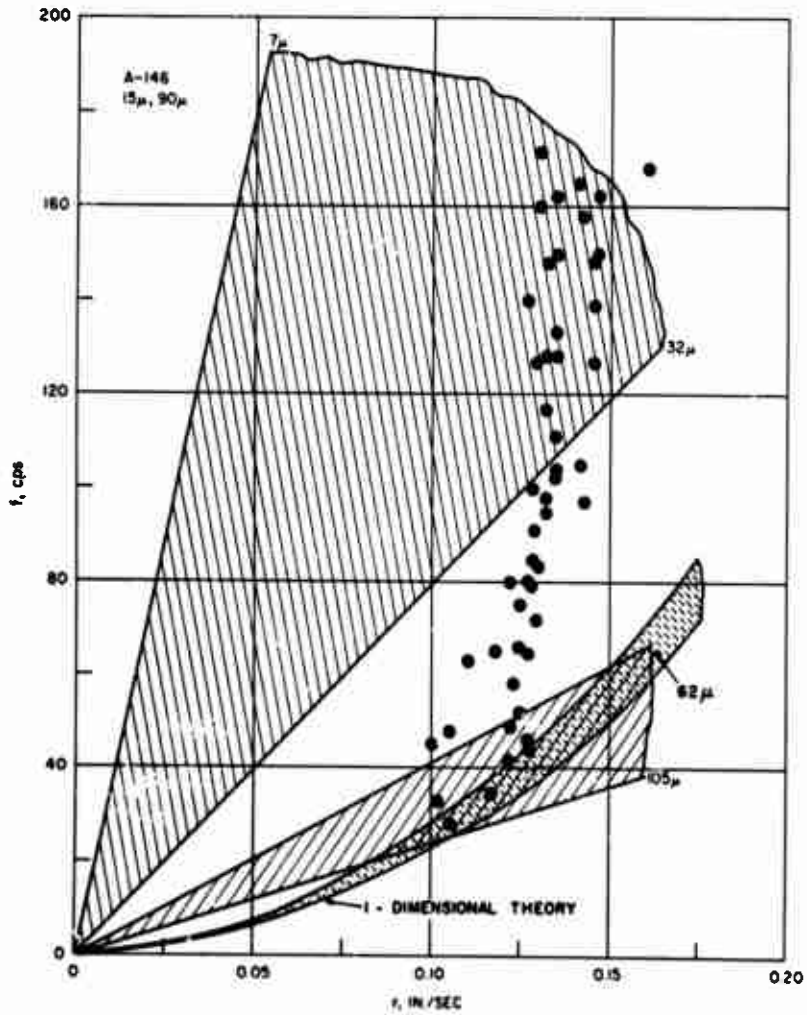

FIG. 4.24. Frequency Versus Burning Rate for A-146.

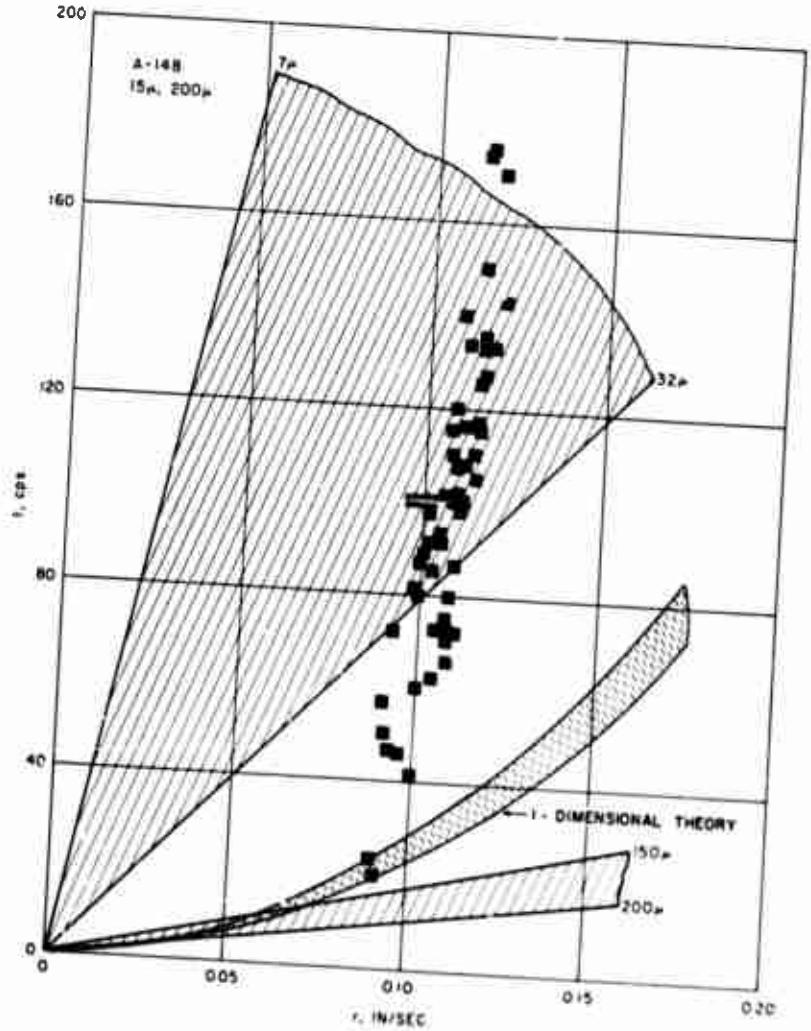

FIG. 4.25. Frequency Versus Burning Rate for A-14B.

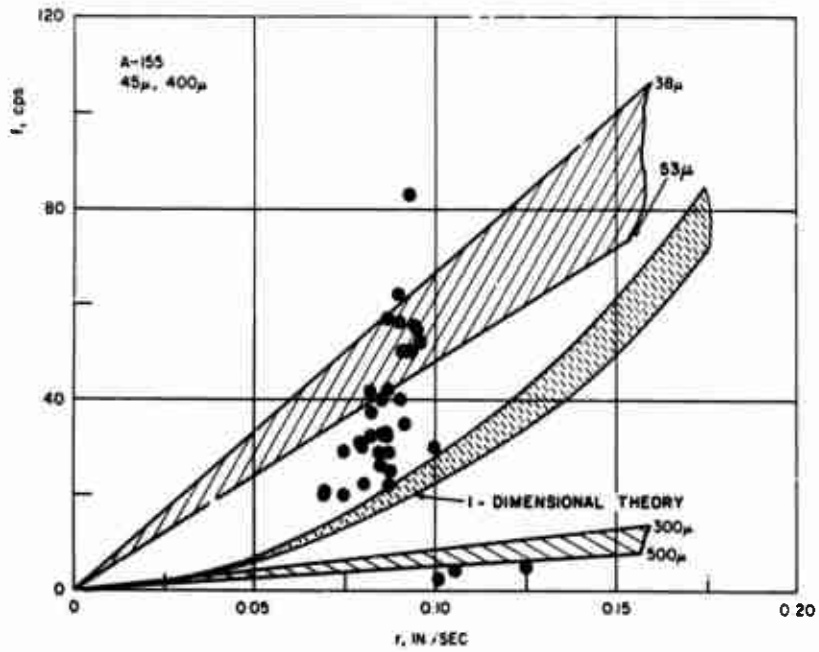

FIG. 4.26. Frequency Versus Burning Rate for A-155.

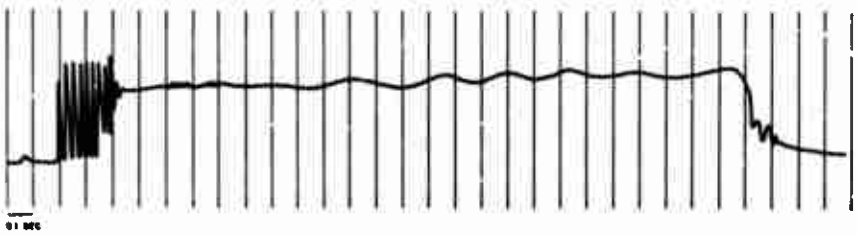

FIG. 4.27. Oscillograph Trace for Propellent A-155 Showing Dual Frequency.

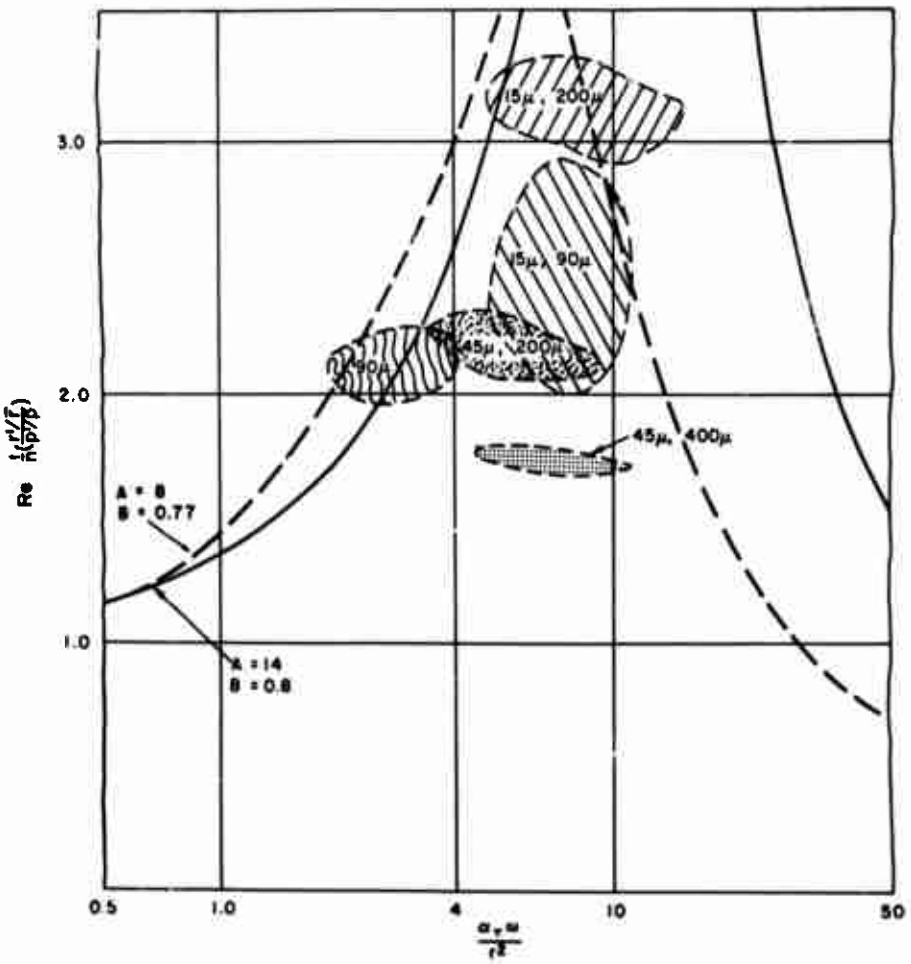

FIG. 4.28. Response Function Versus Nondimensional Frequency.

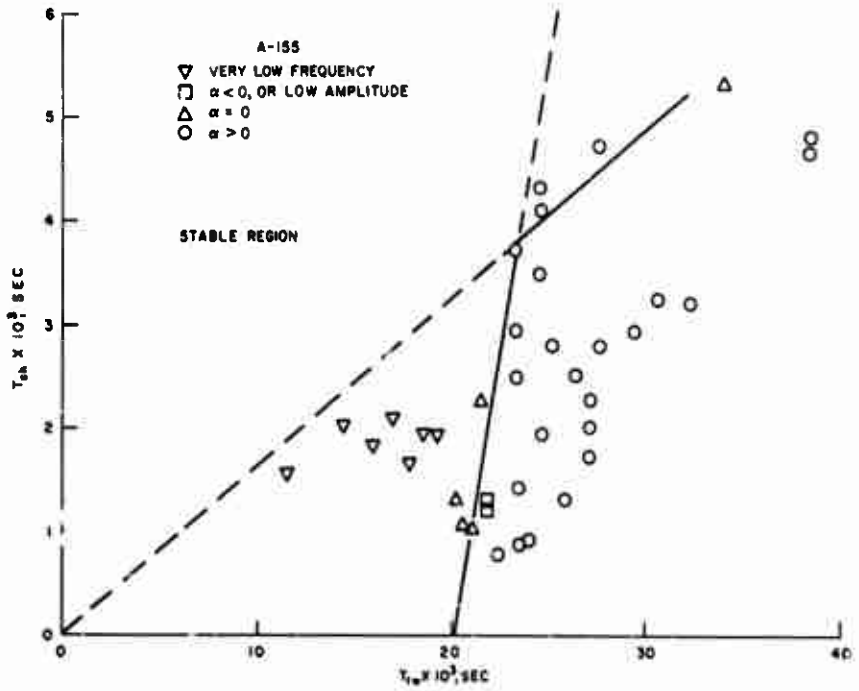

FIG. 4.29. Stsbility Limit Plot of τ_{ch} Versus τ_{tw} for A-155. Dsta tó the right of the lines are in the unstable region.

α = 0 points should lie on the line, snd the α < 0 lines should be to the left of the limit in the stsble domain. In the figure all of the points with α > 0 lie to the right of the solid line that intersects the abscisss et τ_{tw} = 20 milliseconds. The majority of the date lying to the left of this line are the dste et very low frequency. This seems to indicete the possibility of two different stability limits, one corresponding to the very low frequency dste end the second for the remsinder of the date. It will be recalled from Section 4.4 that the theories predict e streight line through the origin es the etebility limit. In Fig. 4.29 the very low frequency dete seem to give a stsbility limit that would egree with theories and yet the frequencies ef the oscilletions ere much lower than would be predicted. This anomaloue behavior needs further inveetigetion in order to underetend the relstion between, snd the reletive effect of, the leyer frequency end one-dimensionel theoriea.

From the above discussion it is apparent that the one-dimensional theories available at present are not adequate to predict the unstable behavior of propellants in a quantitative manner. Nor is it possible to do so with a simple mechanistic argument such as the layer frequency concept. However, by combining aspects of each of these a greater understanding of the problem may possibly be attained. In the following discussion it should be kept in mind that the layer frequency concept results in a range of frequencies under which oscillations occur but gives no indication as to the magnitude of the oscillations, whereas the one-dimensional models give both the frequency and an indication of the magnitude of the oscillations (in the form of the response function). Therefore, the two concepts cannot be combined in an exact sense, but a qualitative combination of the results is very informative. A plot similar to Fig. 4.20-4.26 has been constructed in which the results of the one-dimensional models can be readily included. Figure 4.30 is a log-log plot of the burning rate and the frequency with the layer frequency lines corresponding to A-155 propellant included as well as the line representing the maximum in the response function for A = 14 and B = 0.8 (see Fig. 4.28). If a third axis extending outward from the plane of the paper is considered to represent the real part of the response function, then Fig. 4.30 takes the form of a contour map. On the map there will be three ridges, two corresponding to the layer frequencies, and the third corresponding to the maximum in the one-dimensional theory. By taking a section of the contour at a constant burning rate (r = 0.09 in/sec), a modified form of the response function can be postulated as in Fig. 4.31. The dashed lines represent the approximate effect that could be caused by the layer frequency, and it has been assumed that the two effects would be additive. The magnitude of these ridges due to layer frequency effects are unknown before a series of tests are conducted, but Fig. 4.32 may be used to obtain the frequency that might be expected, given the oxidizer particle size and a particular burn rate. This figure also shows how this result would differ from that expected from a simple one-dimensional analysis, such as the Denison and Baum model.

4.7. SUMMARY

Two prevalent analytical models of solid propellant combustion instability which are relevant to the low-frequency regime have been reduced to a common notation and found to be numerically identical. Nonacoustic data for several propellants have been reduced to a format common with the models, thus allowing a quantitative comparison between theoretical analyses and experimental data of this nature. The possibility of utilizing combustion dynamics models to predict nonacoustic instability behavior has been explored: only qualitative agreement between experimental data and model predictions has been found, and even then several large discrepancies have been discovered. One such discrepancy, the effect of oxidizer particle size, has been explored in detail. A very

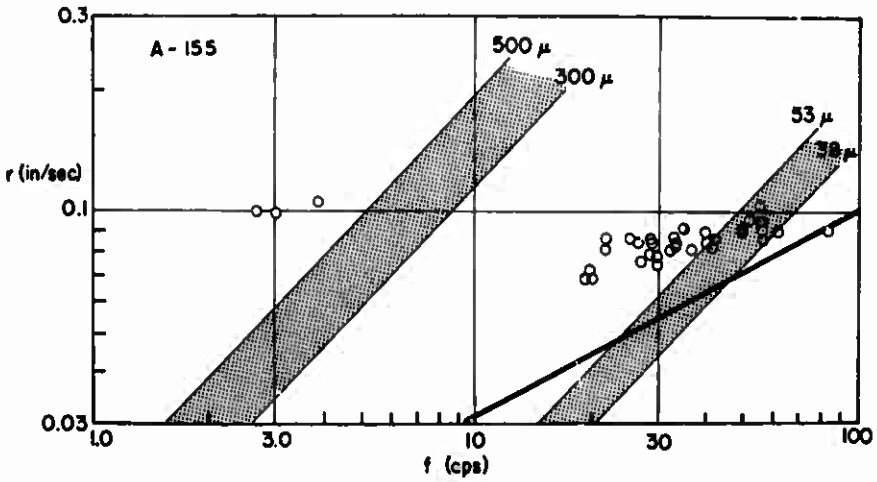

FIG. 4.30. Burning Rate Versus Frequency for A-155 Propellant With Shaded Areas Representing the Layer Frequency Regimes. The heavy solid line is the maximum of the response function calculated from the Denison and Baum model.

simple, phenomenological argument relating frequency of oscillation to the particle size of the oxidizer has been postulated and experimentally examined. This was accomplished by formulating a series of propellants containing bimodal oxidizer blends and testing them in the L* burner. The results obtained can only be explained by considering aspects contained in the models as well as aspects of the layer frequency concept which is related to the oxidizer particle size.

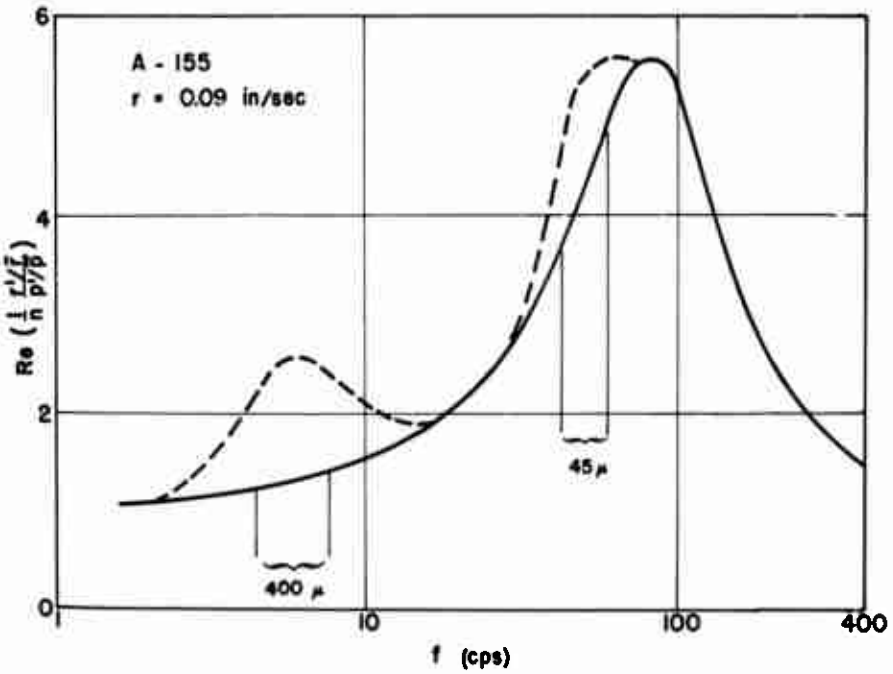

FIG. 4.31. The Modified Response Function With Deviations Included (the Dashed Lines) to Account for Oxidizer Particle Size.

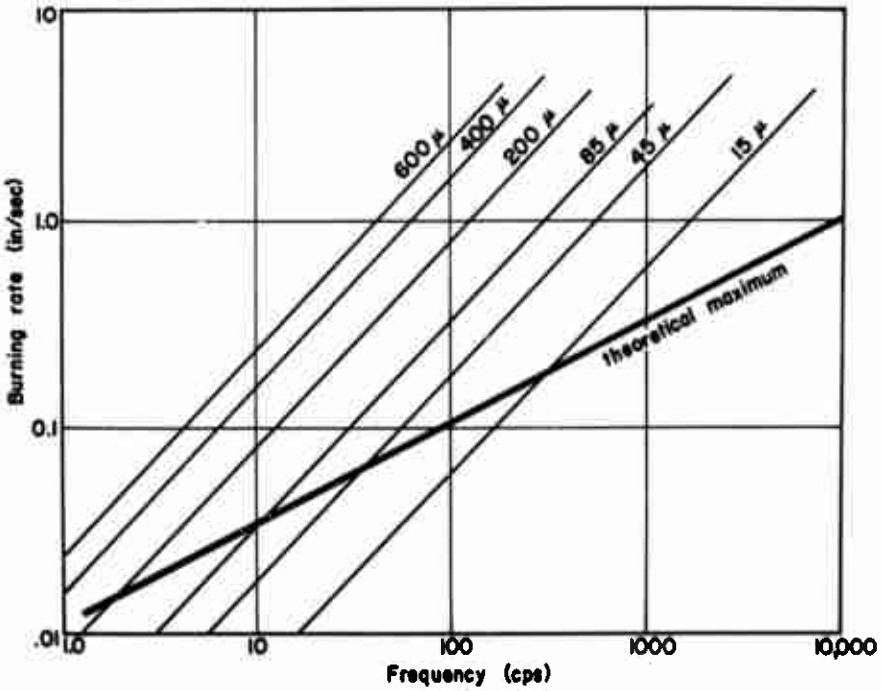

FIG. 4.32. Burning Rate Versus Frequency With the Layer Frequency Lines Included for Typical AP Sizes and the Theoretical Maximum Calculated From a Denison and Bsum Type Model.

5. ACOUSTIC COMBUSTION INSTABILITY

Experimental equipment has been devised which permita the investigation of acoustic instability in the low frequency range characteristic of very large rocket motors (Ref. 31, 32, 33 and 34) snd recent modifications to the equipment permit control of the experimental parameters and acquisition of quantitative information including acoustic response function data (Ref. 1). A cutawsy diagram of the burner used in this investigstion is shown in Fig. 1.

Activity during the present report period included assessment of stability characteristics of several metallized and nonmetallized propellanta, initial tests to determine the acoustic response function of a nonmetallized polyurethane propellant composition, tests with pressed AP-Al pellets which indicate that these spontaneously unstable formulations will couple with and drive acoustic wave modes, and an investigation of nonisentropic phenomena in low frequency acoustic instability of solid propellants.

5.1. TESTS TO DETERMINE RANGE OF UNSTABLE BEHAVIOR

Tests were conducted to determine unstable combustion behavior of two compositions for big booster applications (ANB 3105 and ANB 3254), a metallized and a nonmetallized AP-polyurethsne propellant (A-147 and A-35), and a nonmetallized AP-PBAN composition (A-13). Results of the big booster propellsnt tests are discuased in Appendix B.

An investigation previously conducted with a family of metallized AP-polyurethane propellants (Ref. 1) to determine the range of unatable behavior was expanded to include a new composition. Previous tests on A-139 snd A-91 propellants revealed that A-139, although unstable over a much wider range of pressure and frequency than A-91, was much hsrder to ignite (information on propellant compositions appears in Table 5.1). Since the AP psrticle size was the only parsmeter vsried between A-139 and A-91 it was expected that a propellant with an intermediate oxidizer size might offer a wider range of instability than A-91 and at the same time be easier to ignite than A-139. A 50-pound mix of A-147 was made using 45μ spherical AP. Tests to determine the range of instability were conducted and the results are shown in Fig. 5.2 with A-139 and A-91 included for comparison. The rsnge of instability for A-147 appeared to be less than that for A-91 and ignitability of A-147 did not appear to be greatly improved over A-139; hence, further tests with A-147 are not planned.

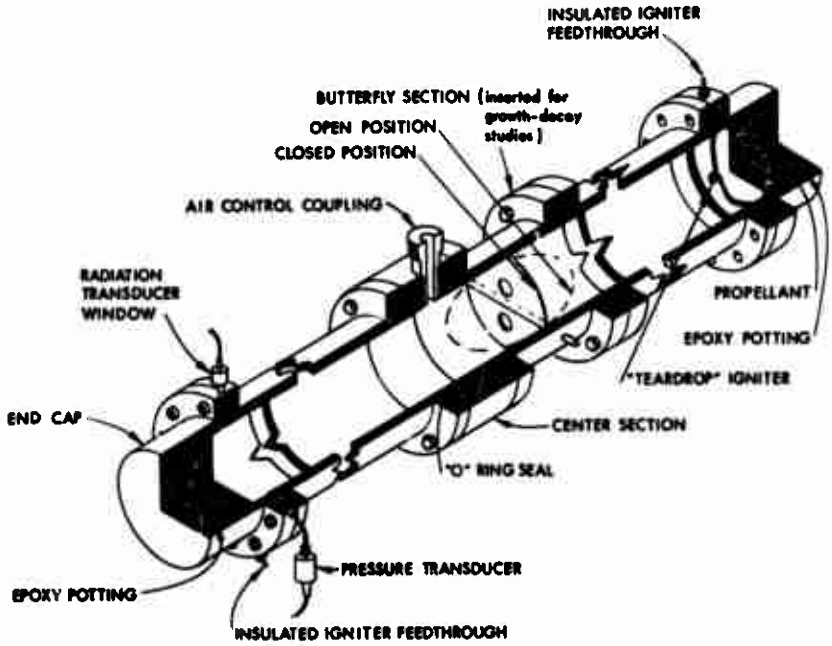

FIG. 5.1. Cutaway Diagram of the 5.5-inch T-8urner.

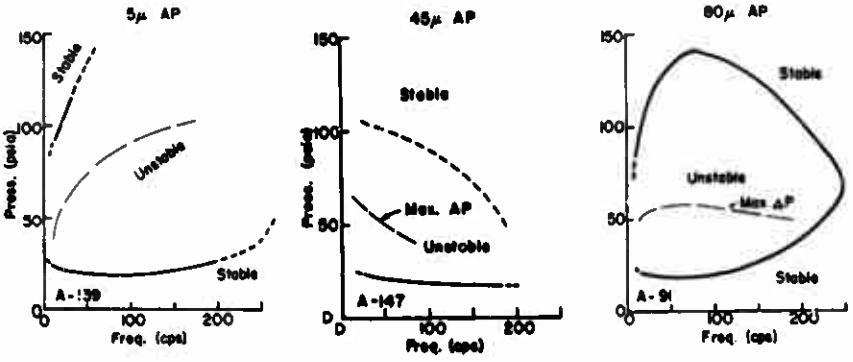

FIG. 5.2. Range of Unstable Combustion Behsvior for A-147 Propellant. A-139 and A-91 compositions are included for comparison. Dashed borderа indicate uncertain dsta while conditions of mаximum acoustic pressure are indicsted by the broken linc in the unstsble sreа.

TABLE 5.1. Compositions Used in Low Frequency Acoustic Instability Resesrch

Designation of composition	Binder		Oxidizer (spherical AP)		Aluminum (spherical)		Other	
	Type	Wt %	Mesn dis.	Wt %	Mesn dis.	Wt %	Type	Wt %
A-13	PBAN	24.0	80 μ	76.00	--	--	--	--
A-35	Polyur-ethane	25.0	80 μ	75.00	--	--	--	--
A-91	do	25.0	80 μ	67.00	5 μ	8	--	--
A-139	do	25.0	15 μ	67.00	5 μ	8	--	--
A-147	do	25.0	45 μ	67.00	5 μ	8	--	--
A-152	do	25.0	80 μ	74.60	--	--	NaCl	0.4
PU	do	20.1	5 μ	23.85	--	--	NaCl	0.05
			45 μ	56.00	--	--	--	--
J-30	--	--	80 μ	94.00	5 μ	4	CuO202	2.00
J-81	--	--	80 μ	88.00	15 μ	4	CuO	8.00

Two unmetallized propellants, A-13 snd A-35 (Tsble 5.1), which have been extensively tested in the 1.5-inch T-burner, were chosen for study in the low frequency range in the 5.5-inch burner. Testing of these two compositions to dste hss been primsrily to determine the range of unstable combustion behsvior. Results are shown in Fig. 5.3.

A notsble festure of tests with A-13 was the simultaneous presence of seversl sxisl acoustic modes during tests when the fundamental mode frequency was below 90 cps. Vslidity of the response function determinstion depends on presence of s single scoustic mode s[illegible]st A-13 response function tests sppesr to be limited to frequencies sbove sbout 90 cps. Tests with A-35 over s range of frequencies similsr to the A-13 tests did not reveal presence of modes higher than the fundamentsl axisl mode snd there does not sppesr to be s combustion-imposed lower frequency limit ss with A-13.

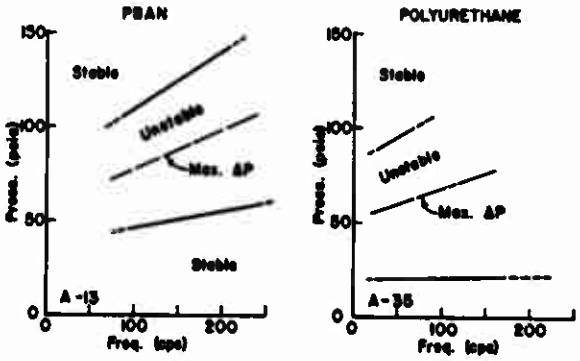

FIG. 5.3. Range of Instability Behavior for Two Unmetallized Propellants.

5.2. PRESSED PELLET INSTABILITY

Spontaneous combustion oscillations observed with AP-Al pressed pellets have been previously reported (Ref. 1). Investigations with metallized propellants which appeared to have a preferred frequency behavior have also been published (Ref. 35), but the correlation of a preferred frequency characteristic with metal combustion in propellant compositions has been indirect. Thus, pressed AP-Al materials appear to offer a means for conducting a definitive study of the relationship between metal combustion and preferred frequency combustion oscillations.

The relevance of pressed pellet combustion oscillations to acoustic instability has not been tested until recently. At least two aspects are involved which determine whether spontaneous combustion oscillations will excite an acoustic wave mode oscillation: (1) whether the combustion oscillations generate a pressure perturbation, and (2) whether the combustion oscillations are capable of being coupled with flow disturbances in a manner which will result in amplification of an acoustic mode (Ref. 36).

Initial tests to determine the extent to which pressed AP-Al materials exhibit acoustic instability have been conducted with J-30 (see Table 5.1) in the 5.5-inch burner. The problems of attaining large pellet size and of mounting the pellets without the use of organic binders or potting compounds which inhibit spontaneous instability, were solved by utilizing an existing die of approximately 1-1/2-in. diameter and arranging the pellets in an array such that seven pellets were accommodated in each end of the burner. Mounting was accomplished by pressing the pellets into a metal disc (Fig. 5.4). The metal disc-pellet assembly was then held in place in the bottom of the burner end-cap by a backing of silicone-glass adhesive tape. Ignition was accomplished by use of the same paint-on material used for propellants.

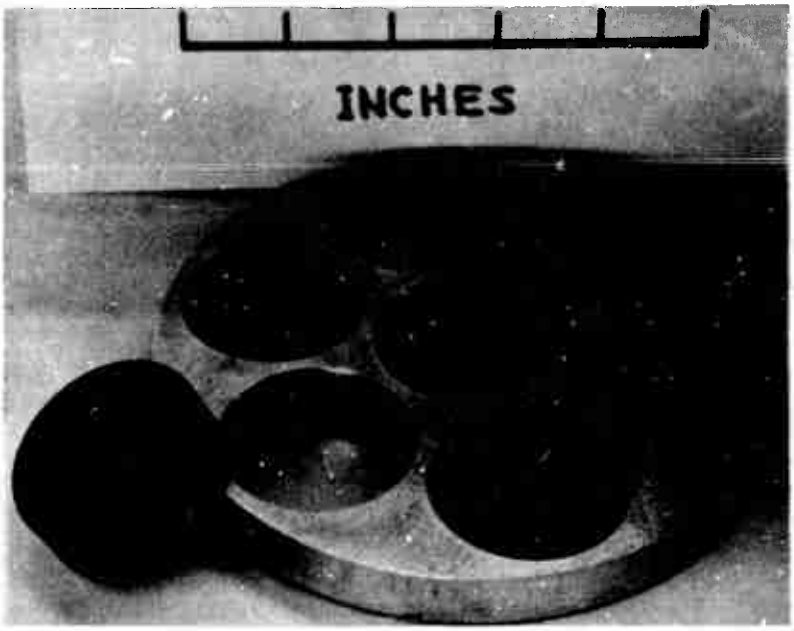

FIG. 5.4. Pressed Pellet Mounting Arrangement for the 5.5-inch Burner.

Test results indicated that coupling did occur and that the pressed pellet material is a good medium for study of the role of metal behavior in producing preferred frequency instability. Further testing, however, will be more readily accomplished by choice of a pressed-pellet formulation that exhibits spontaneous oscillatory behavior at lower pressures than J-30. J-81 (Table 5.1) appears to be a suitable candidate, as noted in Ref. 1.

5.3. INVESTIGATION OF NONISENTROPIC PHENOMENA

5.3.1. Introduction

Knowledge of the response of propellant combustion processes to flow perturbations is vital to any quantitative description of acoustic instability. The acoustic admittance appears as a boundary condition in solution of the wave equation and it describes the flow of energy into or out of the acoustic wave. The admittance is defined as

$$Y \equiv - \frac{v'}{p'} \qquad (5.1)$$

where v' is s velocity perturbstion normal to the propellsnt surface and p' is a pressure perturbation. When written in terms of variables relsted to propellant combustion, the admittance becomes (Ref. 34)

$$Y = -\frac{\bar{v}}{\bar{p}}\left\{\frac{\mu}{\varepsilon} - \frac{o}{\varepsilon}\right\} \qquad (5.2)$$

where $\bar{v}$ is the mean gas velocity, $\bar{p}$ ia the mesn presaure, μ/ε ia the ratio of mssa perturbation to pressure perturbation, and σ/ε is the rstio of denaity to preasure perturbation. It is assumed that the above quantities are cslculated at a plane near the propellant surface but at a location outaide the chemical reaction zone. It is further assumed thst gsa velocity and presaure fluctuations arc described by s stsnding acoustic wave mode, that the flame zone is of a thickness small compsred to other dimensiona in the system, snd that the gss-phase reaction timea are ahort compared to a period of acouatic oscillation snd to the transit time of sn element of gas through the combustion zone. It should be noted that, in geneisl, Y is a complex quantity. However, the real psrt of the complex admittsnce determines whether or not an acouatic wsve will be amplified; the out-of-phase (or imaginsry) component of the combustion response csnnot amplify a pressure perturbation.

The ratio μ/ε ia commonly referred to aa the "reaponse function" and considerable theoretical snd experimental investigation has been devoted to determining its magnitude. Values of the response function, according to T-burner resulta, typicslly fsll in the rsnge between unity snd 5. Less emphasis hsa been put on evsluating o/ε since theoreticsl studies indicste that it is of the order of unity in magnitude. It is this rstio which is sensitive to the nsture of the gss processes in the combustion zone. If the combustion zone behaves isentropically, $o/\varepsilon \to 1/\gamma$, while it spprosches unity if the combuation zone behsves isothermally. This latter situation is often referred to as the "zero-frequency caae". Actual values of this rstio probably lie between these two extremes, varying according to conditions.

In spite of the reduced importance of o/ε to determination of the admittsnce, interest in experimentel investigation of conditions under which nonisentropic behavior sppeers has persisted. Attempts to verify nonisentropic behavior during scoustic instability have, until the present, been negative or inconclusive. In theory the isothermal case sssumes thst the flame tempersture in an oscillsting environment is constsnt. Under typical rocket motor operating conditions the fisme tempersture is relatively insensitive to pressure s., the sbove assumption would appear to be ressonably vslid. Under these conditions, successive elements of gse enter the ecoustic field with different values of entropy which is given by the equation (Ref. 37)

$$s = s_o + \varepsilon R(\sin[\omega t - \pi]), \qquad (5.3)$$

where a_o is a reference value of entropy, ϵ is the ratio of maximum pressure fluctuation to mean pressure, R is the gas constant, ω is the angular frequency of the acoustic wave, and t represents time.

Entropy variations are detected as temperature fluctuations given by the relation

$$T(x,t) = T_f\left\{1 + 2\epsilon\left(\frac{\gamma-1}{\gamma}\right)\sin\frac{\omega x}{2v_g}\cos\left(\omega t - \frac{\omega x}{2v_g}\right)\right\} \qquad (5.4)$$

where T_f is the flame temperature, x is the distance from the propellant surface, and v_g is the gas velocity (Ref. 37)

It was noted in Ref. 37 that at any instant in time there would not only be a sinusoidal temperature variation in space, with amplitude $T_f\,\epsilon\,(\gamma-1)/\gamma$, but that there would also be a time-varying temperature observed at fixed points on the burner. In addition, if one were to observe the magnitude of temperature fluctuations at various points along the burner, it would be found that the amplitude of temperature fluctuations varies with distance from the propellant surface. Maxima in the temperature fluctuation would be found at locations given by

$$x_{T',\,max} = (n + \tfrac{1}{2})\,v_g T, \qquad (5.5)$$

while the temperature fluctuation would be zero at points located at

$$x_{T',\,min} = n\,v_g T, \qquad (5.6)$$

where n represents any positive integer and T is the period of acoustic oscillation. The amplitude of temperature fluctuation (Eq. 5.5) is equal to $2\,T_f\,\epsilon(\gamma-1)/\gamma$, i.e., twice the value of the spatial temperature variation.

Equations 5.4, 5.5, and 5.6 provide a standard for comparing the foregoing theory with experimental observations. The observation of gas temperature variations as a function of space and/or time coupled with knowledge of the acoustic frequency and the gas velocity should be sufficient to verify existence of the entropy wave phenomenon. Sufficiently detailed knowledge of the relationship between the temperature fluctuations and the acoustic pressure would also permit a determination of the o/c term through the "temperature response function" as discussed in Ref. 37 and 38.

Several attempts have been made in the past to detect nonisentropic behavior but these efforts did not yield a positive result. Recent

theoretical studies indicated that the previous experiments may have failed because they were conducted at frequencies ill-suited for displaying of the phenomenon (Ref. 39). Since the NWC 5.5-in. burner was capable of operating within the frequency range of interest, it was decided to attempt to obtain evidence of nonisentropic behavior in that apparatus.

Two types of experiments were conducted: (1) a series in which photographic recording was utilized to obtain space-time records of the light intensity variations in the gas after it left the combustion zone; (2) a series in which high-speed temperature measurements was made using an adaptation of the brightness-emissivity technique. Three propellant compositions were used in the two series of experiments: (1) a bimodal polyurethane-AP composition prepared at Princeton University (designated PU in this report), and cast into metal cups, (2) a modified version of A-35 containing 0.4% NaCl which was designated A-152, and (3) A-13 propellant. Composition of these propellants appears in Table 5.1.

5.3.2. Photographic Studies

The series of photographic experiments utilized a special burner test section which was fitted with a nitrogen-flushed slit window (Fig. 5.5). An optical bench was used to mount a 70 mm streak camera and a long focal length objective lens. A cathode ray oscilloscope and mirror were arranged so that the oscilloscope screen was focused on the film plane in the camera in line with the image of the window slit image. Thus the acoustic pressure trace, which appeared on the cathode ray screen, was recorded simultaneously with the radiant intensity variations that appeared in the slit window on the burner. This arrangement permitted a detailed comparison to be made between events occurring in the burner gas and the acoustic pressure. A block diagram of the equipment arrangement used in the photographic studies is shown in Fig. 5.6.

A portion of streak camera record is shown in Fig. 5.7. The acoustic pressure and approximate position of the propellant surface have been added to the figure as an aid in interpretation. Major features of interest have been inked onto the figure to the left of the photographic record for the same reason. The photographic portion of this figure is a positive so that high and low temperature regions in the figure appear as light and dark areas respectively. Calculations from Eq. 5.5 and 5.6, based on an estimate of the mean value of the gas velocity as it leaves the propellant surface, were made in order to locate the positions of the maximum and minimum temperature variations. These are designated in the figure as T'_{max} and T'_{min} respectively. Note also that a time and distance scale are provided in Fig. 5.7 and that time runs from right to left.

Major features in the reconstructed portion of the record are identified with letters as follows:

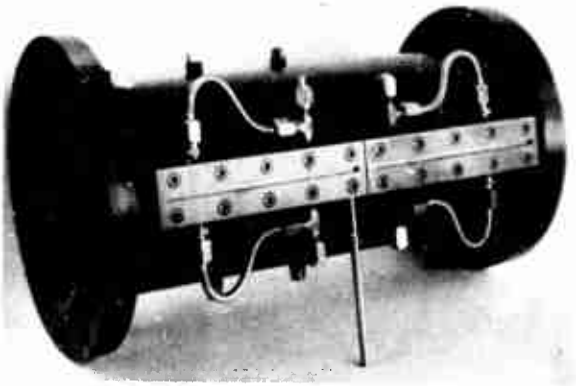

FIG. 5.5. Test Section Containing Nitrogen Flushed Slit Window Used on the 5.5-Inch T-Burner for Photographic Studies of Nonisentropic Phenomena in Low Frequency Acoustic Instability.

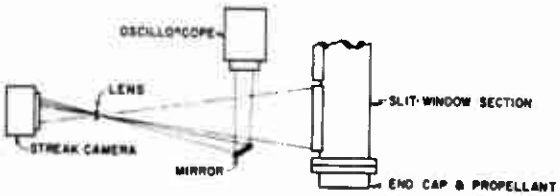

FIG. 5.6. Block Diagram of Streak Camera Arrangement Used for Photographic Study of Nonisentropic Phenomena in the 5.5-Inch Diameter Burner.

A. Periodic vertical darkened zones appear in the record which occur at times when the acoustic pressure is a minimum. These areas appear to be related to adiabatic cooling of gas throughout the burner section covered by the window caused by lowering of the acoustic pressure. (Note that there is also a general brightening at acoustic pressure maxima related to adiabatic heating from compression of the gas in the burner by the acoustic wave.)

B. Dark diagonal lines, designated "B", are relatively persistent in their travel across the section covered by the window. These represent elements of relatively cold gas which appear to have originated from the propellant surface at a time when the acoustic pressure was a minimum. This assertion of the origin of these elements of gas is

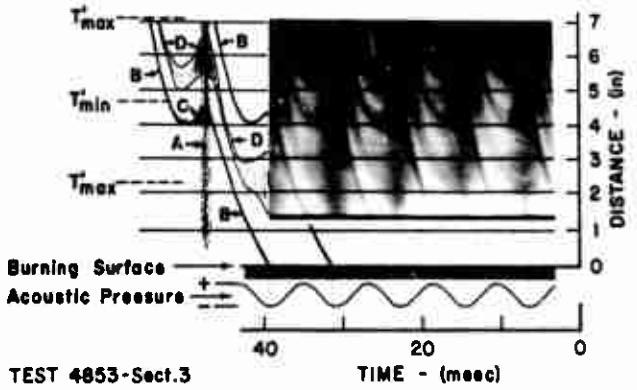

FIG. 5.7. Portion of Streak Camera Record from Test with PU Propellant. Mean burner pressure was 75 psia, acoustic pressure amplitude was 9 psi p-p, time after ignition was 2.3 sec. The position of the burning surface, the acoustic pressure, and some of the major features of the record have been reconstructed for clarity. Points of particular interest in the reconstructed portion of the record are designated by letters in the figure, with appropriate description in the text. Locations of maximum and minimum temperature fluctuations, designated T'_{max} and T'_{min} respectively, were calculated from Eq. 5.5 and 5.6.

based on an extrapolation of the information on the photographic record back to the propellant surface as indicated in the inked reconstruction to the left of the photographic portion of the figure. It was assumed in making the extrapolation that the gas velocity in the region of extrapolation is relatively unaffected by the acoustic wave. If the interpretation given here is correct, a phenomenon is present in these tests that the theory in Section 5.3.1 does not take into account.

C. Apparent inflection points occur in the motion of cold gas elements (designated "C". The photographic record suggests that a significant fluctuation occurs involving, perhaps, a momentary flow reversal. It should be noted that the theory described in Section 5.3.1 assumes uniform gas flow and does not provide for a flow perturbation of the sort indicated in the record.

D. Dark areas designated "D" represent regions of cold gas, which at any instant in time occupy a position midway between "B" elements of gas. Since these appear between areas of gas ("B" designation) which originated at acoustic pressure minima, it seems that the "D" regions are related to the entropy fluctuations referred to in Section 5.3.1.

There are several difficulties related to the above discussion. First is the problem of identification of the cold gas that appears to leave the propellant surface at an acoustic pressure minimum. The extrapolation of an element of gas back to the surface has to be done over more than an inch for which there is no photographic record. In doing the extrapolation, the assumption has been made that the acoustic velocity perturbation in this region is negligible since it is so close to the propellant surface, relative to the acoustic wavelength. Second, the film was overexposed causing a diminishing of the relative importance of cooler regions in the gss. Some of the effects of overexposure have been counteracted by printing on high-contrast material but this may have introduced further distortion of the quality of the photograph. Problems in photographic record interpretation can probably be resolved by repeating tests with altered burner parts which allow the propellant to be moved up to the end of the window and by using a camera lens with smaller aperture than was used in the first test series.

5.3.3. High-Speed Temperature Measurements

The second part of this investigation involved acquisition of high-speed gas temperature data from a region near the propellant surface. The measurement technique utilized an adaptation of the brightness-emissivity approach mentioned in Ref. 37. The apparatus is shown in Fig. 5.8 and consists of: (A) a ribbon filament lamp of known brightness temperature, (B) a syatem of lenses and slits to focus and collimate the light, (C) a rotating perforated metal wheel which periodically interrupts light from the known source, (D) a special test section which fits between the burner and an end cap containing propellant that contains two small nitrogen-flushed windows which permit light from the known source to pass through the burner, and (E) a monochromater equipped with a photomultiplier tube which receives and detects radiation in the sodium D-line portion of the optical spectrum. The photomultiplier signal was recorded on an oscillograph simultaneously with the chamber pressure. Prior to each run, the source was calibrated with a precision pyrometer and a short calibration record was obtained on the oscillograph giving the deflection due to the lamp intensity. During the test, the radiation received by the photomultiplier tube alternated between that from the flame and that of the flame plus radiation from the source. A portion of a test record is shown in Fig. 5.9.

Data reduction following a test was accomplished by making deflection measurements of the pre-run source calibration, and measuring the signal deflections from the photomultiplier and the pressure transducer over one or more cycles of oscillation at selected portions of the test. A typical plot of temperature-pressure data is shown in Fig. 5.10.

Data from selected tests appear in Table 5.2. Columns [a] through [h] represent data derived from the oscillograph recordings. Alphabetical suffixes to the test number are used to identify the portion of the test record from which the data was taken. The time at which the data

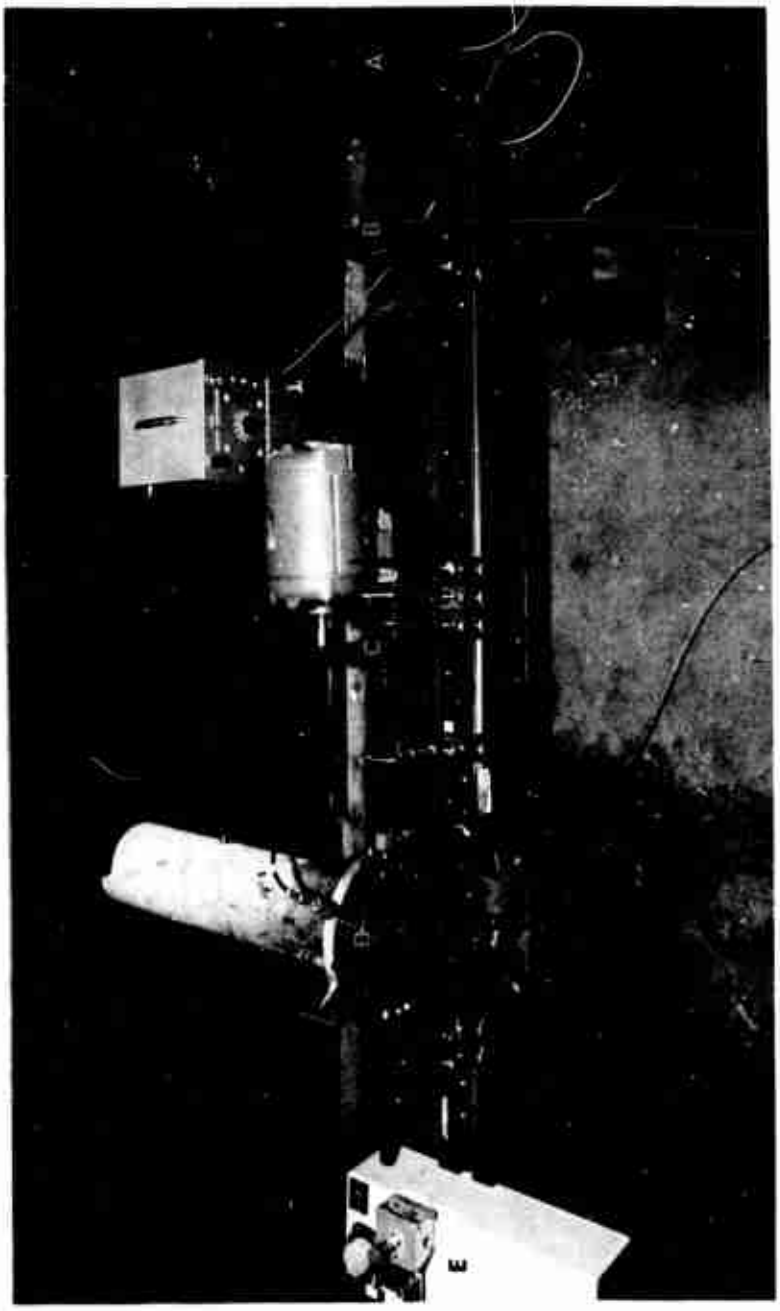

FIG. 5.8. Apparatus Used for Brightness-Emissivity Temperature Determination. Lettered items are described in the text.

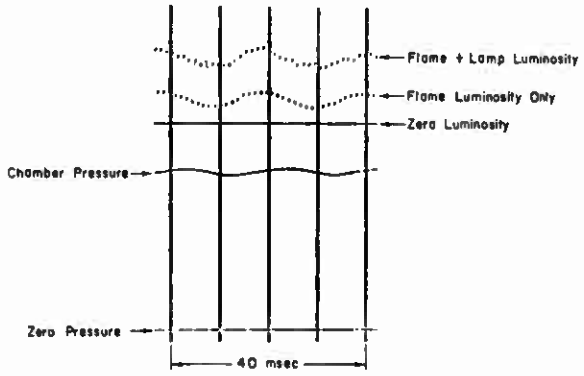

FIG. 5.9. Portion of Test Record From a Test in Which High-Speed Temperature Data was Acquired.

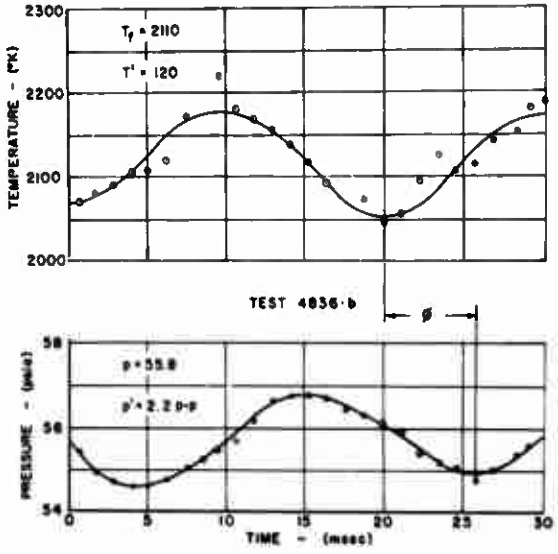

FIG. 5.10. Temperature-Pressure Data Reduced and Plotted on a Common Time Base From Test Record Similar to That Shown in Fig. 5.9.

TABLE 5-2. Pressure-Temperature Data.

Propellant type	Test no.	Time* t sec [a]	Freq f cps [b]	Pressure		Temperature		Severity of pressure oscillation ϵ [g]	Phase** ϕ fraction of cycle [h]	$\frac{\bar{T}}{\gamma}\frac{\gamma-1}{\gamma}\epsilon$ °K p-p [i]	$S\epsilon$*** °K p-p [j]
				Mean $\bar{P}$ psia [c]	Oscillation amplitude psi p-p [d]	Mean $\bar{T}$ °K [e]	Oscillation amplitude °K p-p [f]				
PU	4826A	3.81	15.0	46.5	4.95	2064	44	0.106	0.078	43.8	70.7
	4829B	2.70	37.0	53.7	5.25	2220	100	.098	− .007	43.4	75.0
A-152	4825A	2.30	14.6	44.0	10.0	2008	190	.227	− .415	91.2	48.5
	4825B	2.60	14.6	46.5	9.0	1980	155	.194	− .465	76.8	43.7
	4836C	2.73	46.0	55.95	1.97	2120	120	.039	.026	16.4	9.55
	4836B	3.38	46.0	50.80	2.20	2110	120	.039	.262	16.6	10.67
	4837B	2.26	52.5	68.0	1.23	2130	135	.018	.105	7.70	5.97
A-13	4832A	2.88	81.0	26.7	1.3	2188	100	.049	− .062	21.3	.....
	4832B	3.18	78.7	27.5	2.4	2165	165	.087	− .061	37.8	.....

* Time at which data is taken.

** Phase of temperature fluctuation relative to the pressure fluctuation. Negative sign indicates a temperature lag.

*** S = sensitivity of temperature to pressure. $S = 14.3°K/psi$ for PU propellant and $S = 4.85°K/psi$ for A-152 propellant.

was taken appears in column [a] and is the time elapsed after ignition. Frequency was determined by measurement of the oscillograph record (column [b]) while the pressure and temperature data were obtained from plots similar to that shown in Fig. 5.10. Column [g] was calculated by taking the ratio of the pressure oscillation amplitude to the mean pressure. The phase between temperature and pressure (column [h]) waa computed from measurements of the pressure-temperature plots (as in Fig. 5.10). Columns [i] and [j] are computed temperature fluctuations thst will be discussed in some detail below.

In general, the tabulsted pressure-temperature data show quite a diversity of behavior. The A-152 data represent the most comprehensive complilstion of information available at preaent, but the question of whether the data fits a consistent pattern must await completion of the data analysis. One outstanding feature, for which there is no explanation at present, is the surprisingly high amplitude of temperature oscillation observed in the testa above 40 cps. A comparison of observed temper_ture fluctuation amplitude with calculated amplitudes, baaed on two rather different assumptions suggests that neither of the explanations for the temperature oscillations advanced so far can explain what is observed in the burner. The first comparison is with the temperature fluctuation predicted on the assumption thst the gas in the burner behaves isentropically. This assumption leads to the calculated temperaturea entered in column [i]. Comparison of the isentropic calculation and the observed temperature oscillations indicatea the increaaed difference between the isentropic prediction and the observed vslues. If the assumptions of Section 5.3.1 were valid, the observed temperature oscillation amplitude would not exceed the isentropic value by more than a fsctor of two. As one can aee, the observed amplitudes from tests with frequencies above 40 cpa far exceed the expected range.

Another fscet of the temperature oscillations was considered, namely the effect of a fluctuating flame temperature. It was noted, in comparing mean temperature and mean pressure from PU snd A-152 data, that the temperature was a function of pressure. The dependence of temperature on pressure for these two propellants is indicated in Fig. 5.11. Assuming that the temperature follows the presaure oscillations in the ssme manner as indicated in Fig. 5.11, one can aasign a sensitivity of temperature to pressure which can be used to compute the tempersture oscillation caused by an observed pressure fluctuation. Computations based on the above aaaumptions are entered in column [j] of Table 5.2 and the temperature sensitivity for the two propellants appeara in a footnote in that table. Compariaon of the obaerved and computed dsts indicatea a large disparity and that the temperature senaitivity to pressure does not offer an adequate explanation of the large temperature oscillations observed at the higher frequenciea.

A detailed report is in preparation which describes the photographic and high-apeed temperature measurementa in greater detail. The in formation will be released as a NWC report when completed.

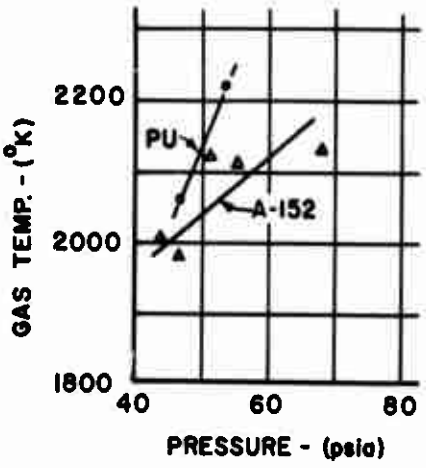

FIG. 5.11. Plot of Measured Mean Gas Temperature and Mean Pressure for PU and A-152 Propellants.

5.3.4. A New Mathematical Model

Detailed interpretation of the streak photography and the temperature data is hampered by presence of phenomena not accounted for in existing theories. It was felt that a mathematical model could be devised which would account for a variable flame temperature and nonuniform flow of gases. Steps in that direction were taken late in the report period.

A new theory is presented here which describes the history of a gas particle from the time it leaves the reaction zone as a function of a parameter ψ which denotes the phasing of the pressure and velocity fields at the emergence of the particle from the combustion zone.

The oscillating components of pressure and velocity were treated as first order perturbation quantities and since the amplitude of the oscillating component of velocity was of the order of the mean velocity, a point clearly shown by the evidence of flow reversal in some of the photographic test records, the nonconvective wave equation was used to describe the acoustic fields. Pressure antinodes at each end of the chamber were used as boundary conditions with the resulting oscillating pressure and velocity fields given by

$$p' = \overline{p}\, \varepsilon \cos(\pi x/L) \cos(\omega t + \psi) \qquad (5.5)$$

and

$$v' = \bar{V} \sin (\pi x/L) \sin (\omega t + \psi) \tag{5.6}$$

respectively. In Eq. 5.5 and 5.6 $\bar{p}$ is the mean pressure, ϵ is the ratio of the maximum value of the pressure perturbation to mean pressure, $\bar{V}$ is the velocity amplitude, x is the distance from the reaction zone and L is the T-burner length. The particle velocity is given by

$$v = \bar{v} + v' \tag{5.7}$$

and the relationship between temperature and pressure given by

$$\frac{T'}{T_r} = \left(\frac{\gamma-1}{\gamma}\right) \frac{p - p_r}{p_r} \tag{5.8}$$

in which p_r was the pressure at a reference plane immediately outside of the flame when the particle in question entered the acoustic field and T_r is the temperature at the reference plane, which is assumed to be constant for this discussion. The reference pressure given by

$$p_r = \bar{p} + \bar{p}\epsilon \cos \psi \tag{5.9}$$

was obtained by adding the mean pressure $\bar{p}$ to the acoustic pressure with x and t set equal to zero. The following expression for relative temperature

$$\frac{T}{T_r} \equiv \frac{T' + T_r}{T_r} =$$

$$1 + \left(\frac{\gamma - 1}{\gamma}\right) \epsilon \left[\frac{\cos (\pi x/L) \cos (\omega t + \psi) - \cos \psi}{1 + \epsilon \cos \psi}\right] \tag{5.10}$$

was obtained by substitution of Eq. 5.7 and 5.9 into Eq. 5.8. In order to evaluate T/T_r it is necessary to determine the relationship between x and t for a given ψ. This is readily obtained from the relation

$$x = \int v \, dt = \int_0^t \left[\bar{v} + \bar{V} \sin \left(\frac{\pi x}{L}\right) \sin (\omega t + \psi)\right] dt \tag{5.11}$$

Solution of Eq. 5.11 thus gives the trajectory of a gas particle leaving the surface at time zero for the assumed boundary conditions and phase angle ψ. Equations 5.10 and 5.11 together give the temperature history and the trajectory of a gas particle subsequent to leaving the surface as a function of the parameter ψ.

Additional steps in modifying the analysis to provide a more adequate description of significant parameters in the problem of nonisentropic behavior need to be undertaken. These include replacing the rigid solid boundary condition at the combustion zone with an acoustic admittance and replacing the constant flame temperature with one which is pressure sensitive.

It is planned to present solutions of the equations in the form of dimensionless plots. With these available, particle trajectories and constant temperature lines may then be superimposed on experimental test records, the phase angle ψ being readily obtained from the pressure record. The relative brightness patterns in the streak data will then provide a qualitative test of the mathematical model.

5.4. SUMMARY

Tests to determine range of unstable combustion behavior on one metallized and two unmetallized propellants were accomplished prior to more definitive testing. It is anticipated that extensive response function testing on the two unmetallized compositions will be accomplished in the near future.

Preliminary testing with a pressed AP-Al composition in the 5.5-inch diameter T-burner demonstrated the feasibility of using such materials in investigating the role of metal combustion in preferred-frequency instability.

Investigation of nonisentropic behavior in the low frequency range revealed that, under the conditions tested, the flame temperature may fluctuate significantly with the acoustic pressure. While it appeared that the flame temperature of two of the propellants tested was a function of the mean pressure, the resulting temperature variation was not large enough in many cases to explain the observed temperature fluctuations. The magnitude of the temperature oscillations and the evidence from the photographic records strongly suggested that factors other than those discussed above were involved. One plausible, but as yet unevaluated, explanation was that the binder and oxidizer were consumed at different rates which vary over a cycle of pressure oscillation, resulting in a fluctuation in the fuel-to-oxidizer ratio.

The observations of nonisentropic behavior strongly suggested that present mathematical models which seek to describe unstable combustion may need additional refinements in order to accurately describe the phenomena that appear to be involved.

6. SUMMARY

Each of the preceding sections contains its own extensive discussion, and the major accomplishments of each section are summarized here in order to provide a comprehensive view of the entire program.

6.1. DECOMPOSITION AND DEFLAGRATION OF AMMONIUM PERCHLORATE

Past and current work has shown that the physical character of the surface residue of AP is significantly dependent on the imposed heating rate. Ammonium perchlorate apparently sublimes under conditions of isothermal decomposition and there is no evidence of a surface melt; under conditions of rapid heating such as burning in a methane atmosphere, a surface melt is observed on the AP; and in the case of self-sustaining deflagration, the surface melt is frothy due to the entrapment of transpiring gases. This frothy melt is probably the site of the major heat release necessary to sustain deflagration.

6.2. BENAVIOR OF ALUMINUM IN COMPOSITE PROPELLANTS

Current work has indicated that an important step in the aluminum agglomeration (sintering together) process is characterized by the fracture of the aluminum oxide coating (below its melting point) due to stress produced by the differential thermal expansion of aluminum and aluminum oxide as the particles are heated by the combustion wave and oxidative self-heating. Molten aluminum flows through the cracka, joins with adjacent particles and is oxidized, thus forming aluminum/aluminum oxide particles. By including this important step of the agglomeration process, it is possible to give a detailed, qualitative description of the behavior of aluminum in composite propellants from the unheated condition in the propellant to the condition of molten balls of aluminum with oxide "caps" burning by a vapor transport mechanism in the gas phase above the propellant surface.

6.3. NONACOUSTIC COMBUSTION INSTABILITY

Two analytical modela of solid propellant combustion instability applicable to the low frequency regime have been reduced to a common notation, were found to be numerically identical, and have been compared with experimental data. Only qualitative agreement between experimental data and model predictions was found, and even then several large

discrepancies were discovered. One discrepancy associated with the heterogeneous nsture of the propellant was experimentally explored in detail. A simple, phenomenological argument relating oscillation frequency to oxidizer particle size was developed and, when applied in conjunction with the analytical models, was found to be useful in interpreting the experimental data.

6.4. ACOUSTIC INSTABILITY

Experiments with pressed AP-Al material in the NWC 5.5-inch T-burner indicate that auch material can be successfully used to investigate the interaction of acoustic waves with spontaneously occurring combustion oscillstions.

Investigation of nonisentropic behavior has shown that pehnomena were involved which were not considered in presently svsilsble mathematical models. Experimental information acquired during this report period indicated that flame temperature variations and gas velocity perturbations were of the same order of importance as the temperature fluctuations induced by variations in entropy. Steps were initiated to synthesize a more relevant mathematical model which will include consideration of nonuniform gaa velocity and a variable flame tempersture, as well as improvements in the methods of obtaining experimental measurements.

Appendix A

BURNING RATE DATA AND TABULAR EXPERIMENTAL DATA OBTAINED WITH RESPECT TO NONACOUSTIC COMBUSTION INSTABILITY

TABLE A-1. Data Obtained With A-146 Propellant.

Run no.	L*, in	Frequency, cps	Pressure, psia	Burning rate in/sec	Growth constant, sec^{-1}	τ_{ch}, msec	Dimensionless frequency $\frac{a_f \omega}{r^2}$	$\omega\tau_c$	Phase shift radians	Real part of the response function
906	20	168	168	.162	.....	.850	7.3	.897	.....	.....
	32	55	195	.168	.....	1.360	2.2	.469	.....	.....
907	18	162	145	.154	.....	.765	7.8	.777	.....	.....
	44.8	.....	158	.159	.....	1.904	.....	.....	.....	.....
908	15.9	165	141	.153	97.3	.676	8.0	.699	.580	1.07
	17.1	150	148	.155	114	.727	7.1	.684	.563	1.08
	19	131	153	.157	39.1	.808	6.1	.661	.570	1.03
	21	131	153	.157	−37.8	.893	6.1	.731	.647	.936
910	14.6	172	121	.144	113	.621	9.5	.669	.559	1.07
	16.1	150	130	.148	54.3	.684	8.3	.679	.578	1.04
	18.5	133	131	.149	36.7	.786	6.8	.655	.567	1.03
	24.2	104	130	.148	.....	1.029	5.4	.671	.....	.....
899	45	56	95	.129	27.2	1.913	3.8	.671	.568	1.05
901	13.8	171	115	.141	.....	.587	9.8	.629	.....	.....
	15.1	165	125	.1465	55.5	.642	8.8	.665	.571	1.04
	16.8	133	125	.1465	70	.714	7.1	.594	.515	1.05
912	14.0	158	120	.143	80.5	.595	8.9	.590	.513	1.05
	15.1	148	125	.1465	85	.642	7.9	.595	.513	1.05
	16.5	139	127	.147	61.8	.701	7.3	.612	.531	1.04
	18.9	127	124	.146	38.5	.803	6.8	.642	.557	1.03
	23.5	105	121	.144	.....	.999	5.8	.659	.....	.....
	28.6	97	122	.145	.....	1.216	5.3	.739	.....	.....
914	12.4	160	98	.131	139	.527	10.7	.529	.458	1.07
	13.0	162	105	.135	126	.553	10.2	.562	.483	1.07
915	14.1	148	102	.133	95	.599	9.6	.555	.483	1.06
	15.8	128	106	.136	96	.672	7.9	.539	.468	1.07
916	23.6	100	93	.127	67	1.003	7.1	.628	.532	1.07
	26.2	98	101	.133	53.3	1.114	6.3	.683	.573	1.06
917	29.3	83	98	.131	*45.8	1.245	5.5	.648	.550	1.06
918	39.2	72	96	.130	−17.5	1.666	4.875	.753	.660	0.97
	42.4	58	85	.122	− 5.3	1.802	4.450	.655	.584	1.00

TABLE A-1. (Contd.).

Run no.	L*, in	Frequency, cps	Pressure, psia	Burning rate in/sec	Growth constant, sec^{-1}	τ_{ch}, msec	Dimensionless frequency $\frac{a_t \omega}{\dot{r}^2}$	$\omega\tau_c$	Phase shift radians	Real part of the response function
919	16.9	117	101	.133	59.2	.718	7.573	.527	.468	1.04
	18.6	111	106	.136	48.8	.791	6.875	.550	.487	1.04
	20.6	102	104	.134	67.4	.876	6.50	.559	.486	1.06
920	15.0	140	90	.126	51	.638	10.08	.560	.497	1.03
	20.5	127	97	.130	85	.871	8.60	.695	.574	1.07
	23.7	128	100	.132	46.8	1.007	8.40	.810	.659	1.05
921	28.5	95	101	.133	91.8	1.211	6.15	.723	.577	1.12
922	23.5	91	95	.129	51.5	.999	6.25	.570	.497	1.05
	26.2	84	97	.130	54.7	1.114	5.675	.586	.504	1.06
923	27.9	75	88	.124	33.6	1.186	5.575	.558	.493	1.04
	31.8	79	95	.129	35.5	1.352	5.425	.668	.568	1.10
	36.5	65	92	.127	31.9	1.551	5.25	.720	.599	1.05
925	46.4	52	87	.1235	.....	1.972	3.90	.643	.....	.....
	50.7	44	90	.126	.....	2.155	3.175	.596	.....	.....
	54.1	46	90	.126	.....	2.299	3.3	.660	.....	.....
	58.3	42	83	.120	20.7	2.478	3.325	.650	.554	1.05
	58.3	42	83	.120	−18.2	2.478	3.325	.650	.597	.95
927	23.0	80	84	.121	39.8	.978	6.25	.490	.441	1.04
	24.3	80	90	.126	45.5	1.033	5.75	.522	.462	1.05
928	27.2	65	81	.1185	57.2	1.156	5.30	.471	.416	1.06
	34.9	66	87	.1235	32.6	1.483	4.95	.614	530	1.05
929	45.3	49	84	.121	18.7	1.925	3.825	.591	.519	1.04
	45.3	49	84	.121	−17.7	1.925	3.825	.591	.549	0.98
930	73.8	34.5	76	.114	−18.2	3.137	3.025	.675	.621	0.94
956	~35	63	70	.109	.....	1.49	6.075	.588	.....	.....
957	~53	48	65	.104	.....	2.25	5.075	.686	.....	.....
958	~85	.....	63	.1025	.....	.....	.....	.....	.....	.....
960	~48	45	60	.0995	.....	2.04	5.2	.576	.....	.....
	~55	33	62	.1015	.....	2.34	3.675	.485	.....	.....
962	~81	28	65	.104	.....	3.44	2.950	.602	.....	.....

TABLE A-2. Data Obtained With A-148 Propellant.

Run no.	L*, in	Frequency, cps	Pressure, psia	Burning rate in/sec	Growth constant, sec^{-1}	τ_{ch}, msec	Dimensionless frequency $\frac{a_f \omega}{\bar{r}^2}$	$\omega\tau_c$	Real part of the response function
1001	19	150	114	.116	.....	.806	13.2	.759	.....
	20.1	125	114	.116	.....	.855	11.0	.671	.....
	23.2	127	115	.117	66.2	.98	11.2	.781	1.07
	23.8	119	113	.116	57.2	1.01	10.5	.754	1.06
	24.9	116	111	.115	36.0	1.06	10.4	.772	1.04
	27.2	108	108	.115	22.3	1.16	9.76	.786	1.03
	31.3	100	105	.113	0	1.33	9.23	.835	1.00
	32.7	98	104	.113	0	1.39	9.04	.855	1.00
	40.2	73	90	.107	28.7	1.71	7.56	.783	1.05
1002	25	100	81	.102	.....	1.06	11.4	.666	.....
	25.6	~100	85	.105	.....	1.09	11.0	.686	.....
	26.5	97	85	.105	.....	1.13	10.7	.688	.....
	27.1	87	82	.103	.....	1.15	9.39	.628	.....
	28.2	91	84.5	.105	.....	1.20	9.99	.685	.....
	28.5	89	84	.104	.....	1.26	9.78	.704	.....
	30.6	85	86	.106	.....	1.30	8.70	.694	.....
	32.2	80	83	.103	.....	1.37	8.48	.688	.....
	33.6	81	80	.102	.....	1.43	9.47	.728	.....
	35.0	80	80	.102	.....	1.49	9.34	.748	.....
1003	33	72	70	.0955	.....	1.42	9.49	.642	.....
	36.6	.....	70	.0955	.....	1.56	.....	.....	.....
	40.2	.....	65	.0915	34.3	1.71	.....	.....	1.06
	45	57	67	.0935	27.2	1.91	7.70	.684	1.05
1124	17.5	115	91	.107	.....	.74	11.5	.534	.....
	18.2	120	94	.108	.....	.78	11.8	.588	.....
	19	110	93	.108	.....	.81	10.8	.560	.....
	19.7	120	93	.108	.....	.83	11.8	.626	.....
	20.7	.....	94	.108	.....	.88	.....	.....	.....
	22	.....	94	.108	.....	.94	.....	.....	.....
1125	28.1	80	82	.104	.....	1.20	8.48	.602	.....
	29.8	80	94	.108	84.0	1.27	7.83	.638	1.11
	33.8	87	97	.109	29.2	1.43	8.35	.781	1.04
	40.6	75	94	.108	25.8	1.73	7.35	.815	1.05
1126	44.7	71	94	.108	19.0	1.90	6.96	.847	1.04
1127	19	100	103.5	.113	28.2	.809	8.92	.508	1.02
	22	110	107.5	.113	5.2	.94	9.81	.650	1.01
	25.9	105	105.0	.112	−16.2	1.10	9.56	.725	.98
1128	18.3	115	107	.115	.....	.78	9.89	.563	.....
	20.4	133	117	.117	76.7	.87	11.1	.726	1.07
	25.3	~ 6.7	120	.118	0	1.07	.55	.045	1.00
1129	50.7	72	93.5	.110	.....	2.16	6.78	.976	.....

TABLE A-2. (Contd.).

Run no.	L*, in	Frequency, cps	Pressure, psia	Burning rate in/sec	Growth constant, sec^{-1}	τ_{ch}, msec	Dimensionless frequency $\frac{\alpha_t \omega}{r^2}$	$\omega\tau_c$	Real part of the response function
A-148A (different burning rate)								.050	
1215	32-39	~ 5.8	265	~.17	~ 0	1.36-1.66	.23	.060	~1.0
1216	28	~16	270	~.17	~ 0	1.19	.63	.119	~1.0
1217	18.0	170	120	.15	31.0	.76	8.65	.812	1.02
	22.2	143	123	.152	−24.3	.94	7.09	.844	.98
	35.2	18.5	120	.15	low amp.	1.50	.94	.174	.....
	~45	62	92	.135		1.91	3.89	.743	.....
1218	14.1	140	94	.135	+	.60	8.79	.527	.....
	14.5	179	109	.144		.62	9.89	.697	.....
	15.7	175	108	.143	~81	.67	9.78	.736	~1.05
	18.1	135	111	.145	~76	.77	7.38	.653	~1.06
	20.7	133	110	.145	~70	.88	7.26	.735	~1.06
	24.1	134	106	.142	~58	1.02	7.58	.859	~1.06
	27.0	117	101	.139	~65	1.15	6.91	.845	~1.08
	30.3	108	96	.137	~57.5	1.29	6.58	.875	~1.07
	33.7	100	93	.135	.....	1.43	6.28	.898	.....
1219	29	133	116	.147	~ 0	1.23	7.01	1.027	1.00
	37	~ 9.5	108	.143	low amp.	1.57	~ .53	~094	.....
	45	72	94	.135	28.2	1.91	4.53	.865	1.05
	48.7	62	84	.128	41.5	2.07	4.36	.814	1.06
1220	50.1	60	76	.121	~68.5	2.13	4.67	.803	1.15
1221	53.4	47	68	.115	.....	2.27	4.04	.670	.....
	57.1	46	71	.117	33.7	2.43	3.84	.702	1.08
	60.5	50	65	.112	44.0	2.57	4.55	.807	1.11
1222	38.5	42	77	.121	~33.0	1.64	3.24	.428	~1.05
1225	28.6	101	87	.130	51.0	1.22	6.86	.775	1.06
	35.5	93	86	.129	46.0	1.51	6.37	.882	1.07
	44.4	91	88	.130	47.5	1.89	6.17	1.079	1.09

TABLE A-3. Data Obtained With A-149 Propellant.

Run no.	L*, in	Frequency, cps	Pressure, psia	Burning rate in/sec	Growth constant, sec^{-1}	τ_{ch} msec	Dimensionless frequency $\frac{a_g \omega}{\dot{r}^2}$	$\omega\tau_c$	Real part of the response function
1016	106.3	10.8	68	.064	.....	4.51	3.0	.306	.....
	116	10.7	69	.064	.....	4.93	3.0	.332	.....
1019	41	30	130	.084	.....	1.74	4.86	.328	.....
	54.5	23.4	150	.089	.....	2.32	3.38	.341	.....
	61.4	20	158	.091	.....	2.61	2.77	.328	.....
	64.4	27.3	158	.091	.....	2.74	3.78	.470	.....
1020	57.5-107	.....	151.5	.089	.....	2.42-4.52	.....	.....	.....
1021	35	18.8	108	.077	.....	1.49	3.64	.176	.....
	37.7	25	110	.078	.....	1.60	4.7	.251	.....
1022	60	20	103	.075	.....	2.55	4.07	.321	.....
1023	70.3	13.3	55	.058	5.42	2.99	4.5	.249	1.04
	89	13.2	58	.059	−4.46	3.78	4.45	.314	.98

TABLE A-4. Data Obtained A-151 Propellant.

Run no.	L^*, in	Frequency, cps	Pressure, psia	Burning rate in/sec	Growth constant, sec^{-1}	τ_{ch} msec	Dimensionless frequency $\frac{a_p \omega}{\gamma^2}$	$\omega\tau_c$	Real part of the response function
1074	56.5	72	101.5	.118	50	1.55	5.9	.700	1.08
1078	21.9	77.0	77	.105	40.8	1.55	8.0	.650	1.06
	29.4	72.0	76.5	.105	.....	1.68	7.5	.770	.....
1080	35.0	47.6	75.0	.104	48.2	1.48	6.60	.442	1.07
1100	24.5	34.5	65.0	.097	.....	1.04	6.60	.356	.....
	34.9	30	68.5	.099	40.9	1.48	5.82	.465	1.05
1101	45.3	40	61.5	.093	.....	1.92	5.3	.482	.....
	51.3	37	65.5	.095	24.5	2.18	4.65	.507	1.05
	57.5	56.5	58.5	.090	58.6	2.44	5.15	.560	1.07
1103	69.7	33.5	58.5	.090	41.6	2.96	4.7	.620	1.12
	78.3	28.5	57.5	.090	21.2	3.33	4.0	.596	1.07
1104	93.2	22	53.5	.086	19.1	3.96	3.94	.548	1.08
1107	14.2	50	75	.104	.....	0.60	5.29	.188	.....
	15.6	55	76	.105	.....	0.66	5.72	.228	.....
	17.0	50	77	.105	.....	0.72	5.19	.226	1.02
	23.4	44	73.5	.103	23.8	0.99	4.74	.274	.....
	34.9	42	71.0	.100	12.8	1.48	4.90	.400	1.00
1115	44.1	40	70.3	.100	~0	1.87	4.56	.470	.....
	50.4	38	68.5	.099	~0	2.14	4.45	.511	.....
	59.3	51.5	65.5	.097	17.0	2.52	3.82	.499	1.04
1117	29.2	50	63.5	.099	23.5	1.24	5.83	.390	1.04
	33.2	55	66.5	.099	34	1.41	6.43	.487	1.07
	41	50	70.3	.103	50	1.74	5.4	.547	1.09
1132	19.6	80	106	.125	~0	0.83	5.85	.417	.....
	44.4	40	72.5	.104	16.8	1.88	4.22	.473	1.02
1133	18.5	66.5	94.0	.120	36.3	0.78	5.28	.334	1.02
	23.1	11.8	97	.120	~0	0.98	0.94	.0726	.....
	24.3	70	95	.119	~0	1.03	5.65	.453	.....
1135	44.9	36.1	54.5	.089	.....	1.91	5.30	.433	.....
	50.8	36	56.5	.090	25.5	2.16	5.08	.488	1.05
1142	.....	47	15.5	~.030	.....	.....	59.6	.....	.....
1144	25	40	71.5	.105	15.4	1.06	4.32	.267	1.02
	29.5	45	68.5	.100	.....	1.56	5.13	.356	.....
1145	34.2	44.6	57.5	.093	40	1.45	5.87	.404	1.04
	38.1	42.8	59.5	.094	14.6	1.62	5.55	.436	1.02
1144	59.6	27.2	52.5	.088	14.2	2.34	3.84	.434	1.04
	.....	55.6	18.5	~.036	.....	.....	49.2	.....	.....
1134	60.8	29.5	51.0	.086	.....	2.58	4.55	.478	.....
1172	61	31	47.5	.075	.....	2.58	6.28	.502	.....
1173	85	25	45	.072	.....	3.60	5.50	.566	.....
1178	16.5	80	86	.104	23	0.70	8.12	.352	1.02
	18.2	70	105	.125	~0	0.77	5.12	.339	.....
	24.6	15	117	.133	~0	1.04	0.97	.098	.....
1179	20.3	67	75.5	.099	.....	0.86	7.80	.363	.....
	21.3	59	73.5	.098	.....	0.90	7.05	.334	.....
	25.7	53.5	80	.102	8.8	1.09	5.88	.366	1.01
	27.6	48.5	85.5	.105	-19.4	1.17	5.05	.356	1.00
	42.2	43	76.0	.100	18.5	1.79	4.93	.484	1.03
	46.5	42	33.5	.060	.....	1.97	19.67	.768	.....

TABLE A-5. Data Obtained With A-155 Propellant.

Run no.	L*, in	Frequency, cps	Pressure, psia	Burning rate in/sec	Growth constant, sec^{-1}	τ_{ch}, msec	Dimensionless frequency $\frac{\alpha_1 \omega}{\bar{r}^2}$	$\omega\tau_c$	Real part of the response function
1165	18.2	83	87.5	.092	57.6	.772	11.72	.402	1.04
	20.8	62	83.5	.090	38.4	.885	9.15	.344	1.03
	21.7	57	80.5	.087	−21.2	.935	8.60	.331	.98
	24.5	50	90.5	.093	8.6	1.04	6.62	.327	1.01
	26.6	50	85.0	.090	.....	1.13	6.12	.355	.....
	28.6	50	88.0	.092	− 8.8	1.22	6.9	.383	.99
	45.6	42	79.5	.087	21.8	1.94	6.50	.512	1.04
1166	31.2	40	76.5	.085	27.5	1.32	6.48	.331	1.04
	40.6	41.5	73.5	.082	36.0	1.73	7.08	.451	1.06
	47.6	37.0	73.5	.082	24.1	2.02	6.30	.469	1.05
1167	69.1	30.0	68.5	.079	16.1	2.94	5.32	.553	1.05
	75.8	29.8	62.5	.075	.....	3.22	6.06	.602	.....
1168	53.7	32.3	72.5	.082	16.1	2.28	5.5	.463	1.04
	65.3	30.8	67.5	.079	22.7	2.78	5.36	.537	1.06
1170	33.8	40	83.5	.090	−24.7	1.43	5.91	.359	.97
	59.5	29	75.0	.084	28.3	2.53	4.82	.460	1.07
1188	82	33.3	78.5	.086	.....	3.48	5.14	.727	.....
	96.4	33.3	77.5	.085	.....	4.1	5.26	.857	.....
	101.6	32	78.5	.086	.....	4.33	4.95	.870	.....
1189	58.2	29.0	81.5	.087	.....	2.47	4.37	.450	.....
	66.0	26.7	77.5	.085	29.3	2.80	4.25	.470	1.07
	69.4	25.3	80.5	.087	.....	2.94	3.80	.467	.....
1190	87.4	22	80.5	.087	.....	3.72	3.32	.513	.....
1191	112	22	71	.081	.....	4.75	3.82	.656	.....
1203	23.4	55.6	109.0	.105	.....	1.02	5.76	.356	.....
	43.5	3.9	110.5	.106	.....	1.85	.39	.045	.....
1205	72	28.5	67.5	.079	.....	3.06	5.25	.542	.....
	76	26.8	64.0	.076	26.0	3.24	5.30	.544	1.08
1206	112	20	53.5	.069	−15.3	4.67	4.80	.588	.93
	118	19.6	53.5	.069	26.2	4.92	4.71	.605	1.13
	125	20	58.5	.073	.....	5.3	3.13	.668	.....
1226	24.1	52	92	.096	−54.8	1.025	6.45	.335	.94
	39.4	2.67	100.5	.101	.....	1.67	.30	.028	.....
1232	20.8	56.0	83.5	.090	−41	.885	7.90	.312	.96
	24.7	55.0	88.0	.094	−32	1.05	7.10	.370	.96
	31.0	54.5	91.5	.095	.....	1.32	6.90	.451	.....
	45.9	3.0	97.5	.099	.....	1.95	.35	.037	.....
	53.0	34.9	86.2	.092	.....	2.25	4.7	.493	.....

TABLE A-6. Data Obtained With A-156A Propellant.

Run no.	L*, in	Frequency, cps	Pressure, psia	Burning rate in/sec	Growth constant, sec^{-1}	τ_{ch} msec	Dimensionless frequency $\frac{a_p \omega}{r^2}$	$\omega\tau_c$	Real part of the response function
1227	55	15	175	.144	.....	2.34	.825	0.220	.....
1229	50.8	40	64	.105	.....	2.16	4.15	.543	.....
1238	25	115	68.5	.108	71.5	1.06	11.3	.766	1.08
	35	100	73.5	.109	35.0	1.49	9.65	.936	1.05
1241	30.4	71	57.5	.102	.....	1.29	7.80	.575	.....
	32.5	77	58.5	.102	.....	1.38	8.45	.667	.....
	34.0	67	57.0	.100	.....	1.44	7.65	.606	.....
	34.7	67	57.5	.101	.....	1.47	7.50	.619	.....
	35.4	71	58.5	.102	.....	1.50	7.80	.669	.....
1242	36	85	34	.072	.....	1.53	18.8	.817	.....
1243	55	64	34	.072	.....	2.34	14.2	.941	.....
1254	120	13	152	.140	~0	5.1	.755	.416	1.0
1255	86-124	.....	189	.145	.....	3.66-5.27	.....	.....	.....
1256	159	14	104	.123	.....	6.76	1.06	.594	.....
1257	19	97	116	.127	.....	.808	5.05	.492	.....
	20-33	14	120	.128	.....	.850-1.40	.975	.075-.124	.....
1258	42	.....	118	.127	.....	1.79	.....	.....	.....
1259	40.3	42.3	73	.108	22.6	1.71	4.15	.454	1.04
	44.0	43.5	70	.107	−13.7	1.87	4.35	.511	0.97
	46.4	44.5	69	.107	~0	1.97	4.45	.551	1.0
1260	56-75	.....	80	.110	.....	2.38-3.19	.....	.....	.....
1262	15.7	50.0	76	.109	+	.57	4.80	.210	.....
	16.1-19.0	50.6	76	.109	~0	.68-.80	4.85	.216-.254	1.0
	20.7	40.0	71	.108	9.9	.88	3.92	.221	1.01
	21-25	45.5	72	.108	22.6	.89-1.06	4.45	.254-.303	1.02
1263	19.3	95	108	.125	46.4	.82	6.95	.489	1.04
	43.4	57	85	.111	27.8	1.85	5.30	.662	1.05
	44.5	43.5	78	.110	~0	1.89	4.11	.516	1.00
1264	18.0	85.6	110	.125	.....	.77	6.27	.414	.....
	19.0	88.4	109	.125	.....	.81	6.43	.450	.....
	20.0	83.5	110	.125	.....	.85	6.11	.446	.....
1265	73.7	32.2	60	.101	.....	3.13	3.62	.633	.....
	87	29.4	66	.106	.....	3.70	3.00	.683	.....

TABLE A-6. (Contd.).

Run no.	L*, in	Frequency, cps	Pressure, psia	Burning rate in/sec	Growth constant, sec^{-1}	τ_{ch}, msec	Dimensionless frequency $\frac{\alpha_t \omega}{r^2}$	$\omega\tau_c$	Real part of the response function
1266	90.1	14.3	66	.106	.....	3.83	1.46	.344	.....
	94.0	14.3	66	.100	.....	4.00	1.46	.359	.....
	104.0	19	66	.106	.....	4.42	1.94	.527	.....
	107.6	15.4	61	.102	.....	4.57	1.69	.442	.....
1267	26	73.5	94	.116	27.6	1.10	6.25	.508	1.03
	27.6	60.4	90	.115	40.0	1.17	5.23	.444	1.05
1268	51.5	25.6	61	.101	0	2.19	2.87	.352	1.00
	55.4	40.0	74	.108	22.5	2.35	3.94	.590	1.05
1269	80.9	42.9	78	.109	.....	3.44	4.12	.927	.....
1270	17	92	106	.124	.....	.72	6.84	.416	.....
	19	87.6	105	.123	28.6	.81	6.62	.446	1.02
1270B	37	13.4	114	.126	.....	1.57	.965	.132	.....
	40	16.6	119	.128	.....	1.70	1.16	.177	.....
	44	14.3	141	.136	.....	1.87	.885	.168	.....

TABLE A-7. Data Obtained With A-157 Propellant.

Run no.	L*, in	Frequency, cps	Pressure, psia	Burning rate in/sec	Growth constant, sec^{-1}	τ_{ch}, msec	Dimensionless frequency $\frac{a_t\omega}{\bar{r}^2}$	$\omega\tau_c$	Real part of the response function
1159	31.9	46	76	.117	27.3	1.36	3.84	.393	1.037
1161	53	33	69.5	.110	.....	2.25	3.12	.466	.....
1163	24.1	62.5	73.5	.115	.....	1.02	5.40	.401	.....
	25.9	70.0	83.5	.120	.....	1.10	5.56	.484	.....
1194	30	47	93.5	.120	31.5	1.28	3.73	.378	1.04
1197	27.1	51.5	88.5	.120	31.8	1.15	4.09	.372	1.04
	30.0	55.0	88.5	.120	32.0	1.28	4.36	.443	1.04
	31.6	61	90.5	.120	.....	1.34	4.85	.514	.....
	34.9	50	87.0	.120	38.4	1.48	3.97	.465	1.06
	39.0	50	83.5	.120	37.0	1.66	3.97	.523	1.06
1198	45.6	22.8	63.0	.103	.....	1.94	2.46	.278	.....
1200	68	27.5	63.5	.103	.....	2.89	2.97	.499	.....
	73	33.3	60.5	.101	.....	3.10	3.72	.649	.....
1202	66.1	36.0	72.5	.114	23.4	2.81	3.16	.635	1.07
	74.1	35.2	75.5	.115	.....	3.15	3.04	.696	.....
	79.3	31.0	58.5	.095	.....	3.37	3.94	.656	.....
1211	20.1	85	98.5	.120	.....	.85	6.75	.454	.....
	27.0	75	96	.120	.....	1.15	5.96	.542	.....
1212	17.6	82	90.5	.120	17.2	.75	6.51	.388	1.01
	26.2	80	90.5	.120	65.2	1.11	6.35	.558	1.07
1213	29	83.5	82	.120	79	1.23	6.64	.645	1.10
1214	70	33.3	41.5	.078	.....	2.98	6.25	.624	.....
1235	16.6	85	85.5	.120	.....	.71	6.75	.378	.....
	17.6	68	86.0	.120	.....	.75	5.40	.321	.....
	18.7	66	85.5	.120	51.0	.79	5.25	.425	1.04
	20.0	67	84.0	.120	41.8	.85	5.32	.358	1.04
	21.1	65	84.0	.120	48.8	.90	5.16	.368	1.04
	22.9	63	83.5	.120	46.8	.97	5.00	.384	1.05
	24.4	55.5	84.0	.120	51.5	1.04	4.41	.363	1.03
	25.4	61	83.0	.120	46.0	1.08	4.85	.414	1.05
	29.7	52.5	83.0	.120	31.2	1.26	4.17	.415	1.04
	31.6	61.5	86.0	.120	.....	1.34	4.88	.517	.....
	34.9	59.0	85.5	.120	.....	1.48	4.68	.549	.....
	36.6	55.5	84.0	.120	.....	1.56	4.41	.543	.....
	38.6	48.5	82.0	.120	.....	1.64	3.86	.500	.....
1237	26.6	60.0	77.5	.119	.....	1.13	4.85	.426	.....
	27.3	61.0	78.5	.119	.....	1.16	4.93	.444	.....
	28.0	67.5	78.5	.119	.....	1.19	5.45	.505	.....
	29.6	57	79.0	.119	.....	1.26	4.60	.452	.....
	31.1	50.0	77.5	.117	48.6	1.32	4.17	.415	1.06
	32.3	53.5	73.5	.115	23.2	1.37	4.64	.461	1.03
	34.0	53.2	78.5	.119	− 9.7	1.44	4.30	.481	.99
	36.6	48.9	78.5	.119	37.2	1.56	3.94	.480	1.06
	39.5	46.2	80.0	.120	32.9	1.68	3.66	.488	1.06
	43.6	46.3	76.0	.117	28.8	1.85	3.87	.537	1.05
	45.4	49.2	73.0	.114	.....	1.93	4.31	.596	.....

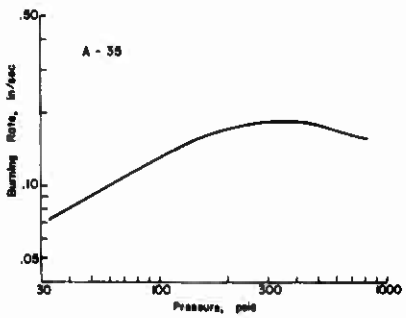

FIG. A-1. Burning Rate for Propellant A-35.

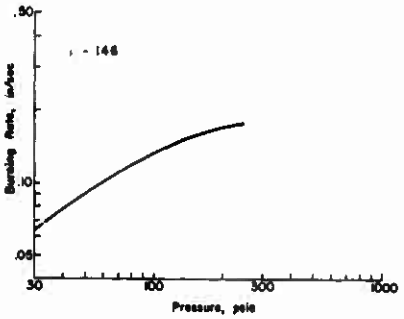

FIG. A-2. Burning Rate for Propellant A-146.

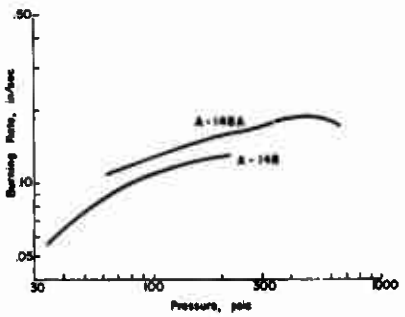

FIG. A-3. Burning Rate for Propellant A-148.

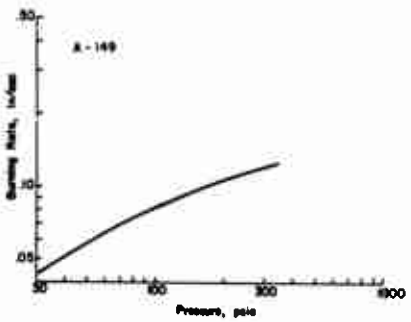

FIG. A-4. Burning Rate for Propellant A-149.

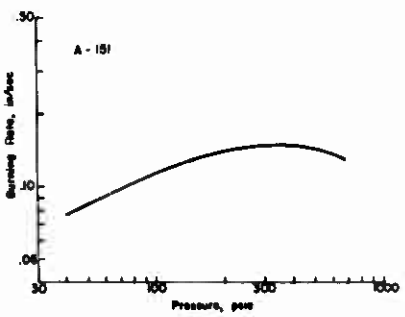

FIG. A-5. Burning Rate for Propellant A-181.

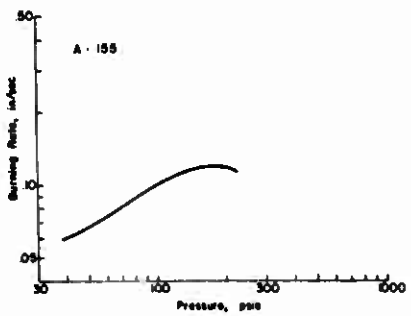

FIG. A-6. Burning Rate for Propellant A-155.

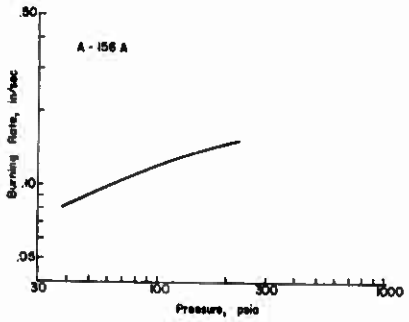

FIG. A-7. Burning Rate for Propellant A-156.

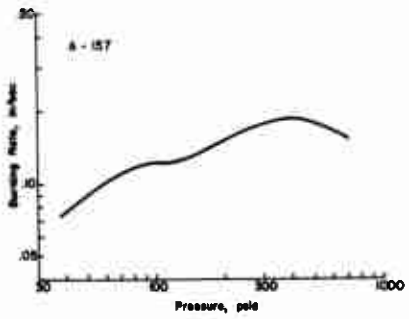

FIG. A-8. Burning Rate for Propellant A-157.

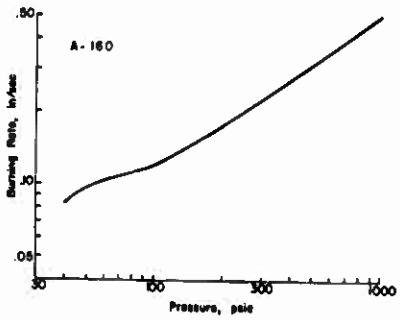

FIG. A-9. Burning Rate for Propellant A-160.

Appendix B

INSTABILITY TESTS ON CANDIDATE BIG BOOSTER PROPELLANTS

Two propellants that had been designed for snd were candidates for use in the large solid booster program were tested in both the L*-burner and the low-frequency T-burner. They were not tested in the conventional T-burner because of the high metal losding in the propellsnts which would csuse high-frequency oscillations to be completely sttenuated.

Testing in the L* burner wss more extensive than that of the "big pipe" due msinly to the ease of testing snd the smaller amount of propellsnt used in the L*-burner. Instability was observed for both propellsnts with the bounds that are normally observed in this burner. The propellsnts both behaved in what would be termed a "normal" fashion and on this basis sre considered as being typical, i.e., nothing occurred that would indicate that they would be more prone to instability thsn any other propellsnt. The dats thst were obtained sre included in Tsbles B-1 snd B-2.

TABLE B-1. Data Obtained With ANB-3105

Run no.	L*, in.	Frequency, cps	Pressure, psia	Growth constsnt, sec^{-1}
1008	11.4	59	80	< 0
1009	7.8	58	66	> 0
	8.7	53	70	~ 0
1010	13.6	44	48	> 0
	15.2	46	50	> 0
	16.7	44	55	< 0
1011	25.1	39	52	~ 0
1012	25.1	37	50	~ 0
	26.2	37	57	~ 0
	27.9	39	67	~ 0
1013	17.8	43	48.5	~ 0
	22.3	45	56.5	~ 0
1014	8.86	52	71.0	19.8
	9.62	52	70.5	~ 0
	10.4	51.6	70.0	-12.7
	16.56	53.0	83.5	~ 0

TABLE B-1. (Contd.)

Run no.	L*, in.	Frequency, cps	Pressure, psis	Growth constant, sec^{-1}
1047	10.56	65.5	46	12.8
	11.41	65.0	50.5	- 7.52
1048	7.7	75	73.5	....
	8.0	68	70.5	22.3
	8.4	66.7	73.4	9.5
	9.1	60.0	73.2	17.7
	10.5	70	80.5	~ 0
1049	13.9	77.3	80.0	11.1
	14.3	68.0	78.5	25.6
	14.9	62.0	76.5	24.1
	16.1	60	70.0	14.7
	18.8	58	72.5	~ 0
1050	6.1	55.5	57.5	17.6
	7.5	54.5	67.0	-21.9
	8.4	58.0	71.5	~ 0
1051	11.2	80.0	69.5	....
	12.1	70.0	60.5	28.0
	13.0	66.7	56.5	....
	14.2	55	50.5	50.5
	15.8	50.0	47.5	32.9
	16.4	50.0	43.4	....
	17.7	47.6	42.5	48.8
1052	26.3	40	39.5	32.3
	28.2	40	40.5	18.8
1053	35.7	33	47.5	7.0
	36.8	36.4	46.5	8.1
	40.1	31.0	38.0	23.2
	41.5	32.1	35.0	14.5
1054	20.3	22.0	25.5	21.0
	21.3	25.0	29.5	18.5
	22.4	26.2	33.4	22.1
	25.0	29.2	37.5	....
1090	21.3	60	71.5	22.6
	9.7	62.5	71.5	-22.9
1092	11-31	....	160	....
1093	10	62	55	~ 0
1094	14.7	40	46.0	12.8
1095	20-33	....	112	....

TABLE B-2. Data Obtained With ANB-3254 Propellant

Run no.	L*, in.	Frequency, cps	Pressure, psia	Growth constant sec^{-1}
1039	22.4	50	60.5	70
	21.8	54	78.5	0
1061	....	....	87	....
1062	....	....	98	....
1070	35	35.6	70.5	24.6
	....	....	100.5	....
1072	38.5	30	50.5	-14.7
1073	47.5	33	67	-13.5
1081	27.8	40	67.5	....
	26.4	37.5	70.5	-16.3
	30.7	31	62.5	29.5
1082	~35	41	67	~ 0
1083	~69	30	57.5	-10.9
1084	7.6	65	92.5	-25.7
1085	~12	55	68.5	-21.8
1086	- 7.2	75	105	33.0
1087	7.6	75	95	-29.0
1088	20.9	50	73.5	32.4
1089	~27	43	83.5	-18.2

LOW FREQUENCY ACOUSTIC TESTS

Seven tests were conducted in the 5.5-inch T-burner rsnging from 15 to 250 cps. The pressure control system wss progrsmmed to provide for a progressively incressing pressure during burning of the propellsnt. The high burning rate of these two propellsnts resulted in s tendency for the relstively grest volume of combustion products to overide the pressure control system snd to create a burner pressure-time history thst deviated considerably from that which wss desired. No oscillstory behavior was observed which could be assigned to combustion-driven processes, except in one test with ANB-3254. Some mild oscillstions were observed in other tests which appeared to be caused by vibration of pressure transducers or induced by the pressure control apparatus. Test informstion is detsiled in Tsble B-3.

CONCLUSIONS

As a result of testing these two propellants, it was concluded that the possibility of either of these propellsnts experiencing pressure coupled acoustic instability or nonscoustic instsbility in the 260-inch motor configurstion would be rather remote. The possibility of velocity

coupled instability waa not tested for and could not be ruled out. However, although the poaaibility of thia type of instability occurring exists, it waa considered unlikely in the 260-inch configuration.

TABLE B-3. 5.5-inch T-Burner Tests

Propel-lant	Test no.	Burner length, ft	Pressure range, psig	Preaaure range of Osc. psig	Freq.	Remarka
ANB 3105	4820	12	20-63	...	→	Low amplitude signal ∿ 250 cpa at end of burn
	4776	24	24-70	...	→	Low amplitude 300 cpa signsl above 25 paig
	4777	24	0-35	...	→	(May be trsnaducer scting up)
ANB 3254	4821	6	0-72	55-72	250	Small amount of higher frequency preaent
	4819	12	40-90	...	Stable	Poor preasure control
	4778	24	30-63	...	Stable	Poor preasure control
	4818	48	0-55	...	Stable	2nd mode in last portion of teat-probably due to air controller

REFERENCES

1. U. S. Naval Ordnance Test Station. Combustion of Solid Propellants and Low Frequency Combustion Instability, by Aerothermochemistry Division. China Lake, Calif., NOTS, June 1967. 244 pp. (NOTS TP 4244.)

2. Angelus, T. A. "Solid-Propellant Combustion Instability," Panel Discussion in Proceedings of the Eighth Symposium (International) on Combustion. Blatimore, Md., Williams and Wilkins Company, 1962. Pp. 921-4.

3. Jet Propulsion Lsboratory. Solid Propellant Propulsion, Chapter IV, Starfinder Motor Development, by Floyd Anderson. Pasadena, Calif., JPL Research Summary No. 36-3. (No date).

4. Piasecki, L. and W. Gin. "Solid Rockets for Lunar and Planetary Spacecraft," ARS Preprint 1462-60 (December 1960).

5. Bircumshaw, L. L. and B. H. Newman. "The Thermal Decomposition of Ammonium Perchlorate. I. Introduction, Experimental, Analysis of Gaseous Products, and Thermal Decomposition Experiments," in ROY SOC LONDON, PROC, Vol. A227 (1954), Pp. 115.

6. Hightower, J. D., snd E. W. Price. "Combustion of Ammonium Perchlorate," in "Eleventh Symposium (International) on Combustion." Pittsburgh, Pa., Combustion Institute, 1967. Pp. 463-72.

7. Hightower, J. D., and E. W. Price. "Two-Dimensional Experimental Studies of the Combuation Zone of Composite Propellants, in "2nd Combustion Conference, Interagency Chemical Rocket Propulsion Group," comp. and ed. by Chemical Propulsion Information Agency. Silver Spring, Md., May 1966. CPIA Publ. No. 105, Vol. 1, Pp. 421-32.

8. Friedman, R., R. G. Nugent, K. E. Rumbel, and A. C. Scurlock. "Deflagration of Ammonium Perchlorate," in "Sixth Symposium (International) on Combustion." New York, N. Y., Reinhold Publishing Corp., 1957. Pp. 612-18.

9. Hightower, J. D., snd E. W. Price. "Experimental Studies of the Combustion Zone of Composite Propellants," in "Interagency Chemical Rocket Propulsion Group/American Institute of Aeronautics and Astronautics Solid Propulsion Conference," comp. and ed. by Chemical Propulsion Information Agency. Silver Spring, Md., July 1966. CPIA Publ. No. 111, Vol. II, Pp. 163-76.

10. Markowitz, M. M., and R. F. Harris. "The Differential Thermal Analysis of Perchlorates. III. The System $LiClO_4$," J PHYS CHEM, Vol. 63, (1959), p. 1519.

11. Crump, J. E. "Surface Characteristics of Quenched Samples of Composite Aluminum Propellants," in "1st Combustion Instability Conference, Interagency Chemical Rocket Propulsion Croup," comp. and ed. by Chemical Propulsion Information Agency. Silver Spring, Md., January 1965. CPIA Publ. No. 68, Vol. 1, Pp. 361-5.

12. Naval Weapons Center. Combustion of Metals, Progress Report, 1 July 1965 - 1 May 1967, by The Metal Combustion Study Croup. China Lake, Calif., NWC, to be published in 1968 as NWC TP 4435.

13. Crump, J. E. "Aluminum Combustion in Composite Propellants," in "2nd Combustion Instability Conference, Interagency Chemicsl Rocket Propulsion Croup," comp. and ed. by Chemical Propulaion Information Agency. Silver Spring, Md., CPIA, May 1966. CPIA Publ. No. 105, Vol. 1, Pp. 321-9.

14. Hart, R. W., and F. T. McClure. "Combustion Instability: Acoustic Interaction with a Burning Propellant Surface," J CHEM PHYS (June 1959), Pp. 1501-14.

15. Bird, J. F., L. Haar, R. W. Hart, and F. T. McClure. "Effect of Solid Propellant Compressibility on Combustion Instability," J CHEM PHYS, Vol. 32 (1960), Pp. 1424-9.

16. Denison, R., and E. Baum. "A Simplified Model of Unstable Burning in Solid Fropellants," ARS J, Vol. 31 (August 1961), Pp. 1112-22.

17. Hart, R. W., R. A. Farrell, and R. H. Cantrell. "Theoretical Study of a Solid Propellant Having a Heterogeneous Surface Reaction. Part I: Acoustic Response, Low and Intermediste Frequencies," COMBUST AND FLAME, Vol. 10 (December 1966), Pp. 367-80.

18. Beckstesd, M. W., snd E. W. Price. "Nonacoustic Combustor Instability," AIAA J, Vol. 5, No. 11 (November 1967), Pp. 1989-96.

19. Coates, R. L., N. S. Cohen, and L. R. Harvil. "An Interpretation of L* Ccmbustion Instaoility in Terms of Acoustic Instaoility Theory," AIAA J, Vol. 5, No. 6 (June 1967), Pp. 1097-1102.

20. Rocketdyne. Effects of Aluminum on Solid-Propellant Combustion Instability, by C. L. Oberg and A. L. Huebner. Canoga Park, Calif., Report No. R-6654, Final Report No. AF49 (638)-1575 (July 1966).

21. Beckstead, M. W. "Non-Acoustic Combustion Instability of Solid Propellants," Univ. of Utah (June 1965). Unpublished Ph.D. Thesis.

22. Beckstead, M. W., N. W. Ryan, and A. D. Baer. "Non-Acoustic Instability of Composite Propellant Combustion," AIAA J, Vol. 4, No. 9 (September 1966), Pp. 1622-8.

23. Powling, J. "Experiments Relating to the Combustion of Ammonium Perchlorate-Based Propellants," in "Eleventh Symposium (International) on Combustion," Pittsburgh, Pa., Combustion Institute, 1967. Pp. 447-56.

24. Beckstead, M. W., and J. D. Hightower. "Surface Temperature of Deflagrating Ammonium Perchlorate Crystals," AIAA J, Vol. 5, No. 10 (October 1967), Pp. 1785-90.

25. Andersen, W. H., and R. E. Peaante. "Reaction Rate and Characteristics of Ammonium Perchlorate in Detonation," in "Eighth Symposium (International) on Combustion." Baltimore, Md., Williams and Wilkins Co., 1962. Pp. 705-10.

26. Jacobs, P. W. M., and A. Russell-Jones. "On the Mechanism of the Decomposition of Ammonium Perchlorate," AIAA J. Vol. 5, No. 4 (April 1967), Pp. 829-30.

27. Miller, R. A. Personal communication, Naval Weapons Center, China Lake, Calif., January 1967.

28. Sutton, G. P. Rocket Propulsion Elements. John Wiley and Sons, Inc., New York and London (1964) 341 pp.

29. Price, E. W. "Review of the Combustion Instability Characteristics of Solid Propellants," presented at the 25th Meeting of the AGARD Combustion and Propulsion Panel, San Diego, Calif., 22-24 April 1965. (To be published)

30. Beckstead, M. W., and F. E. C. Culick. "A Comparison of Analysis and Experiment for the Response Function of a Burning Surface," presented at the Fourth ICRPG Combustion Conference, 9-13 October 1967. Stanford Research Institute, Menlo Park, Calif.

31. U. S. Naval Ordnance Test Station. Low Frequency Combustion Inatability of Solid Rocket Propellants, 1 July - 1 September 1962, by E. W. Price. China Lake, Calif., NOTS, December 1962. (TPR 301, NOTS TP 3107).

32. ------. Low-Frequency Combustion Instability of Solid Rocket Propellants, 1 September 1962 - 1 May 1963, by M. D. Horton, J. L. Eisel, and E. W. Price. China Lake, Calif., NOTS, May 1963. (TPR 318, NOTS TP 3248).

33. ------. Low-Frequency Combustion Instability of Solid Rocket Propellants, by E. W. Price, D. W. Rice and J. E. Crump. China Lake, Calif., NOTS, July 1964. (TPR 360, NOTS TP 3524).

34. Horton, M. D., J. L. Eisel, and E. W. Price. "Low-Prequency Acoustic Oscillatory Combustion," AIAA J, Vol. 1, No. 11 (November 1963), Pp. 2652-4.

35. Eisel, J. L., M. D. Horton, E. W. Price, and D. W. Rice. "Preferred Prequency Oscillatory Combustion of Solid Propellants," AIAA J, Vol. 2, No. 7 (July 1964), Pp. 1319-23.

36. Price, E. W. "Review of the Combustion Instability Characteristics of Solid Propellants," presented at the 25th Meeting of the AGARD Combustion and Propulsion Panel, San Diego, Calif., 22-24 April 1965. (To be published).

37. Princeton University, Department of Aerospace and Mechanical Sciences. Solid Propellant Combustion Instability: Oscillatory Burning of Solid Rocket Propellants, by R. H. Woodward Waesche and Martin Summerfield. Princeton, N. J., Princeton Univ., August 1965. (Aerospace and Mechanical Sciences Report No. 751, under AFOSR Grant - 448-63, Project Task No. 920F-3814.).

38. Hart, R. W. snd P. T. McClure. "Theory of Acoustic Instability in Solid-Propellant Rocket Combustion," in Tenth Symposium (International on Combustion, Pittsburgh, Combustion Institute, 1965, pp. 1047-65.

39. Princeton University, Department of Aerospace and Mechanicsl Sciences. Non-Stesdy Burning Pehnomena of Solid Propellancs: Theory and Experiment, by M. Summerfield, H. Krier, J. S. T'ien and W. A. Sirignano. Princeton, N. J., Princeton Univ., July 1967. (Aerospace and Mechanical Sciences Report No. 793, under AFOSR Contract AF 49(638)1405 Project-Tssk 9713-01.). See elso: Krier, H., J. S. T'ien, W. A. Sirignano and M. Summerfield. Non-Steady Burning Phenomena of Solid Propellants: Theory and Experiments, in ICRPG/AIAA 2nd Solid Propulsion Conference, New York, N. Y., American Institute of Aeronautics and Astronautics, 1967. Pp. 75-88.

UNCLASSIFIED
Security Classification

DOCUMENT CONTROL DATA · R&D

(Security classification of title, body of abstract and indexing annotation must be entered when the overall report is classified)

1. ORIGINATING ACTIVITY (Corporate author) Naval Weapons Center China Lake, California 93555	2a. REPORT SECURITY CLASSIFICATION UNCLASSIFIED 2b. GROUP

3. REPORT TITLE
COMBUSTION OF SOLID PROPELLANTS AND LOW FREQUENCY COMBUSTION INSTABILITY
PROGRESS REPORT 1 APRIL-30 SEPTEMBER 1967

4. DESCRIPTIVE NOTES (Type of report and inclusive dates)
Progress Report, 1 April-30 September 1967

5. AUTHOR(S) (Last name, first name, initial)
Aerothermochemistry Division, Research Department

6. REPORT DATE April 1968	7a. TOTAL NO. OF PAGES 108	7b. NO. OF REFS 39
8a. CONTRACT OR GRANT NO. b. PROJECT NO. NASA Work Order No. 6030 c. d.	9a. ORIGINATOR'S REPORT NUMBER(S) NWC TP 4478 9b. OTHER REPORT NO(S) (Any other numbers that may be assigned this report)	

10. AVAILABILITY/LIMITATION NOTICES
THIS DOCUMENT IS SUBJECT TO SPECIAL EXPORT CONTROLS AND EACH TRANSMITTAL TO FOREIGN GOVERNMENTS OR FOREIGN NATIONALS MAY BE MADE ONLY WITH PRIOR APPROVAL OF THE NAVAL WEAPONS CENTER.

11. SUPPLEMENTARY NOTES	12. SPONSORING MILITARY ACTIVITY Naval Ordnance Systems Command Department of the Navy Washington, D.C. 20360

13. ABSTRACT

This semiannual report summarizes studies of ammonium perchlorate decomposition and deflagration, behavior of aluminum in the combustion zone of propellants, and oscillatory combustion of propellants in several types of experimental arrangements.

DD FORM 1 JAN 64 1473 0101-807-6800

UNCLASSIFIED
Security Classification

UNCLASSIFIED

Security Classification

14. KEY WORDS	LINK A		LINK B		LINK C	
	ROLE	WT	ROLE	WT	ROLE	WT
Combustion Propellant Instsbility Rocket						

INSTRUCTIONS

1. ORIGINATING ACTIVITY: Enter the name and address of the contractor, subcontractor, grantee, Department of Defense activity or other organization (corporate author) issuing the report.

2a. REPORT SECURITY CLASSIFICATION: Enter the overall security classification of the report. Indicate whether "Restricted Data" is included. Marking is to be in accordance with appropriate security regulations.

2b. GROUP: Automatic downgrading is specified in DoD Directive 5200.10 and Armed Forces Industrial Manual. Enter the group number. Also, when applicable, show that optional markings have been used for Group 3 and Group 4 as authorized.

3. REPORT TITLE: Enter the complete report title in all capital letters. Titles in all cases should be unclassified. If a meaningful title cannot be selected without classification, show title classification in all capitals in parenthesis immediately following the title.

4. DESCRIPTIVE NOTES: If appropriate, enter the type of report, e.g., interim, progress, summary, annual, or final. Give the inclusive dates when a specific reporting period is covered.

5. AUTHOR(S): Enter the name(s) of author(s) as shown on or in the report. Enter last name, first name, middle initial. If military, show rank and branch of service. The name of the principal author is an absolute minimum requirement.

6. REPORT DATE: Enter the date of the report as day, month, year; or month, year. If more than one date appears on the report, use date of publication.

7a. TOTAL NUMBER OF PAGES: The total page count should follow normal pagination procedures, i.e., enter the number of pages containing information.

7b. NUMBER OF REFERENCES: Enter the total number of references cited in the report.

8a. CONTRACT OR GRANT NUMBER: If appropriate, enter the applicable number of the contract or grant under which the report was written.

8b, 8c, & 8d. PROJECT NUMBER: Enter the appropriate military department identification, such as project number, subproject number, system numbers, task number, etc.

9a. ORIGINATOR'S REPORT NUMBER(S): Enter the official report number by which the document will be identified and controlled by the originating activity. This number must be unique to this report.

9b. OTHER REPORT NUMBER(S): If the report has been assigned any other report numbers *(either by the originator or by the sponsor)*, also enter this number(s).

10. AVAILABILITY/LIMITATION NOTICES: Enter any limitations on further dissemination of the report, other than those imposed by security classification, using standard statements such as:

(1) "Qualified requesters may obtain copies of this report from DDC."

(2) "Foreign announcement and dissemination of this report by DDC is not authorized."

(3) "U. S. Government agencies may obtain copies of this report directly from DDC. Other qualified DDC users shall request through

_____."

(4) "U. S. military agencies may obtain copies of this report directly from DDC. Other qualified users shall request through

_____."

(5) "All distribution of this report is controlled. Qualified DDC users shall request through

_____."

If the report has been furnished to the Office of Technical Services, Department of Commerce, for sale to the public, indicate this fact and enter the price, if known.

11. SUPPLEMENTARY NOTES: Use for additional explanatory notes.

12. SPONSORING MILITARY ACTIVITY: Enter the name of the departmental project office or laboratory sponsoring *(paying for)* the research and development. Include address.

13. ABSTRACT: Enter an abstract giving a brief and factual summary of the document indicative of the report, even though it may also appear elsewhere in the body of the technical report. If additional space is required, a continuation sheet shall be attached.

It is highly desirable that the abstract of classified reports be unclassified. Each paragraph of the abstract shall end with an indication of the military security classification of the information in the paragraph, represented as *(TS), (S), (C), or (U)*

There is no limitation on the length of the abstract. However, the suggested length is from 150 to 225 words.

14. KEY WORDS: Key words are technically meaningful terms or short phrases that characterize a report and may be used as index entries for cataloging the report. Key words must be selected so that no security classification is required. Identifiers, such as equipment model designation, trade name, military project code name, geographic location, may be used as key words but will be followed by an indication of technical context. The assignment of links, roles, and weights is optional.

UNCLASSIFIED

Security Classification